

ANOMALOUS PLASMA HEATING  
INDUCED BY  
MODULATION OF THE CURRENT-DENSITY PROFILE

by

N.J. Lopes Cardozo

Rijnhuizen Report 85-160

# C O N T E N T S

## INTRODUCTION AND SUMMARY

Chapter 1	<u>The TORTUR III experiment</u>	
	1.1 Introduction	1
	1.2 The machine	3
	1.3 Plasma diagnostics	6
	1.4 The TORTUR III plasma	8
	References	13
Chapter 2	<u>X-ray diagnostics</u>	
	2.1 On the origin of X-rays	15
	2.2 The basic expressions	16
	2.3 Classification of spectral regions	21
	2.4 Instrumentation	22
	References	27
Chapter 3	<u>Theoretical notions connected with the turbulent heating experiments</u>	
	3.1 Introduction	29
	3.2 Plasma turbulence	29
	3.3 Runaway electrons	33
	3.4 Interaction of runaways with collective plasma oscillations	36
	3.5 Current-driven instabilities	39
	3.6 Stability against resistive tearing modes	41
	References	43

Chapter 4	<u>Experimental results</u>	
	4.1 Introduction	45
	4.A.1 Basic discharge, general results	47
	4.A.2 Basic discharge, thermal X-ray emission	50
	4.A.3 Basic discharge, non-thermal X-ray emission	56
	4.B.1 Heating pulse, general results	60
	4.B.2 Heating pulse, X-ray measurements	64
	References	68
Chapter 5	<u>Interpretation of the X-ray measurements</u>	
	5.1 Introduction	69
	5.2 The spectral region 1 to 2 keV	69
	5.3 The spectral region 2 to 5 keV	74
	5.4 The spectral region 5 to 30 keV	77
	5.5 The spectral region 30 to 2 MeV	80
	5.6 Conclusions	82
	References	82
Chapter 6	<u>General interpretation and discussion</u>	
	6.1 Introduction	83
	6.2 The basic discharge	84
	6.3 During the current pulse and shortly after	89
	6.4 The delayed heating	92
	6.5 The relaxation of the pinched current-density profile	96
	6.6 Conclusions concerning the heating pulse experiment	101
	References	102
Acknowledgements		102
Appendices	A	103
	B	104
	C	106
	D	108

## INTRODUCTION AND SUMMARY

With the TORTUR III experiment at the FOM Institute for Plasma Physics in Nieuwegein, a research programme is being carried out concerning anomalous plasma heating. The goals are to study the physics of a mildly turbulent plasma and to investigate the potentials of enhanced ohmic dissipation as a means of heating a thermonuclear plasma.

The plasma we study is generated and confined in a so-called tokamak, a closed magnetic confinement device. The tokamak is widely used in thermonuclear research and is one of the most promising candidates for the fusion reactor. It is a toroidal system in which a current-carrying plasma ring is confined. The current heats the plasma by ohmic dissipation. In the typical tokamak plasma, temperatures up to  $10^7$  K are achieved with only ohmic dissipation as a source of heating. The potential of ohmic heating is limited, however, since the plasma resistivity decreases with increasing temperature. In order to heat the plasma up to ignition temperature ( $\sim 10^8$  K) additional heating is necessary. One method to achieve further heating is to induce anomalous plasma resistivity, which enhances the ohmic dissipation. This approach is studied in the TORTUR III experiment.

In our experiments a short (10  $\mu$ s) high-voltage pulse is applied to a stationary tokamak discharge. The object is to enhance the fluctuation level in the plasma and thus the resistivity. Indeed, a sharp rise of the plasma temperature is found, almost simultaneously with the pulse. However, the temperature falls back to its initial value after a few microseconds. Though the heating may be considerable ( $\sim 50\%$  of the basic temperature), the effect is too short-lived to be of interest as a heating method for a thermonuclear plasma.

In 1982, however, in the TORTUR III experiment a new phenomenon was observed: a second rise of the temperature. This second heating effect is a slow one, extending over several milliseconds. The temperature reaches a maximum 2 ms after the application of the high-voltage pulse. This delay is puzzling since the energy-confinement time - the "memory" - of the plasma is but 1.7 ms. Moreover, during the heating phase the Poynting flux through the plasma surface is not increased. What could be the mechanism of this delayed heating and what reservoir within the plasma supplies the energy?

Many experiments were dedicated to the solution of these questions. They involved the measurement of various plasma parameters, such as the temperature (both of the ions and of the electrons), the density, the emission spectrum (microwaves, visible light, vacuum ultra-violet, soft X-rays and hard X-rays, a spectral range from  $\lambda = 1$  cm, to  $\lambda = 10^{-12}$  m) and the fluctuation spectrum. In this thesis an account is given of these experiments. Emphasis is laid on the X-ray measurements, the latter being the author's diagnostic specialism.

Eventually, the conclusion is reached that the application of the high-voltage pulse results in a modulation of the current-density profile: the (normally already peaked) profile sharpens, the current concentrates in the centre of the plasma column. This is a non-equilibrium situation. It relaxes to the normal current distribution within  $\sim 2$  milliseconds. As long as this relaxation process is not finished, the dissipation is on an enhanced level and anomalous plasma heating is observed.

In fact, this is an expression of the general principle that in the stationary situation the current distribution is such that the dissipation is minimal (for given profiles of the temperature and density). Any perturbation of the equilibrium distribution results in enhanced dissipation. In our experiment the current distribution is pinched, which has two advantages above flattening:

- i) during the relaxation the self-inductance of the plasma decreases, which feeds the plasma current; and
- ii) the additional dissipation is concentrated in the plasma centre.

These aspects have been demonstrated in our experiments.

The major drawback is that the attainable peaking of the profile is limited by the macroscopical stability of the plasma. The method is open for improvement.

Actually, the basic TORTUR III discharge is an experiment on plasma turbulence in itself, as it exhibits a stationary resistance anomaly of about a factor of three. The enhanced resistivity is attributed to the occurrence of a weak current-driven instability of the ion-cyclotron type. Our experiments confirm the general finding that this anomalous resistivity is fairly independent of the electron temperature (in contrast to classical resistivity).

The structure of this thesis is as follows:

Chapter 1 is an introduction to the TORTUR III experiment. It contains a brief description of the machine and the diagnostic equipment, and a listing of some basic plasma parameters.

In Chapter 2, the X-ray diagnostic tools are described and the connection between the velocity distribution of the electrons and the X-ray spectrum is given.

Chapter 3 is a summary of various items from plasma theory, including plasma turbulence, runaway electrons and current-driven instabilities. It is meant as a basis for the interpretational work of the last Chapters.

In Chapter 4, the experimental results are presented. This Chapter is split into two parts: Part A, concerning the basic TORTUR III discharge and Part B, concerning the effects of the application of the high-voltage pulse.

The discussion of the experimental results is found in Chapters 5 and 6.

In Chapter 5 the X-ray measurements are scrutinized. Four spectral regions are distinguished, ranging from  $h\nu = 1$  keV to  $h\nu = 2$  MeV. The specific information obtained from measurements in each region is evaluated and discussed.

Chapter 6 offers a general interpretation of the measurements, both of the basic plasma and of the effects induced by the high-voltage pulse. The modulation of the current-density profile is discussed in detail.

Finally, in Appendix D a short account is given of the author's activity in the field of diagnostics development and the study of microchannelplate detectors.

## C H A P T E R 1

### THE TORTUR III EXPERIMENT

#### 1.1 Introduction

The heart of the TORTUR III experiment is a so-called tokamak. This is a magnetic plasma confinement system, the outward appearance of which is determined by a toroidal vacuum vessel, and a set of poloidal coils that generates a toroidal magnetic field in the vessel. The vacuum vessel is necessary because the plasma has to be formed out of low-pressure, exceedingly pure hydrogen gas. The toroidal field constitutes the main component of the magnetic field in which the plasma is confined. In general, it is kept constant during the plasma confinement.

A current is run through the plasma by operating the plasma ring as the secondary coil of a transformer. The current gives rise to heating through ordinary  $I^2R$  dissipation. Moreover, the poloidal magnetic field generated by the plasma current adds to the steady toroidal field to yield a helical field configuration. Together with an additional vertical field, this field configuration ensures stable confinement under well-defined conditions.

The present TORTUR III tokamak has evolved through numerous modifications out of the TORTUR I device that started its operation in 1974. The main theme of the scientific research programme has ever since been the study of enhanced (anomalous) plasma resistivity induced by pulses on the plasma current [1,2,3,4]. In order to produce these pulses the TORTUR III machine is equipped with high-voltage capacitor banks. A variety of diagnostic tools have been used to evaluate the complex processes brought about by the current pulses.

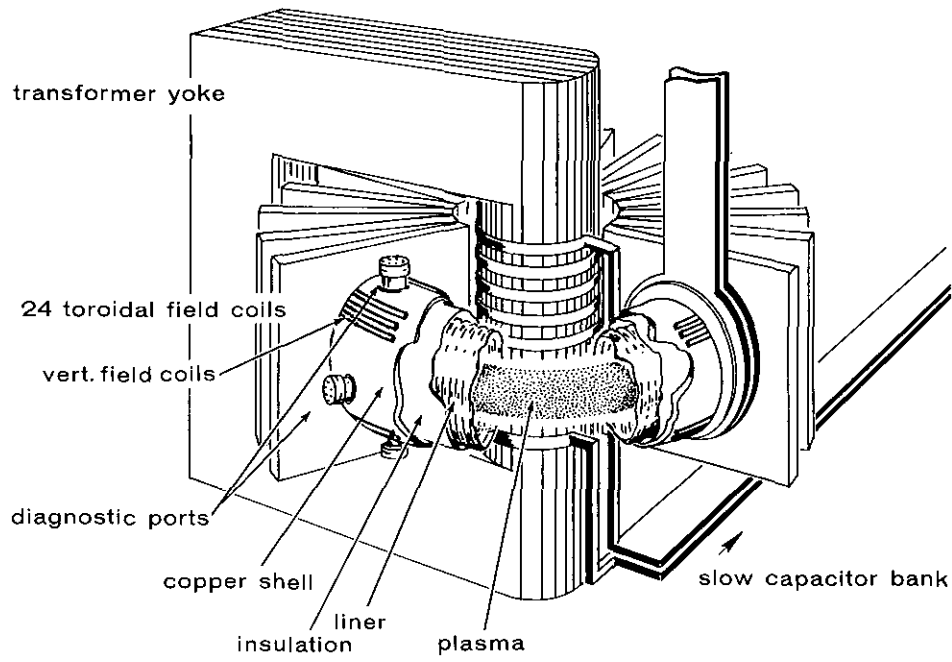


Fig. 1.1. Outline of the TORTUR III tokamak

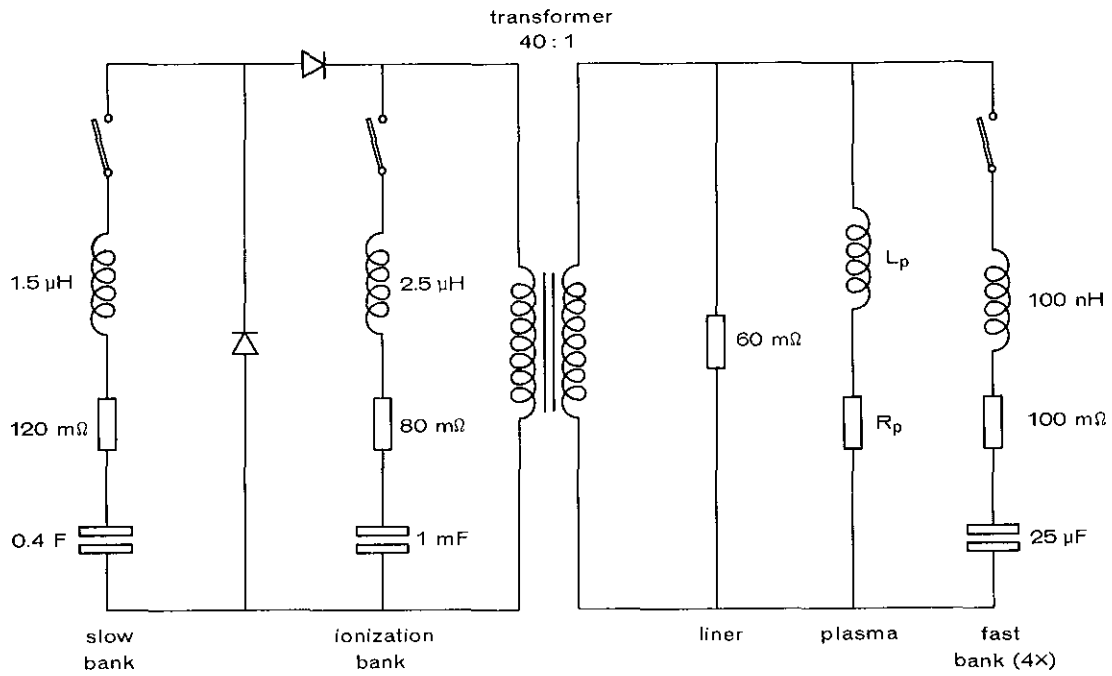


Fig. 1.2. The equivalent electrical circuit.

## 1.2 The machine

An outline of the TORTUR III tokamak is presented in Fig. 1.1, the equivalent electrical circuit is depicted in Fig 1.2. Apart from the vacuum vessel (liner), the toroidal field coils and the transformer yoke, the following features may be noticed:

- A copper shell of 2 cm thickness encloses the liner. This shell suppresses - by means of local induction currents - fluctuations of the plasma position with timescales shorter than the skin time of 2 cm copper ( $\tau = 2 \text{ ms}$ ). Both in poloidal and toroidal direction the shell has insulating gaps to avoid short-circuiting of the currents induced by the magnetic field.
- Vertical field coils are used for the control of the equilibrium position of the plasma column. They are attached closely to the copper shell. The strength and configuration of this control field can be adjusted, but the field cannot be varied during the shot.
- In between the magnetic field coils, ports of the liner emerge through openings in the copper shell. They serve as diagnostic ports. Also the stainless steel limiters that define the plasma boundary are inserted through them. The plasma radius can be chosen in the range 73 to 87 mm.
- The primary coil of the transformer is wound around the central leg of the yoke. In this manner an inductive coupling persists until the yoke has reached saturation. The yoke allows a flux swing of 0.25 Vs.
- The four fast (low-inductance) capacitor banks (40 kV, 25  $\mu\text{F}$ ) are used for the generation of short (10  $\mu\text{s}$ ) current pulses superimposed on the running plasma current. They can be fired at preset times. The current is fed directly to the copper shell. Special care was taken to avoid stray fields at the connection.
- The liner is made of inconel, rigid sections alternate with bellows. The thickness of the inconel of the bellows is 0.2 mm. Thus the skin time is reduced to  $\sim 1 \mu\text{s}$ , which is necessary to transmit the fast voltage pulses to the plasma.

The formation of plasma is initiated by pre-ionization of the test gas (1 mtorr  $\text{H}_2$ ) by means of a 200 watt r.f. signal. The discharge is then started by the ionization bank (5 kV, 1 mF), which rapidly forms a hot plasma. After a few milliseconds an electrolytic

bank (450 V, 0.4 F) takes over the magnetization current, and maintains a steady plasma current until saturation of the yoke puts an end to the discharge. For the plasma formation typically 100 mVs flux swing is used, the quasi-steady state uses the remaining 150 mVs. Figure 1.3 shows typical signals of the plasma current and the loop voltage. Figure 1.4 shows a current pulse delivered by the fast bank.

TABLE 1.1

Main machine parameters of TORTUR III

<u>Machine parameters:</u>	
major radius	$R_0 = 0.460 \text{ m}$
copper shield radius	$r_S = 0.105 \text{ m}$
limiter radius	$a = 0.080 \text{ m}$
magnetic field	$B_0 = 2.9 \text{ T}$
plasma volume	$Vol = 0.06 \text{ m}^3$

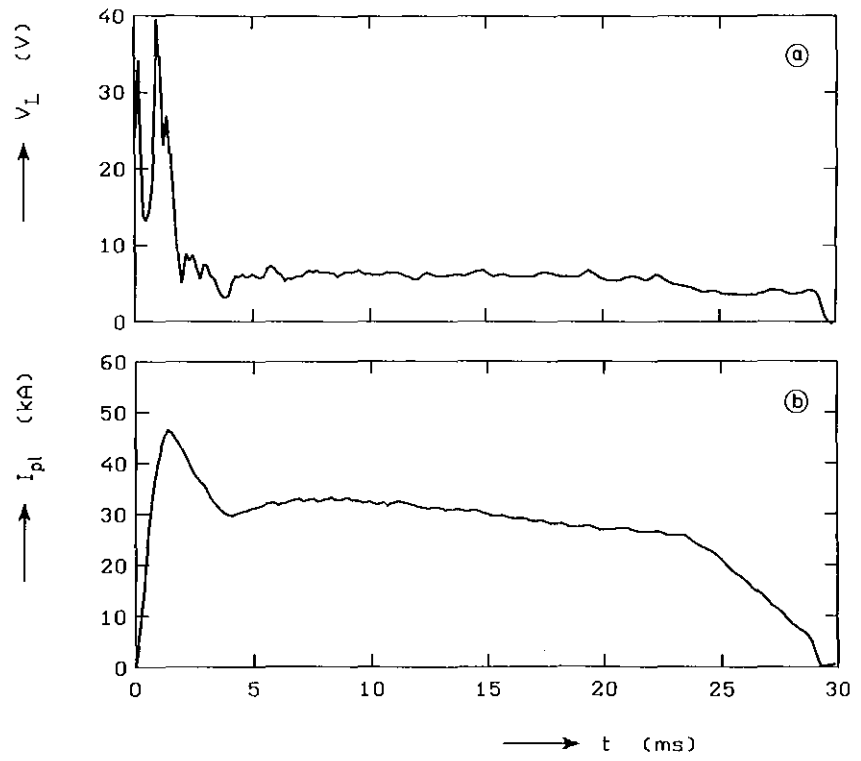


Fig. 1.3. Voltage and current as a function of time for a typical discharge.

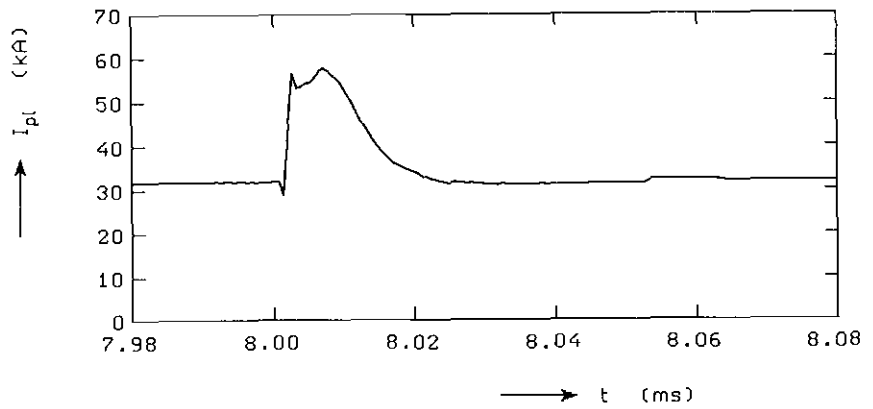


Fig. 1.4. Extra current pulse delivered by the fast bank.

### 1.3 Plasma diagnostics

In order to get detailed information about the physical processes which take place in the plasma, a variety of diagnostic tools have been used (see also Fig. 1.5):

#### Voltage and current:

- Direct measurement of the loop voltage by a loop-voltage divider.
- Measurement of the plasma current by means of Rogovski coils.
- Determination of the plasma position with a sine-cosine coil set (four coils, diametrically positioned around the plasma).

#### Line-integrated density

- A 2.14-mm wave interferometer bridge is used for the determination of the line-integrated plasma density.

#### Density fluctuations [5]:

- Density fluctuations in the outer plasma region are measured by means of the  $90^\circ$  scattered signal from a 4-mm beam launched into the plasma; also passive emission near 2 mm is measured.

#### Electron Cyclotron Emission [6]:

- An ECE six-channel polychromator ( $\lambda = 0.8$  to 3.5 mm) is used for the measurement of time-resolved radial temperature profiles.

#### Thomson scattering [7]:

- A pulsed ruby laser beam (10 ns, 500 MW,  $\lambda = 694.3$  nm) is sent through the plasma and is partially scattered by the free electrons. From the intensity and linewidth of the scattered light the electron density and temperature can be determined at one position and one instant of time. The beam can be positioned either on  $r = 5$  mm or  $r = 60$  mm.

#### Visible light emission:

- An optical multichannel analyser is used for the identification of impurity lines.
- Two monochromators are used to monitor the  $H_\alpha$ -emission of neutral hydrogen and the emission of the  $OII$  425.4 nm line.

#### Vacuum Ultra Violet radiation:

- A 1-m grazing incidence spectrometer performs measurements in the VUV region. These measurements give information on the concentration and ionization states of impurity ions. The spectrometer covers the region  $\lambda = 8$  to 1215 Å.

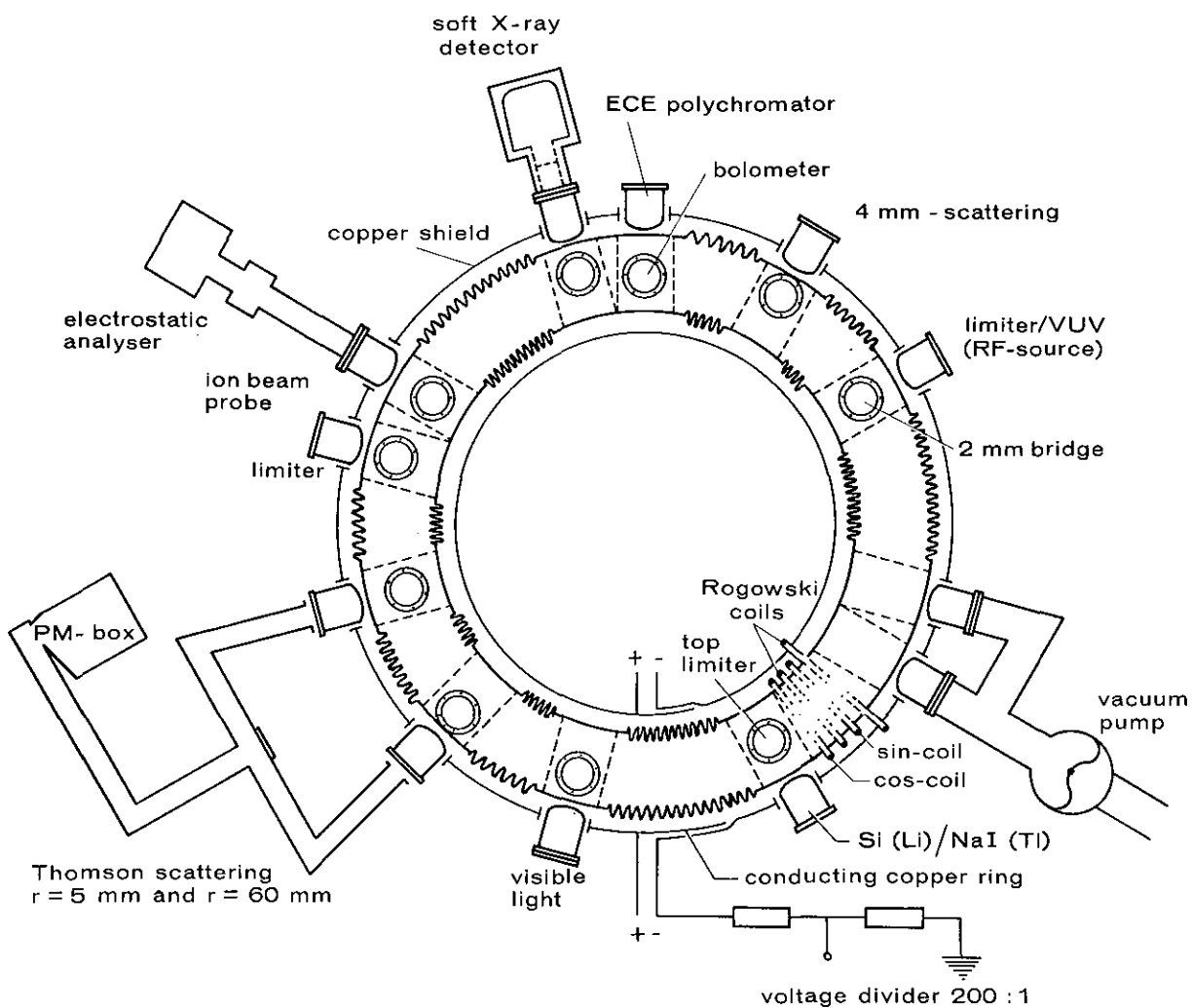


Fig. 1.5. Schematic plan of the diagnostic equipment of TORTUR III.

Soft X-ray emission (< 30 keV):

- A four-channel soft X-ray detector is used to record the evolution of the soft X-ray flux. By means of the foil method the electron temperature can be monitored [1,8].
- A liquid nitrogen-cooled Si(Li) detector is used to construct soft X-ray spectra by means of pulse-height analysis on a many-shot base.

Hard X-ray emission (> 30 keV):

- A big NaI(Tl) scintillation crystal in combination with a photomultiplier tube was used to obtain spectra in the hard X-ray region.
- A small NaI(Tl) scintillator plus photomultiplier was used to monitor the evolution of the hard X-ray flux.

Neutral particle flux [4,9,10]:

- The energy distribution of neutral particles which emerge from the plasma is measured with an eight-channel electrostatic analyser with a stripping cell at the entrance. A neutral beam injector offers the possibility to let the majority of the neutral flux originate at the plasma core. In this way the central ion temperature is evaluated.

Power loss:

- A bolometer measures the power loss to the wall as a function of time.

#### 1.4 The TORTUR III plasma

Anticipating the detailed discussion of the properties of the TORTUR III plasma, we shall present in this section a reference list of basic plasma parameters. The computed values are for a typical discharge as defined by the parameters given in Table 1.2. This type of discharge serves as a standard. When a series of measurements has been performed on a substantially different discharge, this will be mentioned explicitly. The values of the parameters vary during the discharge; those given apply for the quasi-stationary state of the discharge. Tables 1.3 and 1.4 list the standard TORTUR III values of selected plasma parameters. We dwell for a moment on the meaning of these.

TABLE 1.2  
Basic plasma parameters of standard discharges

plasma current	$I_p$	35 kA
loop voltage	$V_L$	4-5 V
electron temperature	$T_e$	{ 700 eV at $r = 5$ mm 250 eV at $r = 60$ mm
ion temperature	$T_i$	400 eV at $r = 5$ mm
electron density	$n_e$	{ $6 \times 10^{19} \text{ m}^{-3}$ at $r = 5$ mm $3 \times 10^{19} \text{ m}^{-3}$ at $r = 60$ mm
effective ion charge	$Z_{\text{eff}}$	1.5 - 2
energy density	$W$	} $\frac{3}{2} k(n_e T_e + n_i T_i) = \left\{ \begin{array}{l} 1.6 \times 10^4 \text{ Jm}^{-3} \text{ at } r = 5 \text{ mm} \\ 1.8 \times 10^3 \text{ Jm}^{-3} \text{ at } r = 60 \text{ mm} \end{array} \right.$
kinetic pressure	$P_k$	
magnetic pressure	$P_B$	$B^2/2\mu_0 = 3.3 \times 10^6 \text{ Jm}^{-3}$
kinetic to magnetic pressure ratio	$\beta$	$P_k/P_B = 0.5\%$ at $r = 5$ mm

TABLE 1.3  
Derived quantities  
(see p. 10-11)

TABLE 1.4  
Quantities depending on the current-density profile,  
computed for the assumption of classical resistivity

TORTUR III values				
quantity	symbol	expression	$r = 5$ mm	$r = 60$ mm
current density	$j$		5.3	1.0 MA/m <sup>2</sup>
drift velocity	$v_D$	$j/n_e \cdot e$	$5.5 \times 10^5$	$2 \times 10^5$ m/s
safety factor	$q$	$\frac{rB_\phi}{RB_\theta}$	1.8	3.5

TABLE 1.3  
Derived quantities

quantity	symbol	Expression (S.I.)	Reduced form ( $T_{e,i}$ in eV)	Value r=5 mm	TORTUR III r=60 mm	
electron-cyclotron frequency	$\omega_{ce}$	$\frac{eB}{m_e}$	$1.8 \times 10^{11} B$	$5.2 \times 10^{11}$		rad/s
ion-cyclotron frequency	$\omega_{ci}$	$\frac{ZeB}{m_i}$	$9.6 \times 10^7 \frac{Z}{A} B$	$2.8 \times 10^8$		rad/s
electron plasma frequency	$\omega_{pe}$	$\left(\frac{n_e e^2}{m_e \epsilon_0}\right)^{\frac{1}{2}}$	$5.6 \times \sqrt{n_e}$	$4.3 \times 10^{11}$	$3.1 \times 10^{11}$	rad/s
ion plasma frequency	$\omega_{pi}$	$\left(\frac{n_i Z^2 e^2}{m_i \epsilon_0}\right)^{\frac{1}{2}}$	$1.3 Z \sqrt{\frac{n_i}{A}}$	$1.0 \times 10^{10}$		rad/s
electron gyroradius	$r_{ce}$	$v_{th,e} / \omega_{ce}$	$3.4 \times 10^{-6} \frac{\sqrt{T_e}}{B}$	$3.1 \times 10^{-5}$	$1.9 \times 10^{-5}$	m
ion gyroradius	$r_{ci}$	$v_{th,i} / \omega_{ci}$	$1.4 \times 10^{-4} \frac{\sqrt{AT_i}}{ZB}$	$1.0 \times 10^{-3}$		m
Debye shielding distance	$\lambda_D$	$\left(\frac{\epsilon_0 k T_e}{n_e e^2}\right)^{\frac{1}{2}}$	$7.4 \times 10^3 \sqrt{\frac{T_e}{n_e}}$	$2.5 \times 10^{-5}$	$2.1 \times 10^{-5}$	m
electron thermal velocity	$v_{th,e}$	$(2kT_e / m_e)^{\frac{1}{2}}$	$5.9 \times 10^5 \sqrt{T_e}$	$1.6 \times 10^7$	$9.3 \times 10^6$	m/s
ion thermal velocity	$v_{th,i}$	$(2kT_i / m_i)^{\frac{1}{2}}$	$1.4 \times 10^4 \sqrt{\frac{T_i}{A}}$	$2.8 \times 10^5$		m/s

ion-acoustic velocity	$v_s$	$(kT_e/m_i)^{1/2}$	$9.8 \times 10^3 \sqrt{\frac{T_e}{A}}$	$2.6 \times 10^5$	$1.5 \times 10^5$	m/s
Alfvén velocity	$v_A$	$B(\mu_0 n_i m_i)^{-1/2}$	$2.2 \times 10^{16} \frac{B}{\sqrt{n_i A}}$	$8.2 \times 10^6$		m/s
electron-ion momentum equipartition time	$\tau_{c,ei}$		$6.9 \times 10^{11} \frac{T_e^{3/2}}{Z^2 n_i \ln \Lambda}$	$7 \times 10^{-6}$	$3 \times 10^{-6}$	s
energy equipartition times:						
electron-ion	$\tau_{eq,ei}$		$3.2 \times 10^{14} \frac{AT_e^{3/2}}{Z^2 n_e \ln \Lambda}$	$5.2 \times 10^{-3}$		s
electron-electron	$\tau_{eq,ee}$		$2.9 \times 10^{11} \frac{T_e^{3/2}}{n_e \ln \Lambda}$	$4.7 \times 10^{-6}$	$2.5 \times 10^{-6}$	s
ion-ion	$\tau_{eq,ii}$		$1.2 \times 10^{13} \frac{\sqrt{A} T_i^{3/2}}{Z^4 n_i \ln \Lambda}$	$1.1 \times 10^{-4}$		s
classical resistivity	$\eta$	$\frac{m_e}{n_e e^2 \tau_{c,ei}}$	$5.0 \times 10^{-5} \frac{Z \ln \Lambda}{T_e^{3/2}}$	$5.0 \times 10^{-8}$		$\Omega m$
runaway field	$E_c$		$2.6 \times 10^{-17} \frac{n_e}{T_e} \ln \Lambda$	40	47	V/m

The total pressure in the plasma is the sum of the kinetic pressure of the particles and the magnetic pressure  $B^2/2\mu_0$ . The value of the kinetic pressure over the magnetic pressure is a measure of the efficiency of the magnetic confinement. The TORTUR III value  $\beta_{\max} = 0.5\%$  is usual for small tokamaks.

The plasma frequency  $\omega_{pe}$  is a basic frequency of collective oscillations of plasma particles: if a group of electrons were slightly displaced with respect to the ions, they would return to their equilibrium position in an oscillatory motion with a frequency  $\omega_{pe}$ . For the ions a similar phenomenon occurs at  $\omega_{pi}$ . This kind of oscillation is always present in a plasma. Note that in our case the cyclotron frequency of the electrons,  $\omega_{ce}$ , is of the same order as  $\omega_{pe}$ . This means that for plasma oscillations the electrons are tied to the magnetic field lines. The parameter  $\omega_{ce}/\omega_{pe}$  plays an important role in the theory on plasma turbulence. For the ions, however,  $\omega_{ci} \ll \omega_{pi}$ . The magnetic field has but little influence on their motion. In fact, the electrons glue the ions to the magnetic field.

The Debye length, which is the effective range of the Coulomb interaction in this environment where free charges tend to shield it, is of the order of the electron gyroradius  $r_{ce}$ . Within a sphere of radius  $\lambda_D$ , however, of the order of  $10^6$  electrons are contained.

Some attention is paid to the important parameter  $\tau_{c,ei}$ , which is usually called the electron-ion collision time, although it really is the momentum equipartition time. We remark that  $\tau_{c,ei}$  is proportional to  $v^3$ . For a maxwellian velocity distribution this means that the resistivity decreases with increasing temperature like  $T_e^{-3/2}$ . This implies that there is a limit to the ohmic heating effect of the plasma current. The time  $\tau_{c,ei}$  is defined as the time it takes an electron, on average, to get scattered over  $90^\circ$ , which it does after many small-angle deflections.

The expressions for the energy equipartition times are valid for maxwellian distributions only. If energy is stored in superthermal particles, the equipartition may take considerably more time.

Since the collision time increases with  $v^3$ , one should not be surprised that there is a critical velocity above which an electron is accelerated freely by the loop voltage. Such electrons are called runaways. The runaway field, or rather  $E/E_C$ , is a measure of the rate of runaway production.

Apart from their thermal motion, the electrons have a mean directed velocity ( $v_D$ ) that corresponds to the local plasma current. Where this velocity approaches certain thresholds, such as the velocity of sound  $v_S$  or the thermal electron velocity, anomalous resistivity can be generated due to so-called current-driven instabilities.

The drift velocity is proportional to the local current density  $j(r)$ . In contrast with the total current  $I_p$  the  $j$ -profile is not easily measured. We can only calculate  $j(r)$  adopting some model for the resistivity. Therefore the values given in Table 1.4 are only an indication. They are computed for a  $j$ -profile as would result from classical resistivity, and should not be regarded as definitive figures.

The current density also determines the pitch of the helical magnetic field. The normalized pitch,  $q$ , is called the safety factor because of its importance for the development of dangerous instabilities. In general, instabilities may develop on surfaces where  $q$  is rational. The simpler the rationality, the faster the instabilities grow.

#### References

- [1] A.W. Kolfshoten, "Experimental studies of anomalous plasma heating in TORTUR II", part of Thesis University of Utrecht, 1982, Rijnhuizen Report 82-141 (1982).
- [2] H.W. Piekaar, "The turbulent heating of a plasma by a high electric field", Thesis University of Utrecht, 1972, Rijnhuizen Report 71-67 (1971).
- [3] H.W. Kalfsbeek, "Magnetic field profiles during turbulent heating in a toroidal hydrogen plasma", Part of Thesis University of Utrecht, 1979, Rijnhuizen Report 78-114 (1978).
- [4] TORTUR TEAM, Proc. 11th Eur. Conf. on Contr. Fusion and Plasma Phys., Aachen, (1983), Part I, p. 409.
- [5] F. Huussen and S. Ikezawa, "Experimental observation of low-frequency spectra in the turbulently-heated TORTUR tokamak plasma", Internal Report 84/023.
- [6] R.M. Niestadt, "ECE measurements on the TORTUR III tokamak", Rijnhuizen Report 83-148 (1983).

- [7] C.J. Barth, "A high transmission, 20-channel polychromator for the Thomson-scattering diagnostic of TORTUR III", Rijnhuizen Report 84-156 (1984).
- [8] N.J. Lopes Cardozo, "Soft X-ray electron temperature measurements on TORTUR", Rijnhuizen Report 84-151 (1984).
- [9] H.J.B.M. Brocken, "Passive and active neutral particle diagnostics for the measurement of ion energy distributions in hot plasmas", Thesis University of Utrecht, 1981.
- [10] F.B. Hendriks and H.J.B.M. Brocken, "Ion temperatures in TORTUR III", Rijnhuizen Report 85-159 (1985).

## C H A P T E R 2

### X-RAY DIAGNOSTICS

#### 2.1 On the origin of X-rays

An X-ray quantum may be generated by one of three distinct processes: Bremsstrahlung, recombination, and line radiation. The former two give rise to a continuous spectrum, the latter to discrete lines. We shall briefly discuss these sources of X-rays.

##### Bremsstrahlung

The scattering of electrons at local fluctuations of the electric field is accompanied by the emission of EM quanta of the electron kinetic energy or less. The source of the field fluctuations may be hydrogen ions or impurity ions, but also some collective oscillation of plasma particles. The X-ray spectrum reflects directly the velocity distribution of the electrons (see Section 2.2). Charged particles that hit solid structures such as the limiter or the liner also produce bremsstrahlung (thick-target radiation). The spectrum of this radiation also reflects the electron velocity distribution. Runaway electrons, which are confined effectively due to the low collisionality, may reach the limiter with an energy they have acquired milliseconds earlier. Hence, a rise of the hard X-ray intensity is not necessarily synchronic with the generation of fast electrons. A good example is the burst of hard X-rays at the end of a tokamak discharge.

Electron-electron interaction does not produce bremsstrahlung unless relativistic effects play a role. This often is the case, but the contribution to the bremsstrahlung flux is small.

##### Recombination

Although a hot hydrogen plasma usually is assumed to be completely ionized, an equilibrium actually exists between ionization and

recombination. If an electron is trapped by an ion, a photon is emitted of the electron kinetic energy plus the ionization energy of the ion. In a pure hydrogen plasma, recombination contributes but modestly to the soft X-ray flux. However, the probability of recombination is a strong function of the ion charge and the ionization potential. In a plasma with  $T_e = 500$  eV, contaminated with few per cents of oxygen, recombination completely outshines bremsstrahlung.

A second form of recombination is dielectronic recombination. In this process the capture of the electron provokes an inner shell excitation of the ion. The continuum part of the spectrum is usually not much affected, but the intensity of the relevant lines may be enhanced significantly [2].

### Line radiation

Inner shell transitions of not fully stripped ions give rise to emission lines in the soft X-ray region. They convey information on species and ionization states of impurities, but they may act as a disturbance of the continuous spectrum. Line radiation is generated mostly in the cold outer regions of the plasma, where light impurities are not fully stripped. Lines of heavy impurities are also found in the hot core.

Distinct as the physical origins of X-ray quanta may be, in the flux that leaves the plasma all photons are mixed together. The implications for the interpretation of spectra are discussed in Section 2.2.

## 2.2 The basic expressions

We shall present in this section expressions for the X-ray spectrum which are used in the analysis of the experimental results. The expressions given are approximate, the approximations made are usual for the kind of analysis we will perform [6,7,10]. The more accurate expressions can be found in literature, e.g., in [11,12] and references therein.

We consider an electron with kinetic energy  $\epsilon_e$  moving through an ion cloud of density  $n_i$ . Then, according to Kramer's rule, the power spectrum of the emitted radiation is flat up to photon energy  $\epsilon = \epsilon_e$  and has the value [5]:

$$I_e(\epsilon) = 3.76 \times 10^{-29} \frac{Z^2 n_i}{\sqrt{\epsilon_e}} \quad \text{s}^{-1} \quad (\epsilon \text{ in J}) \quad , \quad (2.1)$$

$$= 9.40 \times 10^{-20} \frac{Z^2 n_i}{\sqrt{\epsilon_e}} \quad \text{s}^{-1} \quad (\epsilon \text{ in eV}) \quad . \quad (2.2)$$

$I_e(\epsilon)d\epsilon$  is the energy radiated per second, in  $4\pi$  steradians, in the photon energy interval  $(\epsilon, \epsilon + d\epsilon)$  by an electron of kinetic energy  $\epsilon_e$  moving through an ion cloud of density  $n_i$ . This expression loses its validity when  $\epsilon_e$  approaches relativistic values [5].

For many electrons, with  $g(\epsilon_e)d\epsilon_e$  the number of electrons with kinetic energy between  $\epsilon_e$  and  $\epsilon_e + d\epsilon_e$  contained in one cubic metre of plasma, the bremsstrahlung spectrum reads:

$$I(\epsilon) = 9.40 \times 10^{-20} Z^2 n_i \int_{\epsilon}^{\infty} \frac{g(\epsilon_e)}{\sqrt{\epsilon_e}} d\epsilon_e \quad , \quad (2.3)$$

where  $I(\epsilon)d\epsilon$  is the energy radiated in the spectral interval  $(\epsilon, \epsilon+d\epsilon)$ , in  $4\pi$  steradians, in one second, by one cubic metre plasma of ion density  $n_i$  and ion charge  $Z_i$ .

Note that  $g(\epsilon)$  appears linearly in the integrand: if  $g(\epsilon)$  is written as a sum of distribution functions, the resulting spectrum is the sum of the corresponding spectra. This holds if spectra are mixed by line-of-sight integration, but also if, for instance, two quasi-temperatures coexist.

The distribution function can be reconstructed by differentiating the spectrum with respect to  $\epsilon$ :

$$\frac{dI}{d\epsilon}(\epsilon) = - 9.40 \times 10^{-20} Z^2 n_i \frac{g(\epsilon)}{\sqrt{\epsilon}} \quad . \quad (2.4)$$

From this expression, we see that the slope of the bremsstrahlung spectrum should be negative: if a spectrum exhibits a local positive slope, this must be due to a source other than bremsstrahlung, e.g., instrumental response function, line radiation or recombination steps. Expression (2.4) is not adequate for an accurate determination of  $g(\epsilon)$  from the X-ray spectrum: detailed accounts on this subject are given in Refs. [5,8].

For the maxwellian distribution

$$q(\epsilon) = \sqrt{\frac{4}{\pi}} \frac{n_e \sqrt{\epsilon}}{T_e^{3/2}} e^{-\epsilon/T_e}, \quad (2.5)$$

the bremsstrahlung spectrum takes the form:

$$I(\epsilon) = 9.40 \times 10^{-20} z^2 \frac{n_i n_e}{\sqrt{T_e}} e^{-\epsilon/T_e}. \quad (2.6)$$

A plot of  $\log(I)$  versus  $\epsilon$  shows a straight line, the slope of which equals  $-1/T_e$  (Fig. 2.1).

If photons are counted, the relevant spectrum is:

$$\frac{dN}{d\epsilon}(\epsilon) = \frac{I(\epsilon)}{\epsilon}. \quad (2.7)$$

The recombination spectrum has the same energy dependence as the bremsstrahlung spectrum. Therefore the spectral intensity of the total continuum radiation (bremsstrahlung + recombination) is frequently written in the form:

$$I(\epsilon) = 9.40 \times 10^{-20} n_e^2 \frac{e^{-\epsilon/T_e}}{\sqrt{T_e}} \times \xi(T_e). \quad (2.8)$$

$\xi(T_e)$  is called the enhancement factor, as it denotes the enhancement over pure hydrogen plasma bremsstrahlung. For a pure hydrogen plasma  $\xi$  takes the form:

$$\begin{aligned} \xi(T_e) &= \frac{n_{H^+}}{n_e} \left\{ z_H^2 + \left[ 2 \frac{\chi_H}{T_e} e^{\chi_H/T_e} + \sum_{\nu=2} \frac{2\chi_H}{T_e} \frac{1}{\nu^3} e^{\chi_H/\nu^2 T_e} \right] \right\} \\ &\approx 1 + \frac{27.2}{T_e} \sum_{\nu=1} \frac{1}{\nu^3} = 1 + \frac{33}{T_e}, \end{aligned} \quad (2.9)$$

with  $n_e, n_{H^+}$  : density of electrons and protons, respectively,  
 $z_H$  : charge of hydrogen ion = 1,  
 $\chi_H$  : ionization potential of hydrogen = 13.6 eV.

In an impure plasma, where the densities of the different ion species are denoted by  $n_j$  ( $j$ : label of the species) and the ion charges by  $Z_j$ , with  $n_e = \sum n_j \times Z_j$ , the generalized form reads:

$$\xi(T_e) = \sum_j \frac{n_j}{n_e} \{ Z_j^2 + f_j \} \quad , \quad (2.10)$$

$$f_j = Z_j^2 \left[ \frac{\zeta}{n^3} \frac{\chi_j}{T_e} e^{-\chi_j/T_e} + \sum_{\nu=1} \frac{2\chi_H}{T_e} \frac{Z_j^2}{(n+\nu)^3} e^{-Z_j^2 \chi_H / (n+\nu)^2 T_e} \right] \quad , \quad (2.11)$$

with  $n$  : the principal quantum number of the lowest shell with unoccupied places,

$\zeta$  : the number of free places in that shell,

$\chi_j$  : the ionization energy of the recombined state.

For  $T_e > \chi_j$  the  $f_j$  have approximately a  $T_e^{-1}$  dependence, which means that the recombination subsides with increasing temperature. The higher the temperature, however, the higher the ionization states of the impurity ions, which results in a rather wild behaviour of  $\xi$  as a function of  $T_e$  (Fig. 2.2).

We see that the recombination flux spoils the simple dependence of  $I(\epsilon)$  on the effective ion charge  $Z_{eff}$ , which is defined by:

$$Z_{eff} = \frac{1}{n_e} \sum_j n_j Z_j^2 \quad .$$

If we want to calculate  $Z_{eff}$  from the X-ray intensity, we must have additional information about the dominant impurities.

A more accurate expression for  $I(\epsilon)$  of a maxwellian plasma takes into account the Gaunt factors for free-free and free-bound transitions [3]:

$$\xi(T_e) = \sum_j \frac{n_j}{n_e} \{ q_{ff} Z_j^2 + q_{fb} f_j \} \quad .$$

In (2.10) all Gaunt factors are taken unity, which is usually a good approximation within 20% except for hydrogen for which  $q_{ff} \approx 0.5$  [6]. Since in our case the contribution of recombination is always dominant, the use of (2.10) introduces but a small error.

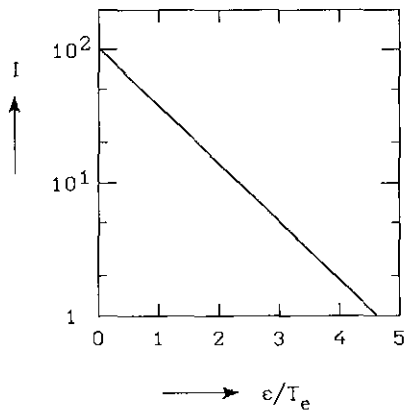


Fig. 2.1.  
The typical form of a bremsstrahlung spectrum.

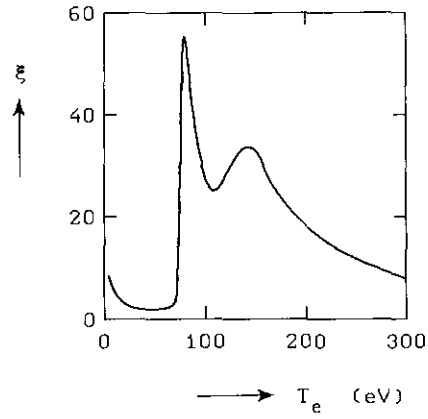


Fig. 2.2.  
The enhancement factor  $\xi$  calculated for a hydrogen plasma contaminated with 0.1% oxygen (corona equilibrium).

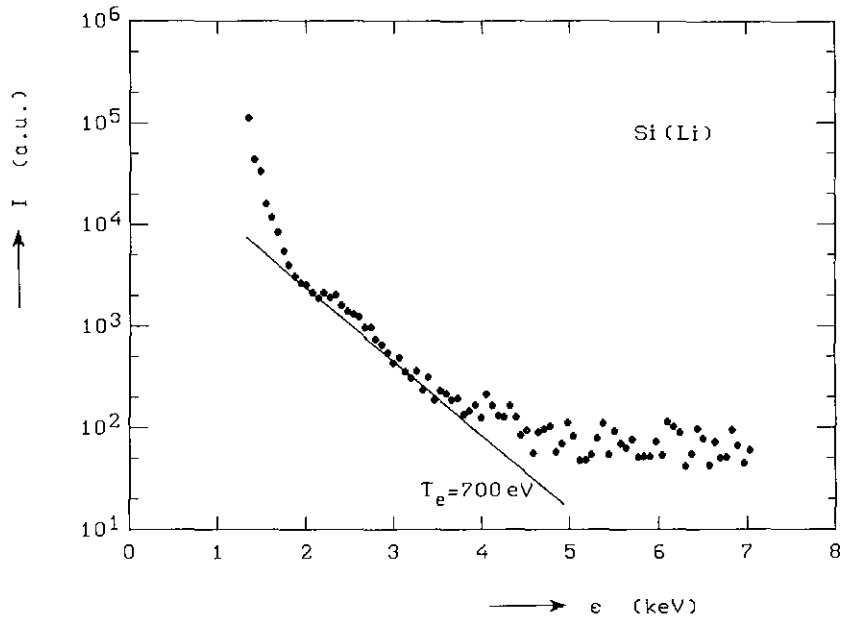


Fig. 2.3. A typical X-ray spectrum from the TORTUR III plasma.

The angular distribution of the radiation generated by a moving electron is peaked in the forward direction for electrons of all energies above 10 keV. For electrons below 100 keV kinetic energy, the peaking is, however, relatively broad [4]. This effect should be brought into account when the spectrum of a non-isotropic electron velocity distribution, in particular the runaway tail, is calculated.

### 2.3 Classification of spectral regions

In order to give a survey of the distinct spectral regions that will have our attention, a typical X-ray spectrum taken from TORTUR III is shown in Fig. 2.3.

We distinguish the following spectral regions:

0 - 1 keV: Radiation in this region is filtered out in our experiments. All lines of light impurities (carbon and oxygen) fall in this range. Iron has lines at 950-1150 eV in this region.

1 - 2 keV: In the TORTUR III case the radiation detected in this interval shows an apparent temperature  $T_e = 150$  eV. This flux dominates the low energy part of the spectrum.

2 - 4 keV: Here, the spectrum shows a neat thermal continuum, corresponding to  $T_e = 670$  eV. Radiation from the hot plasma centre dominates this region. Also line radiation of heavy impurities is observed.

For photon energies exceeding 5 keV a distinct tail is observed. This tail stretches to energies up to mega-electronvolts and grows during the discharge. Up to about 30 keV the X-rays are called soft, more energetic photons are called hard.

The soft and the hard X-rays have been measured by two detection systems each, one for spectral resolution, and one for temporal resolution. The instruments are described in the next section.

#### 2.4. Instrumentation

##### The four-channel soft X-ray analyser: PLATO [14]

A schematic drawing of the instrument is shown in Fig. 2.4. The main components are a vacuum chamber in which four soft X-ray detectors are placed, and a collimation system that defines the field of view of each detector. The four detectors look essentially at the same plasma volume. Four foil exchange wheels give the possibility to place one of four foils between each detector and the plasma. We used beryllium foils ranging in thickness from 30 to 200 micron.

PLATO is used to perform absolute intensity measurements with a time resolution of 100  $\mu$ s. The exchangeable foils enable us to monitor the electron temperature with the same time resolution by means of the foil method [17,11]. The principles of this method are as follows: a soft X-ray detector yields the integral over the photon energy  $\epsilon$  of the X-ray spectrum, weighed by the product of the detection efficiency and the transmission of any absorber between plasma and detector. The spectrum of both bremsstrahlung and recombination has the form (2.8):

$$I(\epsilon) \sim \frac{n_e^2}{\sqrt{T_e}} e^{-\epsilon/T_e} ,$$

with  $\epsilon$  the photon energy. Because the relative yield  $R$  of two detectors with different absorber foils is, to good approximation, a function of  $T_e$  only, evaluation of the flux in two detection channels suffices in principle to obtain the electron temperature. The electron density  $n_e$  is a common factor and does not appear in  $R$ . Due to the line-of-sight integration the radial  $T_e$ -profile should be taken into account when interpreting  $R$ . However, usually the X-ray emissivity is peaked in the hottest part of the plasma, hence  $R$  is determined mainly by the maximum value of  $T_e$  found on the line of sight.

In PLATO we use four detectors simultaneously: two surface-barrier diodes (SBD) and two MgF<sub>2</sub>-coated channeltrons (CEM). Hence, we obtain three types of the relative yield  $R$ : SBD-SBD, CEM-CEM, and the hybrid SBD-CEM. Of these, the hybrid ratio offers the best temperature resolution. This is caused by the contrasting detection efficiencies of the two types of detectors. Actually, it is in PLATO that the hybrid method is successfully applied for the first time [15,16].

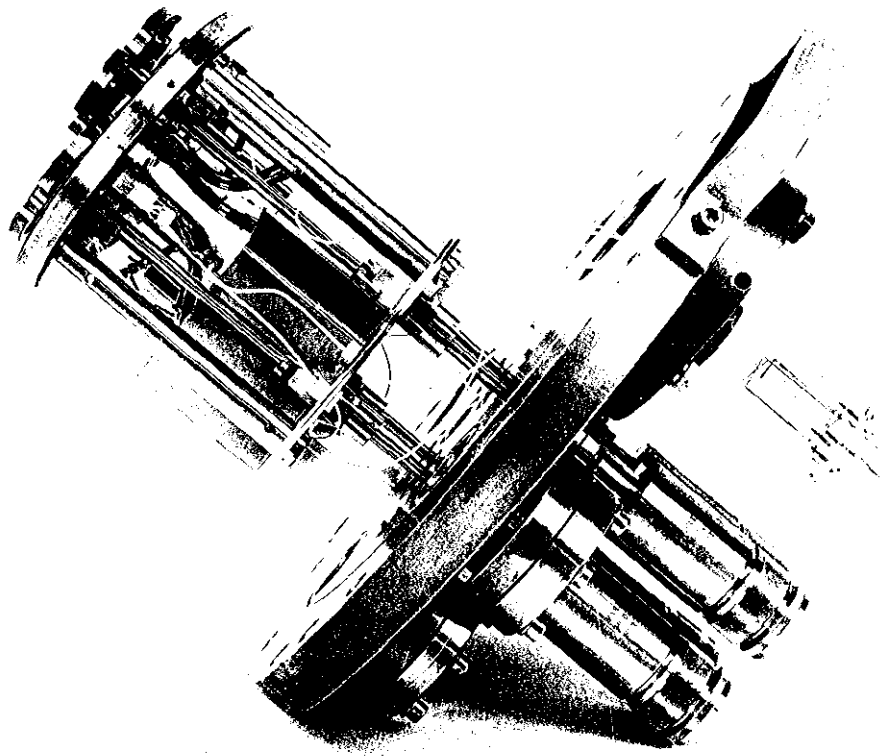
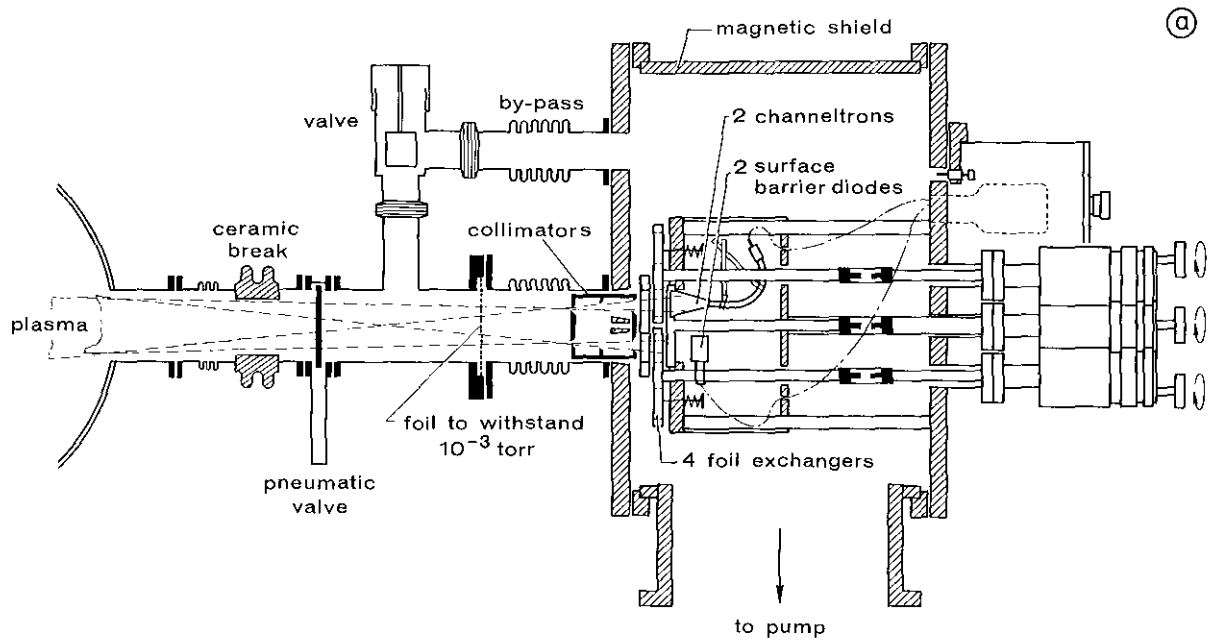


Fig. 2.4 a,b. The four-channel X-ray analyser.

### The Si(Li) detector

An Ortec model 7416-06215 liquid-nitrogen cooled lithium-drifted silicon detector system (see Fig. 2.5) is used for spectral measurements in the energy range 1-30 keV. The actual detector is 3.0 mm thick, which means it becomes transparent for photons exceeding 50 keV (1% absorption). In the spectral range 1-30 keV, each detected quantum produces a charge pulse proportional to its energy (one  $ee^-$ -pair is formed per  $\sim 3.5$  eV). The pulse is amplified directly by a low noise pre-amp of which the input FET is LN-cooled. The pre-amplified pulse is shaped and amplified in an Ortec amplifier/pile-up rejector. Pulses of 2-5  $\mu$ s width in the order of 1-1000 mV are produced. Pulse-height analysis is carried out by means of two Tracor Northern pulse-height analysers: TN 1710 and TN 7200 which can be gated at different sample intervals during the discharge. Count rates up to  $3 \times 10^4$  counts/second are used.

The energy resolution of the system is 280 eV (FWHM) at 5.9 keV. As the count rate is limited (to avoid pile-up) and the spectrum falls off with increasing photon energy, the soft part of the spectrum tends to drown the tail. For measurements in the superthermal region, 3-30 keV, the softer quanta are filtered out to bring out the tail.

An evacuated tube with exchangeable diaphragms at both ends is used to define the field of view and to regulate the intensity. The pressure in the tube is regulated too, so that the air in the tube forms a tuneable absorption filter.

For the energy calibration two radioactive sources are used:  
Fe<sup>55</sup> : 5.9 keV line, and  
Cs<sup>137</sup> : 32.2 keV line.

### The hard X-ray monitor

A NaI(Tl) scintillator-photomultiplier system is used to monitor the hard X-ray flux with good time resolution. The sensitivity lays in the range: 50 keV-0.5 MeV. The output signal is stored in a ADC, with a time resolution of 50  $\mu$ s second during 50 ms, and a triggered time-window of 1  $\mu$ s resolution (100 samples). The system is placed at about 60 cm distance from the torus. No shielding or collimation is applied.

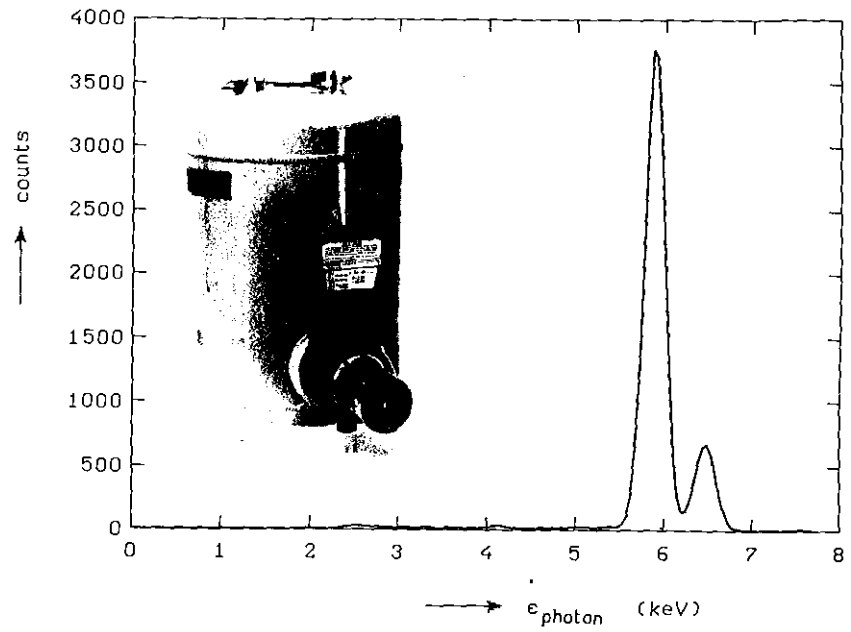


Fig. 2.5. A calibration spectrum ( $\text{Fe}^{55}$ ) taken with the Si(Li) detector (insert).

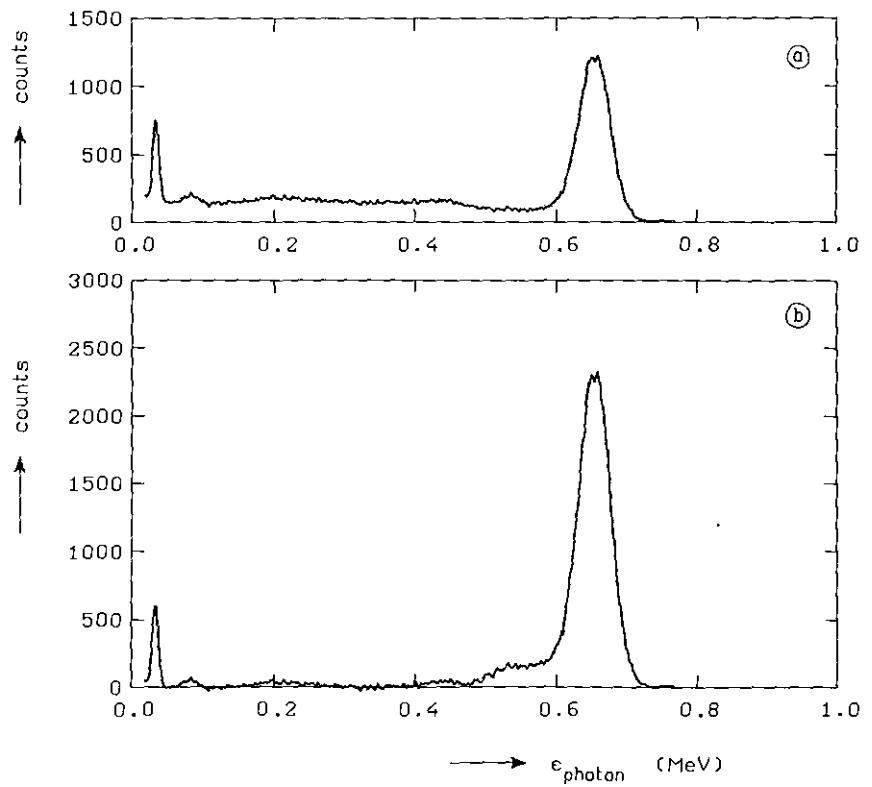


Fig. 2.6a,b. The spectrum of the  $\text{Cs}^{137}$  calibration source, taken with the NaI(Tl) detector: a. without, and b. with correction for the Compton effect.

### The NaI(Tl) scintillator

A NaI(Tl) crystal scintillator attached to a photomultiplier tube is used for hard X-ray spectral measurements. Pulse-height analysis is carried out with the TN 7200 and the TN 1710 pulse-height analysers, pulse-shaping and amplification with an Ortec model 450 research amplifier. The system responds linearly within 1% in the energy range 30 keV to 1.4 MeV.

Apart from the photo-effect, a photon that enters the crystal may decay into a softer photon and a Compton electron. The Compton electron gives rise to a light flash which is detected by the photomultiplier. The photon may escape from the crystal. In that case the detected energy is lower than that of the incident photon. As a result the spectrum of a single line shows, apart from a main peak, a continuous intensity at lower energies. The bigger the crystal, the more chance a secondary photon has to be captured in the crystal, and the more intensity is found in the main peak. The crystal we used has the dimensions:  $\emptyset = 6.25$  cm, length = 6.25 cm. The measured spectra were corrected for the Compton effect (see Fig. 2.6). Correction is not possible for the Compton effect due to photons of energy exceeding the detection range. Hence, the correction cannot be performed accurately for spectra that have a flat tail which extends too far over the border of the detection range.

For calibration we used a  $\text{Cs}^{137}$  (662 keV, 32.2 keV) and a  $\text{Co}^{60}$  (1.17, 1.33 MeV) radioactive source.

The whole system is placed in a lead castle of 5 cm wall thickness to reduce penetration of hard stray photons. A  $\emptyset = 2$  mm lead collimator is placed in front of the crystal. For X-ray energies of 1 MeV or more, however, the lead shielding becomes transparent.

In most discharges we could not measure after about  $t = 10$  ms, due to too high intensity.

References

- [1] C. Breton et al., "Ionization equilibrium and radiation cooling of a high temperature plasma", Report EUR-CEA-FC-853 (1976).
- [2] C. De Michelis and M. Mattioli, Nucl. Fusion 21 (1981) 677.
- [3] S. von Goeler et al., Nucl. Fusion 15 (1975) 301.
- [4] S. von Goeler et al., "Determination of the electron velocity distribution from the soft and hard X-ray emission during lower hybrid current drive on PLT", Report PPPL 2012 (1983).
- [5] S. von Goeler et al., "X-ray analysis of non-maxwellian distributions (current drive)", Report PPPL 2010 (1983).
- [6] R.D. Gill et al., Nucl. Fusion 19 (1979) 1003.
- [7] K.W. Hill et al., "Low energy X-ray emission from magnetic fusion plasmas", Report PPPL 1887 (1982).
- [8] K. Bernhardt and K. Wiesemann, Plasma Phys. 24 (1982) 867.
- [9] P. Brouquet, "Spectrométrie à fort taux de comptage pour l'étude du rayonnement X mou application du plasma WEGA", Report EUR-CEA-FC-1002 (1979).
- [10] W.R. Wing, Course of Plasma Diagnostics and Data Acquisition Systems, Varenna 1975, p. 324.
- [11] P. Smeulders, "Soft X-ray fluxes as a diagnostic for hot plasmas", Thesis University of Utrecht, 1979, Report IPP 2/233 (1979).
- [12] J.E. Rice et al., "Continuum X-ray emission from the Alcator A tokamak", Report PFC/JA-81-5 (1981).
- [13] S.M. Shafroth et al., "Scintillation spectroscopy of gamma radiation", Vol. 1, Gordon & Breach, London, 1967.
- [14] A.W. Kolfshoten, "Experimental studies of anomalous plasma heating in TORTUR II", part of Thesis University of Utrecht, 1982, Rijnhuizen Report 82-141 (1982).
- [15] N.J. Lopes Cardozo, Rev. Sci. Instrum. 55 (1984) 1077.
- [16] N.J. Lopes Cardozo, "Soft X-ray electron temperature measurements on TORTUR", Rijnhuizen Report 84-151 (1984).
- [17] F.C. Jahoda et al., Phys. Rev. 119 (1960) 843.



## C H A P T E R 3

### THEORETICAL NOTIONS CONNECTED WITH THE TURBULENT HEATING EXPERIMENTS

#### 3.1 Introduction

In the interpretation of experiments on turbulent plasma heating many fields of plasma theory come together. We do not only want to know what laws govern the anomalous resistivity, but we must concern ourselves with the power balance as a whole, e.g. with anomalous heat conduction and particle transport. Furthermore, the short current pulse that is applied in the TORTUR III experiment is such that we must consider the plasma stability against ideal MHD and resistive tearing modes during the pulse.

In this chapter we will briefly quote some capita of the vast body of literature existing on these fields. This selection is by no means meant as a review. Its purpose is merely to provide some basic material on topics that will recur in Chapters 5 and 6.

#### 3.2 Plasma turbulence

Plasma turbulence is found in many experiments, under widely different conditions. A systematic survey of the turbulent states that can occur is given in Table 3.1 [1]. The TORTUR III experiments are found low in the central columns. The important parameter for the behaviour of the plasma is found to be the normalized electric field  $E/E_C$ , where  $E_C$  is the runaway field (see Section 3.3). Indeed for many experiments, the anomaly of the resistivity is found to scale with  $E/E_C$  (see Fig. 3.1 [2]). The turbulent state is quite generally found to occur for  $E/E_C \gtrsim 0.003 \sigma_{c1}/\sigma$  (broken line in Fig. 3.1), which is equivalent to the condition:

$$\gamma \equiv v_D/v_S \gtrsim \gamma_{cr} \gtrsim 1 .$$

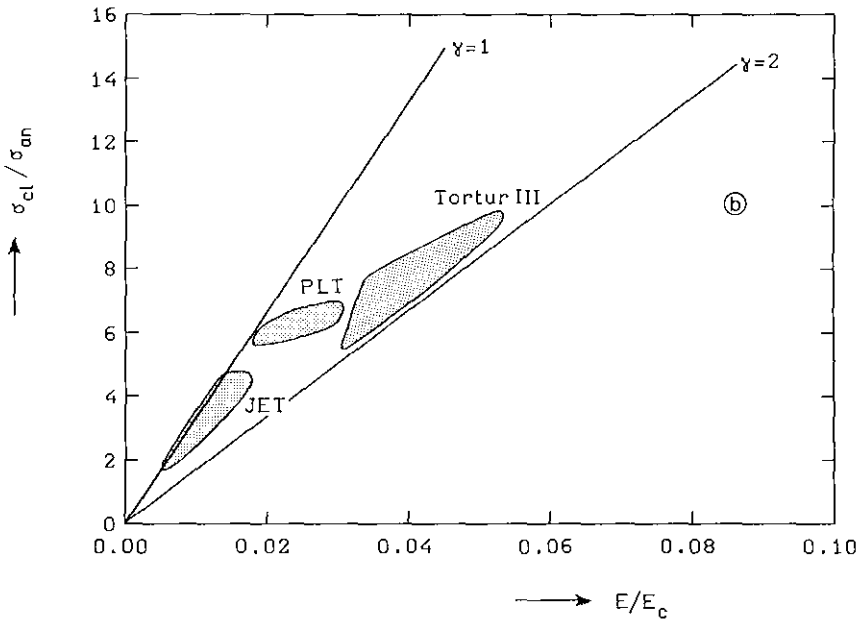
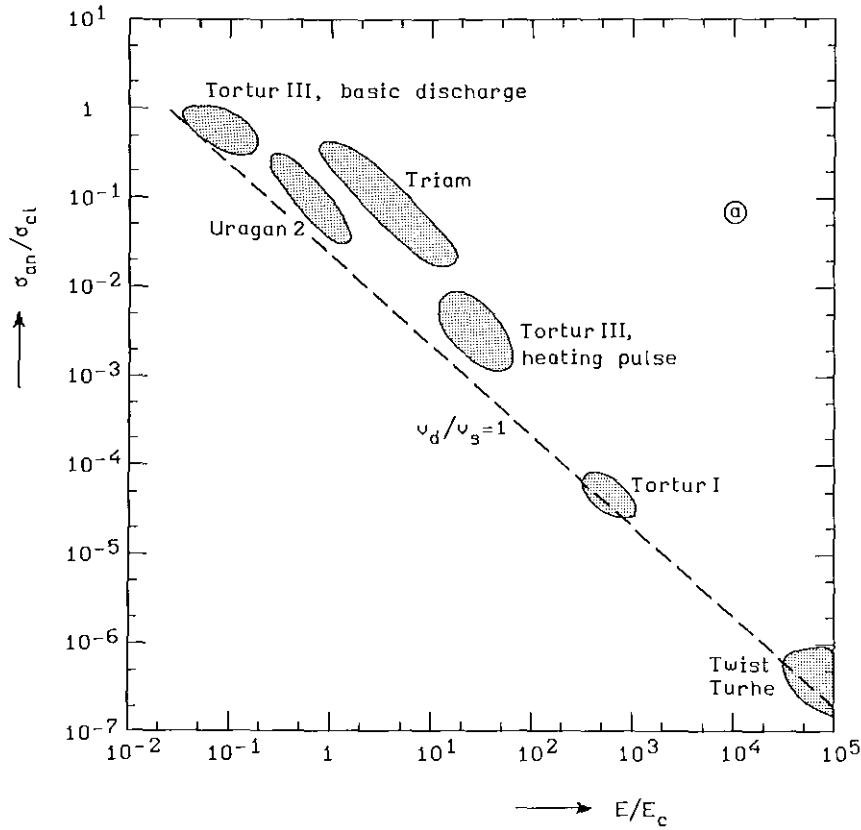


Fig. 3.1a. Ratio of  $\frac{\sigma_{\text{anomalous}}}{\sigma_{\text{classical}}}$  as a function of  $\frac{E}{E_D}$ . Values found in literature are quoted. ( $E_D$  -Dreicer field- is related to  $E_c$  by  $E_D = 0.2 E_c$ ).

3.1b. Idem, for the typical tokamak regime. ( $\gamma = \nu_D/\nu_S$ ).

		$E/E_D \leq 0.02$	$0.02 < E/E_D \leq 1$	$1 < E/E_D \leq 1000$	$E/E_D > 1000$
		classical regime classical collision theory collision-dominated "true runaways"	weak turbulence accelerative regime	'bulk' turbulence minority tail effects	strong turbulence non-linear theories
		quasi-linear theories beam-plasma interaction by anomalous Doppler effect and Cerenkov resonance			
$\frac{\omega_{ce}}{\omega_{pe}} < 1$	$\frac{T_e}{T_i} \gtrsim 3$	$\sigma = \sigma_{cl}$  (Spitzer resistivity)	$\sigma/\sigma_{cl} \sim E_D/E \quad \gamma \approx 1$ T-P interaction: Cerenkov resonance plasma modes: IA, LM	$\sigma/\sigma_{cl} \sim E_D/E \quad \gamma \geq 1$ bulk: IA turbulence T-P interaction: Cerenkov plasma modes: IA, LM	two-stream instability ion-acoustic instability stop runaway production
	$\frac{T_e}{T_i} \lesssim 3$		$\sigma/\sigma_{cl} \sim E_D/E \quad \gamma \gtrsim 1$ T-P interaction: Cerenkov plasma modes: IC, DW, MS	$\sigma/\sigma_{cl} \sim E_D/E \quad \gamma \geq 1$ bulk: IC turbulence T-P interaction: Cerenkov plasma modes: IC, DW, MS	
$\frac{\omega_{ce}}{\omega_{pe}} > 1$	$\frac{T_e}{T_i} \gtrsim 3$		$\sigma/\sigma_{cl} \sim E_D/E \quad \gamma \gtrsim 1$ T-P interaction: A.D. res. plasma modes: IA, DW, MS	$\sigma/\sigma_{cl} \sim E_D/E \quad \gamma \geq 1$ bulk: IA turbulence T-P interaction: A.D. res. plasma modes: IA, DW, MS	
	$\frac{T_e}{T_i} \lesssim 3$		$\sigma/\sigma_{cl} \sim E_D/E \quad \gamma \geq 1$ T-P interaction: A.D. res plasma modes: IC, DW, MS	$\sigma/\sigma_{cl} \sim E_D/E \quad \gamma \geq 1$ bulk: IC turbulence T-P interaction: A.D. res. plasma modes: IC, DW, MS	
			TORTUR III plateau	TORTUR III heating pulse	

TABLE 3.1: A systematic survey of turbulent plasma states.

Abbreviations: T-P interaction: tail-plasma interaction      DW : Drift waves  
A.D. resonance : Anomalous Doppler resonance      MS : Magnetic sound waves  
IA : Ion-acoustic waves      LM : Langmuir oscillations.  
IC : Ion-cyclotron waves

This condition implies that the drift velocity should exceed a certain threshold related to  $v_S$  in order to bring the plasma in a turbulent state. Such turbulence is called current-driven. The critical value of  $\gamma$ ,  $\gamma_{cr}$  depends on such parameters as  $T_e/T_i$  and  $\omega_{ce}/\omega_{pe}$ , and on the particular type of turbulence that is excited [3-9].

Provided the current is more or less stable (more precise:  $\dot{j}/j \ll \nu_{eff}$ , where  $\nu_{eff}$  is the effective collision frequency) the plasma again satisfies Ohm's law, with an enhanced resistivity  $\eta_{an}$ . The anomalous resistivity itself, although triggered by  $v_D$ , is no strong function of the drift velocity.

These findings are explained qualitatively by the marginal stability concept [6,7,10]. We sketch a simplified picture here. Let us assume that at some instant, the local drift velocity rises and exceeds a critical value: the local current drives some collective oscillation unstable, whereupon the resistivity rises sharply; then the current is cut down, the instability quenches and the process starts again. After a transition period, the plasma tends to an equilibrium for which the drift velocity just takes on its critical value. The latter depends on slowly varying plasma conditions, which tune the equilibrium in the course of many rise-quench periods. The growth and quenching of the instability then, is a repeating phenomenon which acts as an effective collision frequency. The processes inducing the current-driven instabilities are microscopic, but they lead to a macroscopic (averaged over the plasma) anomalous resistivity.

The macroscopic description of the marginally stable state says [2]:

- $v_D/v_S \sim n_e^{-1/2}$ ,
- $\eta_{eff}$  ( $\equiv m_e \nu_{eff}/n_e e^2$ ) is no strong function of the local drift velocity, nor of the electron temperature.

Much theoretical work has been done to calculate the effective resistivity from the microscopic behaviour, i.e. the growth and damping of the collective oscillations. As many types of oscillations may couple with each other and transport processes play a role, this approach is difficult to do analytically. The best way to attack the problem has turned out to be numerical simulation [6,7,11,12].

In this thesis we will not be concerned much with the microscopical processes, but will instead try to come to an understanding of the plasma in terms of macroscopical parameters, such as the current density profile and the profiles of temperature and density. In this chapter we will give some basic material on topics that will recur in Chapters 5 and 6, in which the experimental results are discussed.

### 3.3 Runaway electrons\* [13,14]

An electron in a tokamak plasma is subject to the electrical force

$$F_E = eE ,$$

exerted by the loop voltage, which tends to accelerate the electron along the magnetic field lines. This force is counteracted by the Coulomb interactions, which cause a transfer of momentum from the electron to ions and other electrons. The effect of these collisions can conveniently be written in the form of a drag force:

$$F_D = m_e v \nu(v) .$$

Here,  $v$  is the electron speed and  $\nu(v)$  is the collision frequency, which has  $v^{-3}$  dependence:

$$\nu(v) = \frac{e^4 n_e \ln \Lambda}{2\pi \epsilon_0^2 m_e^2 v^3} = 1.60 \times 10^6 \frac{n_e}{v^3} \ln \Lambda ,$$

where  $\ln \Lambda$  is the Coulomb logarithm:  $\ln \Lambda = 32.2 + \frac{1}{2} \ln(T_e^3 / Z^2 n_e)$  ( $\approx 15$  in a tokamak).

The critical speed  $v_c$  is defined as the speed at which the drag balances the electrical force  $F_E$ :

$$v_c^2 = (e^3 n_e \ln \Lambda) / (2\pi \epsilon_0^2 m_e E) = 9.14 \times 10^{-6} \frac{n_e}{E} \ln \Lambda .$$

For  $\ln \Lambda = 15$ :  $v_c = 3.7 \times 10^7 \sqrt{\frac{n_e}{10^{19}} \frac{1}{E}} .$

Clearly, electrons with velocities  $v > v_c$  will be gradually accelerated by the electric field and eventually reach a free fall state.

---

\*In this section we use the definitions given by Knoepfel and Spong [13] in their review paper on runaway electrons.

These electrons have virtually no interaction with other plasma particles and are called runaways. Interaction with collective plasma modes is possible, however, and in that way a runaway population may affect the state of the thermal plasma. This subject is discussed in Section 3.4.

Another quantity used frequently in the analysis of runaway associated phenomena is the critical field ( $E_c$ ), e.g. the field which will let a thermal electron ( $v = v_{th} = (2kT_e/m_e)^{1/2}$ ) run away:

$$E_c = 9.14 \times 10^{-6} \ln \Lambda n_e / v_{th}^2 = 2.60 \times 10^{-17} \frac{n_e}{T_e} \ln \Lambda \quad (T_e \text{ in eV}) .$$

With the substitution  $\ln \Lambda = 15$  we find the rule of thumb:

$$E_c \approx 4 \frac{n_e}{10^{19}} \frac{1}{T_e \text{ (keV)}} \quad E_c \text{ in V/m .}$$

The electron velocity distribution function is nearly isotropic for velocities  $v \ll v_c$ , but in the vicinity of  $v_c$  it is strongly deformed. The runaway tail is essentially one-dimensional. The deformation has its bearing on the soft X-ray spectrum, where, roughly speaking, a tail begins to grow at the energy  $\epsilon_c$  corresponding to the critical velocity:

$$\begin{aligned} \epsilon_c &= 2.6 \times 10^{-17} \frac{n_e}{E} \ln \Lambda \quad (\epsilon_c \text{ in eV}) \\ &\approx 4 \frac{n_e}{10^{19}} \frac{1}{E} \quad (\epsilon_c \text{ in keV}) . \end{aligned}$$

The rate of runaway production ( $\lambda$ ) has been the subject of numerous investigations, both analytical and numerical. We shall use the expression [13]:

$$\lambda = K(Z_{eff}) n_e v(v_{th}) \left( \frac{E}{E_c} \right)^\alpha \exp \left[ - \frac{E_c}{4E} - \frac{\sqrt{(Z_{eff} + 1)E_c}}{E} \right]$$

with  $\alpha = 3(Z_{eff} + 1)/16$  and  $K(Z_{eff}) \approx 0.4$  for  $Z_{eff} = 1 - 3$ .

For TORTUR III, with  $E/E_C \approx 0.03$  and  $Z_{\text{eff}} \approx 2$ , we estimate for the total number of runaways at  $t = 10$  ms

$$N_{\text{RA}} \leq 4 \times 10^{12} .$$

Runaways are born predominantly in the region of the plasma where  $E_C/E$  has its smallest value, which is generally in the plasma centre. As long as they are confined and not scattered by interaction with collective plasma oscillations, they gain speed until the velocity of light is approached. The free fall is described by:

$$\dot{p} = eE \rightarrow p(t) = p(0) + e \int_0^t E(t') dt' .$$

In Fig. 3.2  $v$ ,  $p$  and  $\epsilon$  of a free-falling electron under the influence of a constant field are depicted.

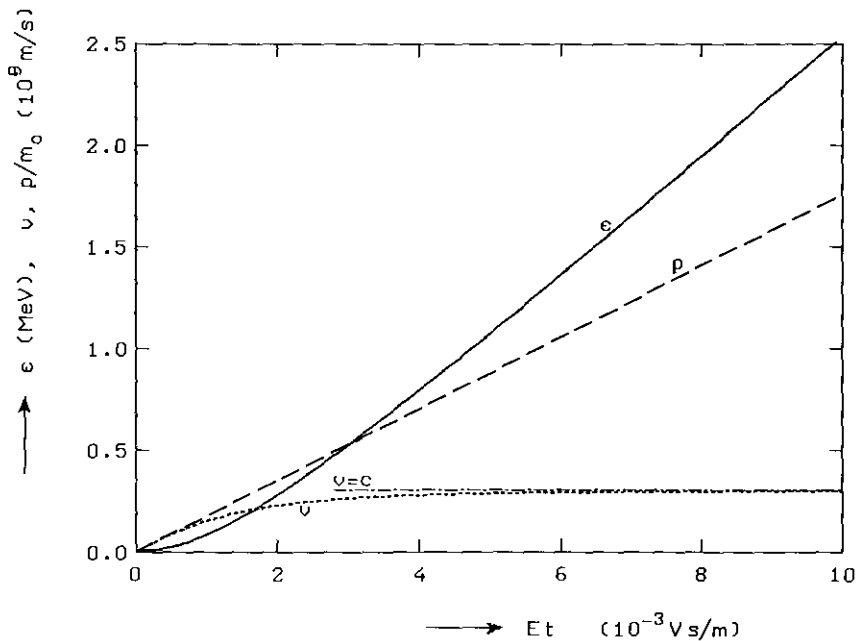


Fig. 3.2. Momentum ( $p$ ), velocity ( $v$ ) and energy ( $\epsilon$ ) of a free-falling electron in a field  $E$  as a function of  $Et$ .

A runaway population carries current, roughly approximated by

$$I_{RA} = N_{RA} \frac{ec}{2\pi R} = \frac{N_{RA}}{2\pi R} 5 \times 10^{-11} \text{ Am} ,$$

where  $N_{RA}$  is the absolute number of runaways and  $R$  is the major radius of the torus. For TORTUR III the estimated runaway current  $I_{RA} \lesssim 40$  A, which is a negligible fraction of the plasma current.

A condition for the confinement of a runaway is that the Lorentz force exerted on the electron by the poloidal magnetic field can balance the centrifugal force:

$$ev_{\parallel} B_G \geq \gamma m_0 v_{\parallel}^2 / R ,$$

with  $\gamma = (1 - v^2/c^2)^{-1/2}$ .

From this condition it follows that a runaway is lost if its velocity exceeds a critical value given by:

$$\sqrt{\gamma^2 - 1} = \frac{\mu_0 e}{2\pi m_0 c} \frac{R}{a} I_p .$$

For TORTUR III this implies that electrons with up to 10 MeV longitudinal energy may be confined.

Because of their low collisionality, runaways may be confined much longer than the confinement time of thermal electrons. Runaways that do get scattered in pitch angle may get trapped in local mirrors (field ripple) and produce strongly enhanced cyclotron radiation. Trapped runaways do not carry current, but still a considerable amount of energy can be stored in them.

### 3.4 Interaction of runaways with collective plasma oscillations [13,14,15,16,17,18,19,20,21]

The runaway electrons may be immune to Coulomb scattering, they still can interact with collective plasma modes such as ion-cyclotron waves, ion-acoustic waves, Langmuir oscillations or drift waves. The reason why the interaction exists in spite of the high electron velocity is twofold. First, the collective modes bunch ions together and thus

produce quasi-particles of much larger effective charge than a single ion. Second and most important, for oblique waves the phase velocity in the direction of the electron velocity can be indefinitely high, so as to allow resonant interaction between wave and electron. The Doppler-shifted resonance condition has the general form:

$$\vec{k} \cdot \vec{v} = \omega_k + n\omega_{ce} \quad n = 0, \pm 1, \pm 2, \dots,$$

where  $z$  is the direction of the electron velocity (see Fig. 3.3).

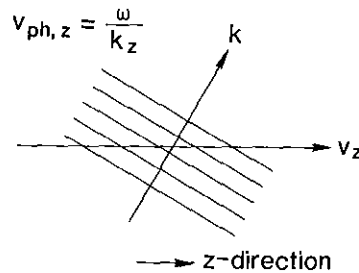


Fig. 3.3. Interaction of a wave with an electron.

For  $n=0$  the phase velocity in the  $z$ -direction equals the electron speed; the interaction is called Cerenkov resonance. In this resonance there is an exchange of energy between the electron and the wave. This leads to nonlinear growth of the wave if  $df(v)/dv > 0$ , e.g. on the positive slopes of the electron velocity distribution function. Resonance on a negative slope leads to Landau damping of the wave.

For  $n=1,2,\dots$ , the resonant interaction is called the anomalous Doppler effect. Here the transverse field of the wave force is in resonance with the cyclotron rotation of the electron. The result is that longitudinal energy of the electron is converted into transversal energy, with, for  $\omega \ll \omega_{ce}$ , only little exchange with the wave: the electron is scattered elastically in pitch angle. The resonance condition allows interaction of the precipitating electrons with low-frequency waves. This pitch-angle scattering can lead to electrons trapped in local mirrors, to enhanced cyclotron emission and to dissipative trapped electron instabilities.

For  $n=-1,-2,\dots$ , the resonance is called the normal Doppler effect. It occurs only for waves with  $\omega_k > \omega_{ce}$ , e.g. high frequency electromagnetic waves. This mode can convert transverse energy of the electron into longitudinal energy.

These types of resonance can lead to instabilities of  $f(v)$ , which are generally of a cyclic nature: a tail grows gradually until an unstable distribution is formed and nonlinear generation of plasma oscillations restores  $f(v)$ . Such instabilities are usually accompanied by voltage spikes, current steps, strongly enhanced cyclotron radiation and X-ray bursts [13,14].

One type of tail instability, described by Parail and Pogutse, is a result of an interplay between the Cerenkov resonance and the anomalous Doppler effect. They showed that a developing runaway tail goes unstable with respect to the anomalous Doppler effect if the highest velocity in the tail ( $v_b$ ) exceeds some critical value, which for Langmuir oscillations is [20,21]:

$$v_b > 3(\omega_{ce}/\omega_{pe})^{3/2} v_c \quad (v_c = \text{critical runaway velocity}) .$$

A bump in  $f(v)$  is formed which drives the  $n=0$  resonance unstable. The combined action of the two instabilities then rapidly cuts off the runaway tail.

So far we have been vague about the actual type of collective mode that is excited. The reason is that any kind of wave that can exist in the specific plasma and satisfies the resonance condition can be the vehicle of an instability. Moreover, one type of plasma wave couples with various others, which makes the actual process of a complicated nature.

Papadopoulos [14] proposed a model in which density fluctuations produce an enhanced resistivity which results, by increasing the loop voltage, in a runaway tail. The latter, in turn, excites high frequency waves that decay and produce density fluctuations. In this way a steady-state anomalous resistivity could be created. We note that in this scheme the runaway tail generates the turbulence that produces anomalous resistivity. Contrastingly, in the case of current-driven turbulence the generation of collective oscillations is due to the drift velocity of the thermal bulk.

### 3.5 Current-driven instabilities

A special class of instabilities that induces anomalous resistivity are those driven by the current itself. The main types of current-driven instabilities are the Buneman instability (two-stream instability), the ion-acoustic instability and the ion-cyclotron instability.

The Buneman instability arises when the drift velocity  $v_D = j/n_e e$  exceeds the electron thermal velocity:

$$\text{Buneman} \quad v_D > v_{th,e} ,$$

i.e., when the velocity distributions of the ions and the electrons are separated in velocity space. The instability develops within  $10 \omega_{pe}^{-1}$  and cuts down the current, thereby heating predominantly the electrons. Thus  $v_{th,e}$  is increased and the Buneman mode is stabilized. The threshold condition implies that very high current densities are required for the Buneman instability. In TORTUR III, for instance, the streaming parameter  $v_D/v_{th,e} \leq 0.03$ .

The ion-acoustic instability can grow at lower values of  $v_D$ , when  $v_D$  exceeds the ion-sound velocity  $v_S$ , but it depends critically on the ratio  $T_e/T_i$ :

$$\text{Ion acoustic} \quad v_D > v_S , \quad T_e/T_i \geq 3 \quad [16,22] .$$

For  $T_i \approx T_e$ ,  $v_S$  is too close to the thermal-ion velocity, which causes heavy ion Landau damping. In a plasma with  $T_i \approx T_e$ , the condition on the drift velocity becomes  $v_D > v_{th,e}$ , in which case we have entered the domain of the Buneman instability. The actual critical drift velocity is a function of  $T_e/T_i$  (see Fig. 3.4).

The ion-cyclotron instability is not Landau-damped and therefore can occur in a plasma even when  $T_e/T_i \approx 1$ . The condition on the drift velocity reads:

$$\begin{aligned} \text{Ion cyclotron} \quad v_d > u_{cr} &= 15 (T_i/T_e)^{3/2} \sqrt{m_e/m_i} v_{th,e} , \\ &\approx 20 (T_i/T_e)^{3/2} v_S \quad [3,16] . \end{aligned}$$

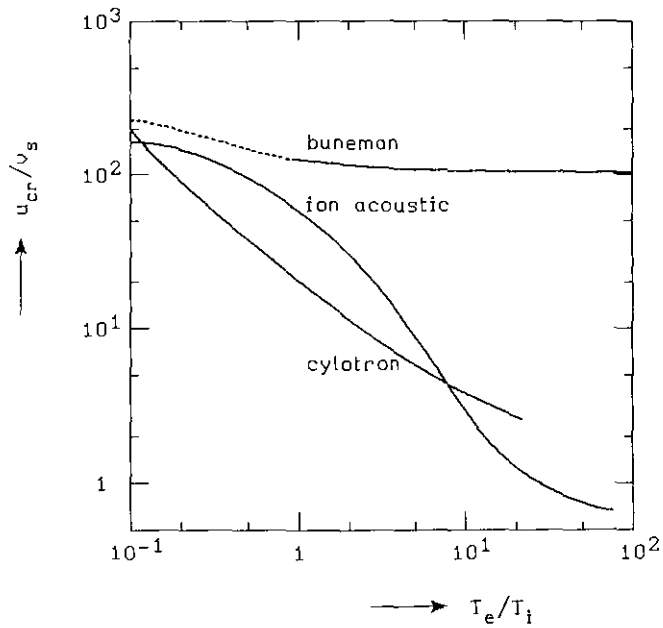


Fig. 3.4. The critical drift velocity for current-driven modes in a hydrogen plasma, as a function of  $T_e/T_i$ . (Adapted from J.M. Kindel and C.F. Kennel [3].)

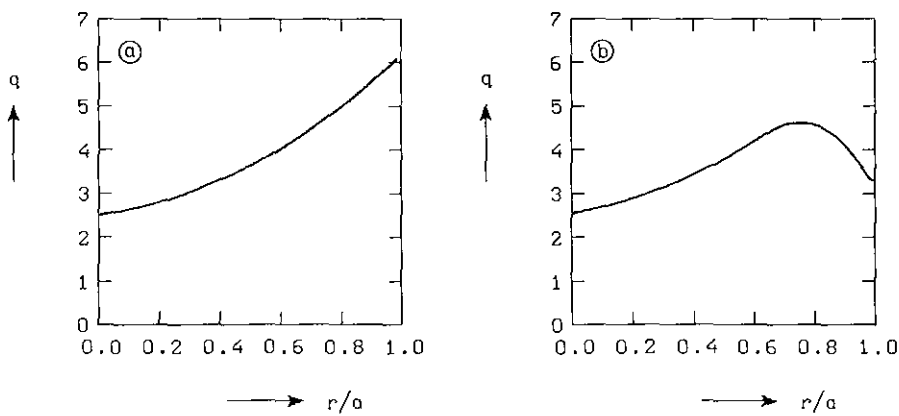


Fig. 3.5a,b. Sketch of the  $q$ -profile before (a) and during (b) the application of the current pulse.

As is seen in Fig. 3.4, in the TORTUR III discharge the ion-cyclotron instability should be the one most easily triggered [3]. The mean drift velocity is subcritical even for this mode. If we take  $q \geq 2$  in the centre, we find  $v_D \lesssim 10^6$  m/s, whereas  $u_{cr} \approx 1.8 \times 10^6$  m/s (with  $T_i/T_e \approx 0.5$ ). However, according to the marginal stability concept, a current-driven mode can be triggered due to local and temporal variations of  $v_D$  even if the mean drift velocity is below the critical value.

Summarizing, we must state that theory is not very clear about the type of turbulence that should be present in the TORTUR III plasma. Possibly, modes other than current-driven play an important role. We mention gradient-driven modes (drift waves) or trapped electron instabilities. The effects of such instabilities on the plasma resistivity are difficult to evaluate.

### 3.6 Stability against resistive tearing modes

In the turbulent heating experiment in TORTUR III, a current spike of 30 kA is induced on top of the running current. The duration of the current pulse is 20  $\mu$ s. At first, the current does not spread over the entire cross-section of the column but runs in a skin of 2.5 cm width (the skin time is reduced by turbulence-induced resistivity in the skin [6,7]). This skin current misshapes the hollow q-profile.

In the normal TORTUR III discharge the q-profile has a form as sketched in Fig. 3.5a. We do not know its shape exactly, because we lack information on the actual current density profile. The skin current results in a double-valued q-profile, of a form depicted in Fig. 3.5b. As was shown by Kolfschoten [25] this hollow current density profile can be a MHD equilibrium situation. Such a q-profile is unstable against the growth of resistive tearing modes, which tend to connect the neighbouring rational q-surfaces. Thereby, magnetic islands are formed in the plasma boundary. These modes can grow within 5  $\mu$ s [6,7,23,24]. These modes and possibly other mechanisms are assumed responsible for the rapid spread of the current skin over the plasma cross-section that was measured by Kalfsbeek [6,7] in a forerunner of TORTUR III (see Fig. 3.6). This process is referred to as 'skin implosion'. The poloidal field due to the extra current exerts a magnetic pressure that is but a small fraction of the pressure of the toroidal field. Hence, the toroidal field cannot be pinched and the skin implosion has to produce breakage of magnetic field lines.

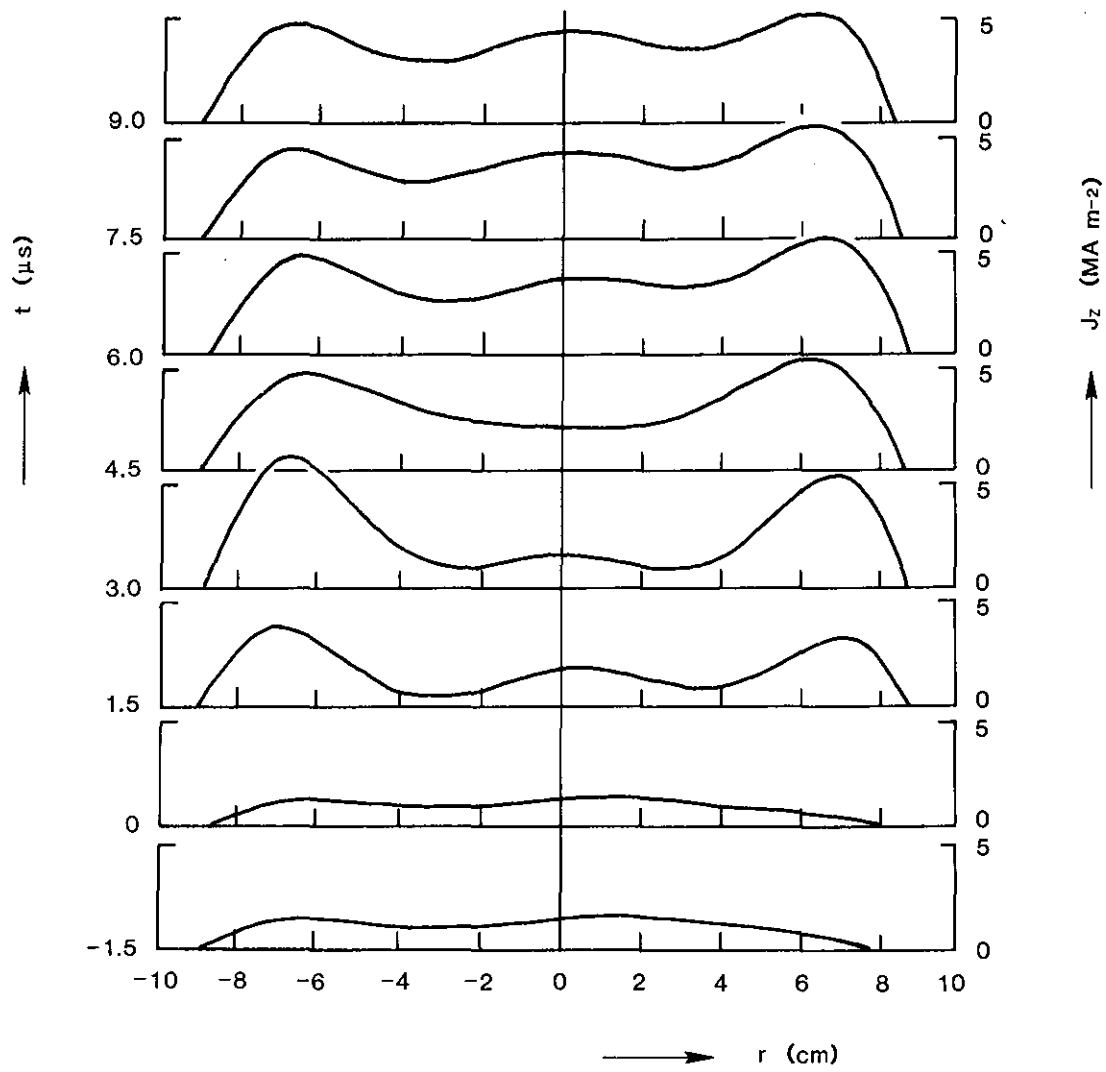


Fig. 3.6. The implosion of the current skin as measured in TORTUR III by Kalfsbeek [6].

References

- [1] H. de Kluiver et al., to be published.
- [2] H. de Kluiver, "Current-driven turbulence in plasmas", Rijnhuizen Report 77-106 (1977).
- [3] J.M. Kindel and C.F. Kennel, J. Geophys. Res. 76 (1971) 3055.
- [4] L.I. Grigor'eva et al., Sov. Phys.-JETP 33 (1971) 329.
- [5] G. Benford, J. Plasma Phys. 15 (1976) 431.
- [6] H.W. Kalfsbeek, "Numerical calculations on the anomalous current penetration in a toroidal hydrogen plasma", Part of Thesis University of Utrecht, 1979, Rijnhuizen Report 78-113 (1978).
- [7] H.W. Kalfsbeek, "Magnetic field profiles during turbulent heating in a toroidal hydrogen plasma", Part of Thesis University of Utrecht, 1979, Rijnhuizen Report 78-114 (1978).
- [8] D.R. Dakin et al., J. Plasma Phys. 15 (1976) 175.
- [9] A.S. Sakharov and S. Kuhn, Phys. Fluids 26 (1983) 3482.
- [10] W. Manheimer and J.P. Boris, Comments Plasma Phys. and Controlled Fusion 3 (1977) 15.
- [11] M.Z. Caponi and R.C. Davidson, Phys. Fluids 17 (1974) 1394.
- [12] M.Z. Caponi and R.C. Davidson, Phys. Rev. Lett. 31 (1973) 86.
- [13] H. Knoepfel and D.A. Spong, Nucl. Fusion 19 (1979) 785.
- [14] K. Papadopoulos, Rev. Geophys. and Space Phys. 15 (1977) 113.
- [15] B.B. Kadomtsev and O.P. Pogutse, Sov. Phys.-JETP 26 (1968) 1146.
- [16] B.B. Kadomtsev, "Plasma turbulence", Academic Press, New York (1965).
- [17] K. Papadopoulos et al., Nucl. Fusion 17 (1977) 1087.
- [18] Y. Mok, Thesis University of Maryland, 1979.
- [19] B. Coppi et al., Nucl. Fusion 16 (1976) 309.
- [20] V.V. Parail and O.P. Pogutse, Sov. J. Plasma Phys. 2 (1976) 125.
- [21] V.V. Parail and O.P. Pogutse, Nucl. Fusion 18 (1978) 303.
- [22] T.H. Stix, "The theory of plasma waves", McGraw Hill, New York, Advanced Physics Monographs, 1962.
- [23] G. Bateman, "MHD instabilities", MIT Press, Cambridge, Mass., 1980.
- [24] H.P. Furth et al., Phys. Fluids 16 (1973) 1054.
- [25] A.W. Kolfshoten, "Equilibrium studies of skin-like pressure and current-density profiles", part of Thesis University of Utrecht, 1982, Rijnhuizen Report 81-134 (1981).



## C H A P T E R 4

### EXPERIMENTAL RESULTS

#### 4.1 Introduction

In this chapter the results of recent experiments on the turbulent heating of the TORTUR III plasma are presented. A limited amount of analysis is offered, and only straightforward conclusions are drawn. More involved arguments and an attempt to synthesize a consistent physical picture are left for Chapters 5 and 6.

The experiments all follow basically the same plan. First, a mildly turbulent plasma is created which is quasi-stationary during more than 20 ms. We call this plasma the basic plasma. Then, a current spike is induced on top of the plateau current. A study is made of the heating effect of a power injection of this type.

Actually, the formation of the basic, mildly turbulent plasma is an experiment on plasma turbulence in itself. The plasma is rapidly formed by the steeply rising (30 kA/ms) predischage current. After this initial highly turbulent phase the plasma can be kept alive in one of two distinct quasi-stationary regimes. One we call the classical tokamak regime, the other is called mildly turbulent. The tokamak regime is characterized by a loop voltage of 2 V at a plasma current of 20 kA, a central electron temperature of 500 eV and quite narrow temperature and density profiles:  $\text{FWHM}(T_e) = 7$  cm. This state is reached if we let the plasma current decay after the predischage current maximum of 45 kA to  $I_p < 25$  kA before we start the supply of current with the second capacitor bank. This regime is not the subject of the present study, but it will be referred to occasionally.

The mildly turbulent state is reached if we clamp the current directly after the predischage, at a level of 30 to 40 kA. In this regime the central electron temperature is typically 800 eV and the ion temperature 400 eV. The loop voltage is anomalously high: 5 V, which means  $E/E_c \approx 0.03$ . Both the temperature and the density profiles are broader in this case:  $\text{FWHM}(T_e) = 10$  cm.

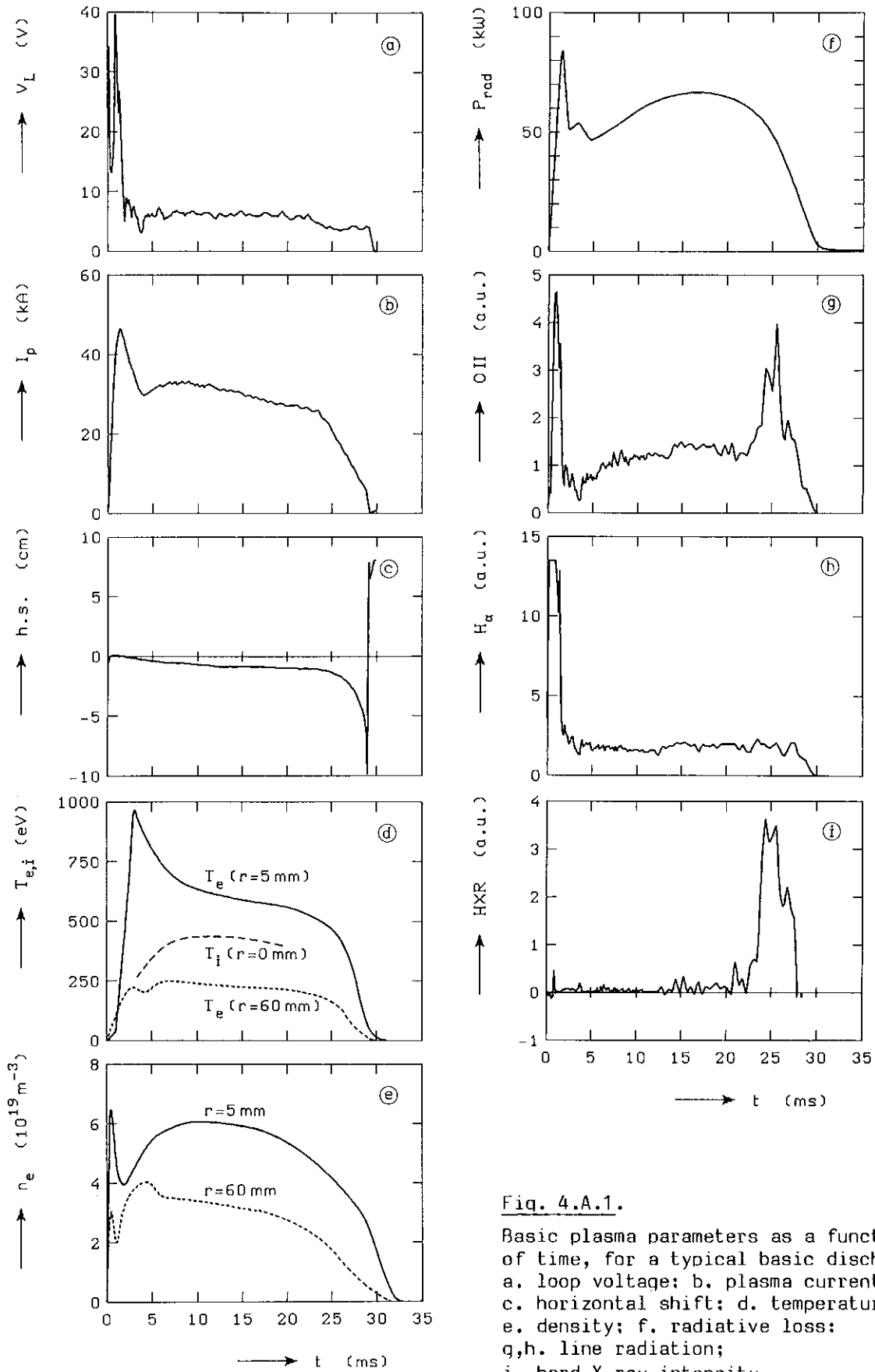


Fig. 4.A.1.

Basic plasma parameters as a function of time, for a typical basic discharge:  
 a. loop voltage; b. plasma current;  
 c. horizontal shift; d. temperature;  
 e. density; f. radiative loss;  
 g,h. line radiation;  
 i. hard X-ray intensity.

On the Thomson-scattering signal deviations from the gaussian are observed that are indicative of bunches of electrons moving at  $v = 6 \times 10^6$  m/s. Thus our basic plasma raises many questions such as why are the profiles so broad and what mechanism produces the enhanced resistivity? Results of experiments dedicated to the solution of such questions are found in part A of this chapter.

The superposition of the current pulse on the plateau current is really quite another experiment. In this case  $E/E_C \approx 5$ , and we may expect strong deformations of the electron velocity distribution. After an initial 50  $\mu$ s of turmoil in which the centre is heated and cooled again, the plasma seems to resume its basic condition. Then we see a transient effect, the rise and decline of which take 5 ms. The most striking features are the retarded heating of the ions and electrons, the temporal absence of the hard and the very soft X-ray flux, and the marked increase of the low frequency density fluctuations in the plasma edge. Measurements of the effects of the heating pulse are presented in part B of this chapter.

As is seen in Chapter 3, collective oscillations that are present in the mildly turbulent plasma can interact with the electrons, both thermal and runaway. Some information about the oscillations is obtained from the Thomson-scattering signal and from density fluctuation measurements in the edge plasma. Information about the electron velocity distribution function is obtained from Thomson scattering, ECE and X-ray measurements. As to X-rays, our special attention has been directed to the development of the runaway tail, the population of the superthermal region, the lull in the X-ray emission directly after the current pulse, and to the evolution of the X-ray spectrum in the 4 ms following the pulse.

#### 4.A.1. Basic discharge, general results [1,2,3]

In Fig. 4.A.1, measurements of the basic plasma parameters  $I_p$ ,  $V_{loop}$ ,  $T_e$ ,  $T_i$ ,  $n_e$  and the horizontal displacement are shown, together with a set of monitor signals: radiative power losses and hard X-rays. We notice that the electrons are heated rapidly within the first three milliseconds of the discharge. The ions are not yet heated in this phase. Both the line intensities and the total radiative power loss  $P_{rad}$  exhibit an initial peak where the plasma burns through the radiation barrier. The density is high almost from the very beginning of the discharge.

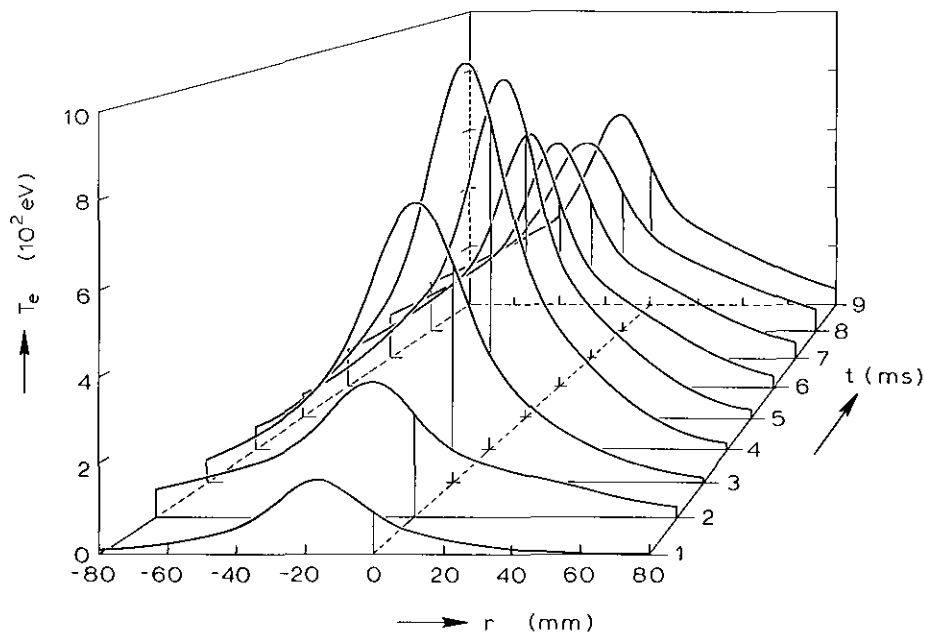


Fig. 4.A.2. The evolution of the  $T_e$ -profile, as measured by ECE.

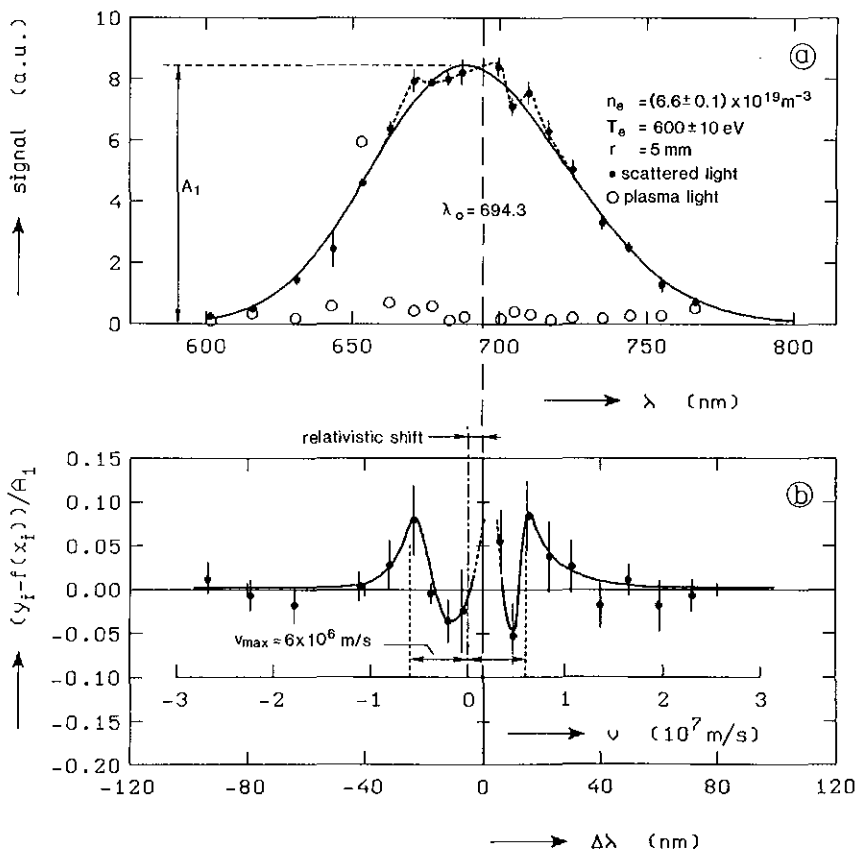


Fig. 4.A.3ab. The Thomson-scattering spectrum (a) and the deviations from the gaussian (b).

The loop voltage and the plasma current are stationary from 5 to 25 ms, in which the total power input P is 150 to 175 kW. Of this power 50 to 70 kW is lost due to radiation, most of which is line radiation and recombination radiation. The remaining 100 kW is lost to the limiters by heat and particle transport. A rough calculation yields for the heat diffusion coefficient  $D_H = 1.0$  to  $1.5 \text{ m}^2/\text{s}$ , which is a perfectly normal tokamak value. In the plateau about

$$W_p = 3/2 (n_e T_e + n_i T_i) \times e \times \text{plasma volume} = 300 \text{ J} \quad (T_{e,i} \text{ in eV})$$

is present in the thermal motion of the particles. The magnetic field energy is  $2.5 \times 10^5 \text{ J}$ . For the energy confinement time  $\tau_\epsilon = W_p/P$ , we find  $\tau_\epsilon = 1.5 - 2 \text{ ms}$  as a mean value.

We compare this value to the outcome of some scaling laws:

$$\text{TFTR [4]:} \quad \tau_\epsilon = 7 \times 10^{-22} a R^2 \bar{n}_e q(a) = 2.0 \text{ ms} ,$$

$$\text{TFR:} \quad \tau_\epsilon = 4.9 \times 10^{-21} a^2 R \bar{n}_e \sqrt{q(a)}$$

$$= 1.1 \text{ ms} ,$$

and we find that our experimental value is nothing exceptional.

The hard X-ray monitor shows a spiky activity in the first milliseconds, followed by a period of rest. Then, a runaway tail develops gradually, until an intense burst marks the end of the discharge. Typically  $\ll 1$  mrem per shot were detected in the direct vicinity of the limiter.

Figure 4.A.2 shows the development of the radial  $T_e$ -profile, as measured by ECE spectrometry [5]. The typical profile is bell-shaped like a gaussian, but the central part is peaked more sharply, whereas the flanks are relatively flat. The plasma has a hot core with a radius of 3 to 4 cm, surrounded by a broad (4 to 5 cm) layer of 100 to 300 eV.

In Fig. 4.A.3a, a Thomson-scattering spectrum is shown. The deviations from the gaussian, shown in detail in Fig. 4.A.3b are systematical. Their position corresponds to a velocity, perpendicular to the magnetic field lines, of  $\pm 6 \times 10^6 \text{ ms}^{-1}$ .

#### 4.A.2 Basic discharge, thermal X-ray emission

A detailed soft X-ray spectrum was obtained with the Si(Li) detector (see Fig. 4.A.4). The spectrum was taken in the interval 2-10 ms, i.e. after the initial hard X-ray burst and before the runaway tail has developed so far that it spoils the spectrum. It is a compilation of 50 shots. The count rate was taken 10 to 20 kHz. The spectrum has been corrected for the attenuation in absorbers that were placed between detector and plasma: 65.5 micron beryllium, 1.9 cm air, 2 micron Makrofol, and on the detector: 0.1 micron silicon (dead layer) and 100 Å gold. The transmittance of the detector (3.0 mm Si) which results in a decreasing detection efficiency towards higher energies was also brought into account. The energy scale was calibrated at 5.9 keV and 32.2 keV. The resolution of the detector is 280 eV at 5.9 keV.

In this spectrum the flux in the energy region 1-2 keV is dominant. The slope of this part of the spectrum corresponds to  $T_e = 150$  eV. For energies lower than 1 keV the attenuation in the foils is too big for a sensible reconstruction of the spectrum.

In the range 2-4 keV the spectrum is typical of thermal emission of a plasma with  $T_e = 670$  eV, which corresponds to the central electron temperature. This flux is recognized unambiguously as the continuum emission of the hot plasma core. On top of this continuum a distinct hump is found. Figure 4.A.5 shows this hump on a linear scale, where the thermal continuum has been subtracted from the signal. In Table 4.A.1 the relevant lines of compounds of stainless steel 305 (the limiter material) are listed.

TABLE 4.1

Lines of compounds of stainless steel  
in the energy range 2-3 keV [6,7]

P	K-lines	2.0 - 2.3 keV
S	K-lines	2.3 - 2.6 keV
Cl	K-lines	2.6 - 3.0 keV
Nb	L-lines	2.3 - 2.6 keV

Small amounts of sulphur and phosphorus are found in stainless steel 305: maximally 0.030% and 0.045%, respectively. Chlorine is often found in tokamaks as a result of the chemical cleaning of the vacuum chamber. Traces of niobium (or molybdenum in other types) are added to

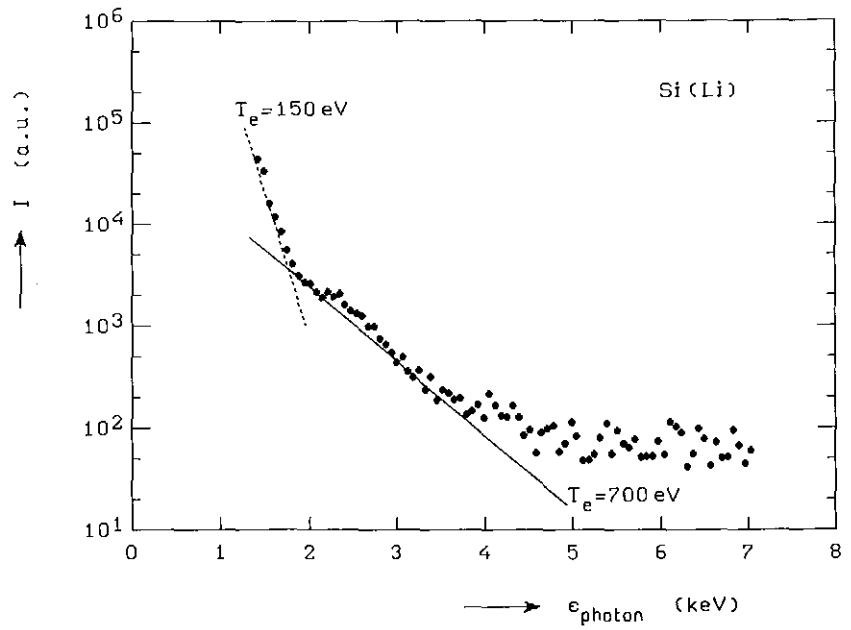


Fig. 4.A.4. Soft X-ray spectrum of the basic plasma, taken with the Si(Li) detector.

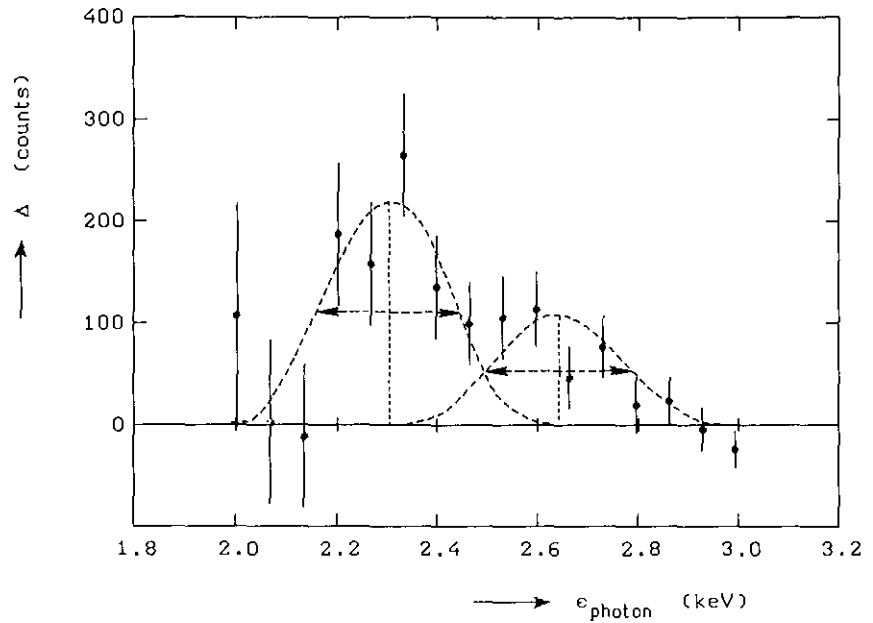


Fig. 4.A.5. Detail of the hump on the spectrum between  $\epsilon = 2 \text{ keV}$  and  $\epsilon = 3 \text{ keV}$ . Two lines are indicated tentatively.

the stainless steel to improve the brazing quality. The energy of the lines depends on the degree of ionization of the impurity. Correspondingly in Table 4.1 energy ranges rather than specific lines are listed. We cannot distinguish sharply particular lines, but in chlorine and niobium we have good candidates to account for the observed line radiation. From the observed line intensity we estimate  $n_{Cl} < 10^{-4} n_e$  [6].

For energies exceeding 4 keV, the spectrum shows a tail due to a non-thermal electron population.

Results obtained with the four-channel analyser PLATO are presented in Fig. 4.A.6. The signals of two channeltrons (ch 1 and ch 2) and two surface-barrier diodes (ch 3 and ch 4) of three plasma shots are shown. In these shots the plasma conditions were unaltered but the foil setting differed:

- In shot A (first column), the vacuum valve between torus and detector was closed, so that only hard X-rays could penetrate PLATO.

The signals show hard X-ray activity in the final stage of the discharge. This burst shows little reproducibility, hence subtracting a zero shot will not clean the soft X-ray signals from this effect. This means that, in the absence of a more sophisticated correction, the soft X-ray signals are interpretable only where they exceed the hard X-ray contribution by far.

Furthermore, some  $dI/dt$  pick-up is present on the SBD-signals. This occurs in the period that the soft X-ray flux is still low according to the undisturbed channeltron signals.

- In shot B a pair of equal foils were placed before both channeltrons, and another matched pair before the surface-barrier diodes. Thus mutual calibration of the detectors of one type was performed. The sensitivity of the surface-barrier diodes differed about 10%, for the channeltrons the difference was about 60%. The following foils were used:

ch 1 CEM	47 $\mu$ Be + 8 $\mu$ Makrofol	FT = 1% at $\epsilon$ = 1.12 keV
ch 2 CEM	48 $\mu$ Be + 8 $\mu$ Makrofol	FT = 1% at $\epsilon$ = 1.12 keV
ch 3 SBD	31 $\mu$ Be + 8 $\mu$ Makrofol	FT = 1% at $\epsilon$ = 1.05 keV
ch 4 SBD	31 $\mu$ Be + 8 $\mu$ Makrofol	FT = 1% at $\epsilon$ = 1.05 keV.

(FT = foil transmission, for the surface-barrier diodes also the dead layer and the gold contact layer act as absorbers).

- In shot C, the foil setting was such that the foil method could be applied to infer  $T_e$ :

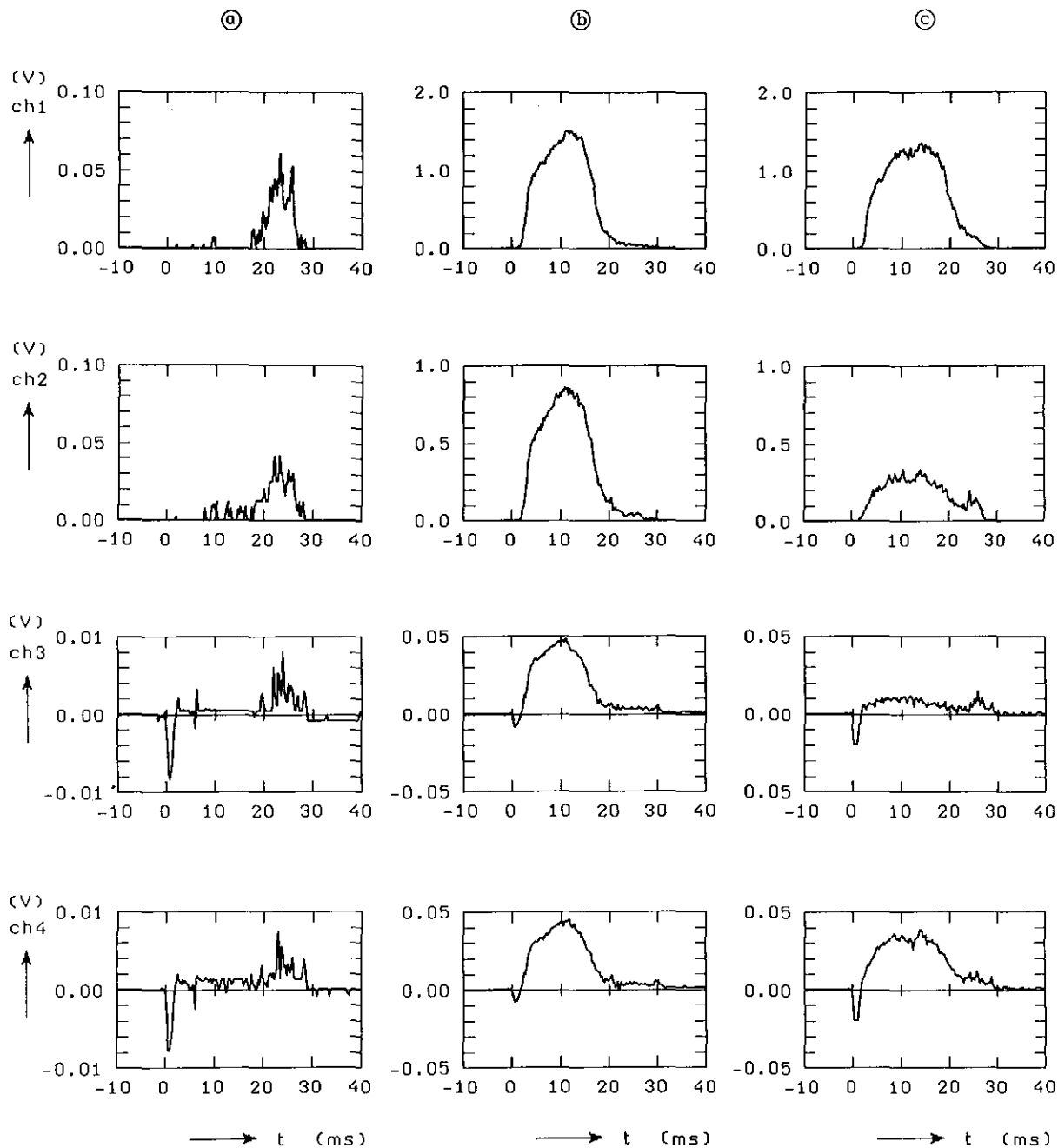


Fig. 4.A.6. Soft X-ray intensities as measured with PLATO.  
(a) zero shot (valve between plasma and detector closed).  
(b) and (c) two shots with different foil combinations.  
(See text page 52).

ch 1 CEM	47 $\mu$ Be + 8 $\mu$ Makrofol	FT = 1% at $\epsilon = 1.12$ keV
ch 2 CEM	94 $\mu$ Be + 8 $\mu$ Makrofol	FT = 1% at $\epsilon = 1.32$ keV
ch 3 SBD	82 $\mu$ Be + 8 $\mu$ Makrofol	FT = 1% at $\epsilon = 1.28$ keV
ch 4 SBD	31 $\mu$ Be + 8 $\mu$ Makrofol.	FT = 1% at $\epsilon = 1.05$ keV.

The signals in column B and C underwent some corrections that are briefly mentioned here: the channeltron output was corrected for the nonlinearity in the response due to saturation at count rates higher than 500 kHz (output 0.5 V). A saturation model was used to calculate the time- and intensity-dependent correction (see App. A). The SBD-signals were corrected for base line drift due to an AC-coupling with a time constant of 200 ms.

A note on absolute intensities: in the determination of  $T_e$  by means of the foil method, the absolute intensity plays no role. It does give, however, information on  $Z_{\text{eff}}$ . We can compute the signals we may expect, adopting laser-scattering values for the electron temperature and density profiles, and assuming, for instance, an oxygen contamination of 1% ( $Z_{\text{eff}} \approx 1.5$ ) throughout the plasma. We then find the following values:

CEM-output	calculated 50 to 300 kHz	measured value .1 MHz;
SBD-output	calculated 5 mV	measured value 30 mV.

The uncertainty in the calculated CEM-output stems from uncertainty in the calibration of CEM's: the quantum efficiency was found to have deteriorated by a factor 10 during the experimental period.

We see that the fluxes are strongly enhanced over the flux of a normal, moderately polluted 700 eV tokamak plasma. This fact is in accordance with the Si(Li) measurements, where the main soft X-ray intensity was found to come from a cool part of the plasma and not from the hot core. This  $\epsilon < 2$  keV flux is strongly enhanced by some mechanism. A discussion of this enhancement is presented in Sect. 5.2. We can deduce an apparent  $T_e$ -value from the measurements by means of the foil method. The result is shown in Fig. 4.A.7. In Fig. 4.A.8 the product of the spectral intensity and the foil transmission is depicted for typical foils used and the spectrum as measured with the Si(Li) detector. Evidently it is the  $\epsilon < 2$  keV flux that mainly determines the intensities and, therefore, the inferred temperatures. We are not surprised then, to find temperature values in the range 200 to 300 eV, namely somewhere between 150 eV and the core temperature. Note that the three independent measurements of  $T_e$  are in fair agreement with each other.

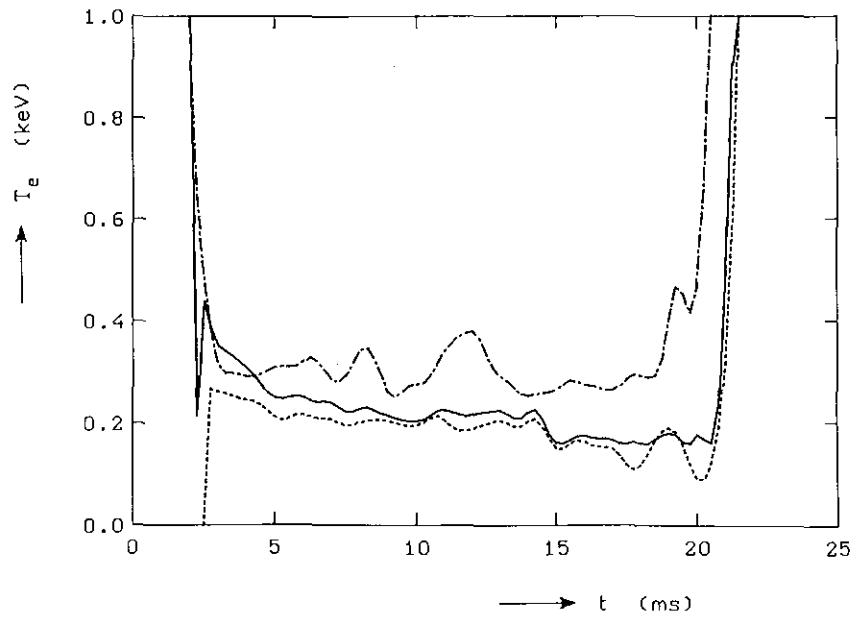


Fig. 4.A.7. The electron temperature  $T_e$  as a function of time as measured with the foil method. The three curves are independent measurements with different detector combinations:  $\cdots$  = CEM/CEM;  $----$  = SBD/SBD;  $—$  = CEM/SBD (hybrid).

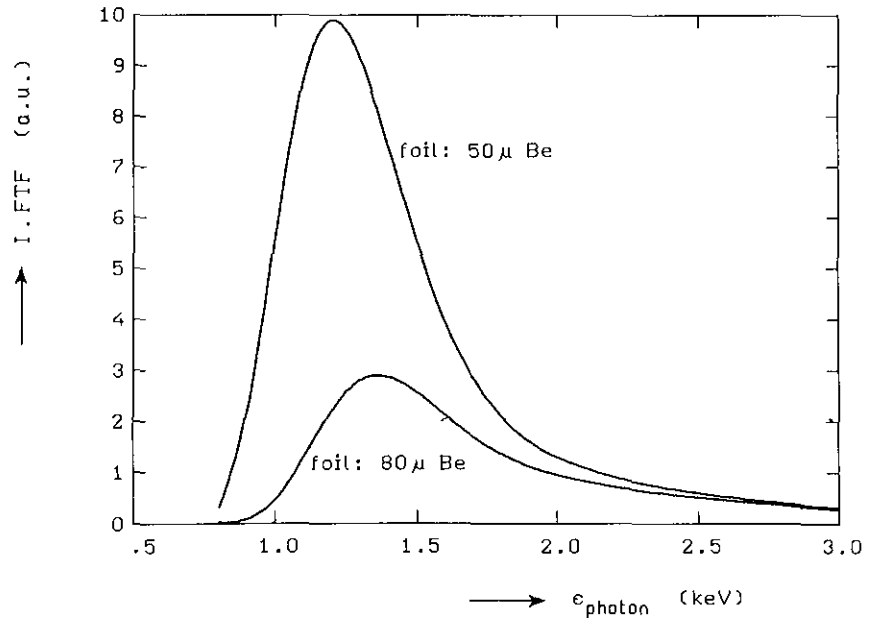


Fig. 4.A.8. The output of a surface-barrier diode is proportional to  $\int FI \cdot DE \cdot I(\epsilon) d\epsilon$ , where  $FI$  is the foil transmission and  $DE$  is the detection efficiency. The figure shows the integrand for the typical spectrum (see Fig. 4.A.4) and foils used in the experiment.

We summarize the most important features of the soft X-ray measurements in the basic discharge:

- the dominant flux is emitted in the region  $\epsilon < 2$  keV,
- this flux is apparently a continuum radiation from a  $T_e = 150$  eV plasma,
- this flux begins to grow at 2 ms, then rises rapidly until 5 ms, when the growth suddenly subsides and the intensity more or less stabilizes,
- in the energy range 2 to 4 keV continuum radiation of the hot plasma core is dominant,
- line emission is found at 2.3 to 2.7 keV, probably due to niobium (L-lines) and chlorine (K-lines).

#### 4.A.3 Basic discharge, non-thermal X-ray emission

Measurements in the energy range 2-30 keV were obtained with the Si(Li) detector. In order to get reasonable count rates in the energy region of interest, the intense low energy radiation was filtered out with Al- and Be-foils, with a cut-off at  $\epsilon = 3$  keV. The spectrum shown in Fig. 4.A.9 is collected in 12 shots. The pulse-height analyser was gated in the intervals 4-8 ms and 6-10 ms, in six shots each. In the figure the thermal continuum is indicated by a line. Due to the poor statistics this spectrum has little detail. Its purpose is merely to show how the non-thermal part of the spectrum fits to the thermal part. The little plateau near  $\epsilon = 6$  keV occurs systematically. This feature is discussed in Section 5.4.

Figure 4.A.10 shows two hard X-ray spectra taken with the NaI detector, in the intervals 2-4.5 and 4.5-7 ms. They are corrected for the distortion due to the Compton effect in the crystal. The dip at 40 keV is an artefact due to a diaphragm used: a stainless steel plate of 1 mm thickness, containing an aperture. As 1 mm of stainless steel has a cut-off at 40 keV, the field of view of the detector is much larger for photons of higher energy than for the softer ones. This effect causes the observed dip. In the figure the function  $Tr(\epsilon) = 1 + A \times TM$  (with  $TM =$  transmission 1 mm Fe) is shown, for  $A = 5$ . The constant  $A$  denotes the ratio of the area of the steel plate seen by the detector to the area of the aperture.  $A$  is not well-known, hence we cannot perform an accurate correction.

The general conclusion is that a runaway tail grows with time and reaches energies exceeding 750 keV.

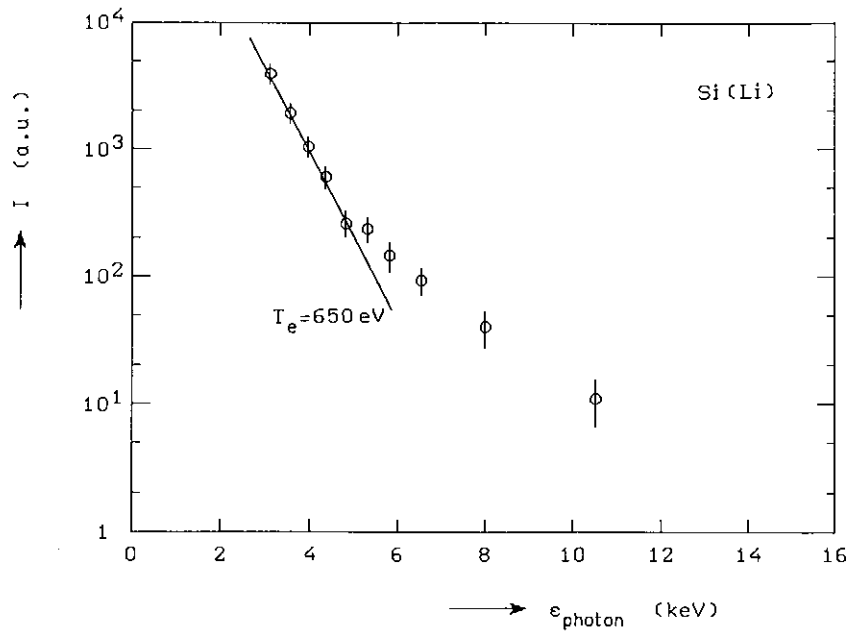


Fig. 4.A.9. Soft X-ray spectrum of the basic plasma, taken with the Si(Li) detector; low energy part filtered out.

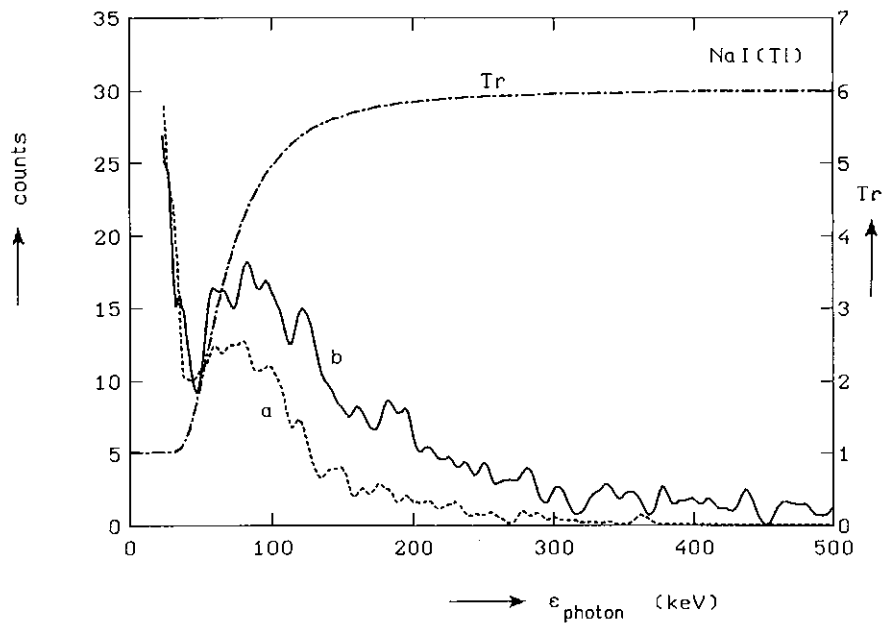


Fig. 4.A.10. Hard X-ray spectra of the basic plasma, taken with the NaI(Tl) detector in the sample intervals: a. 2 - 4.5 ms and b. 4.5 - 7 ms. Tr = transmission stainless steel plate with diaphragm (see text p. 56).

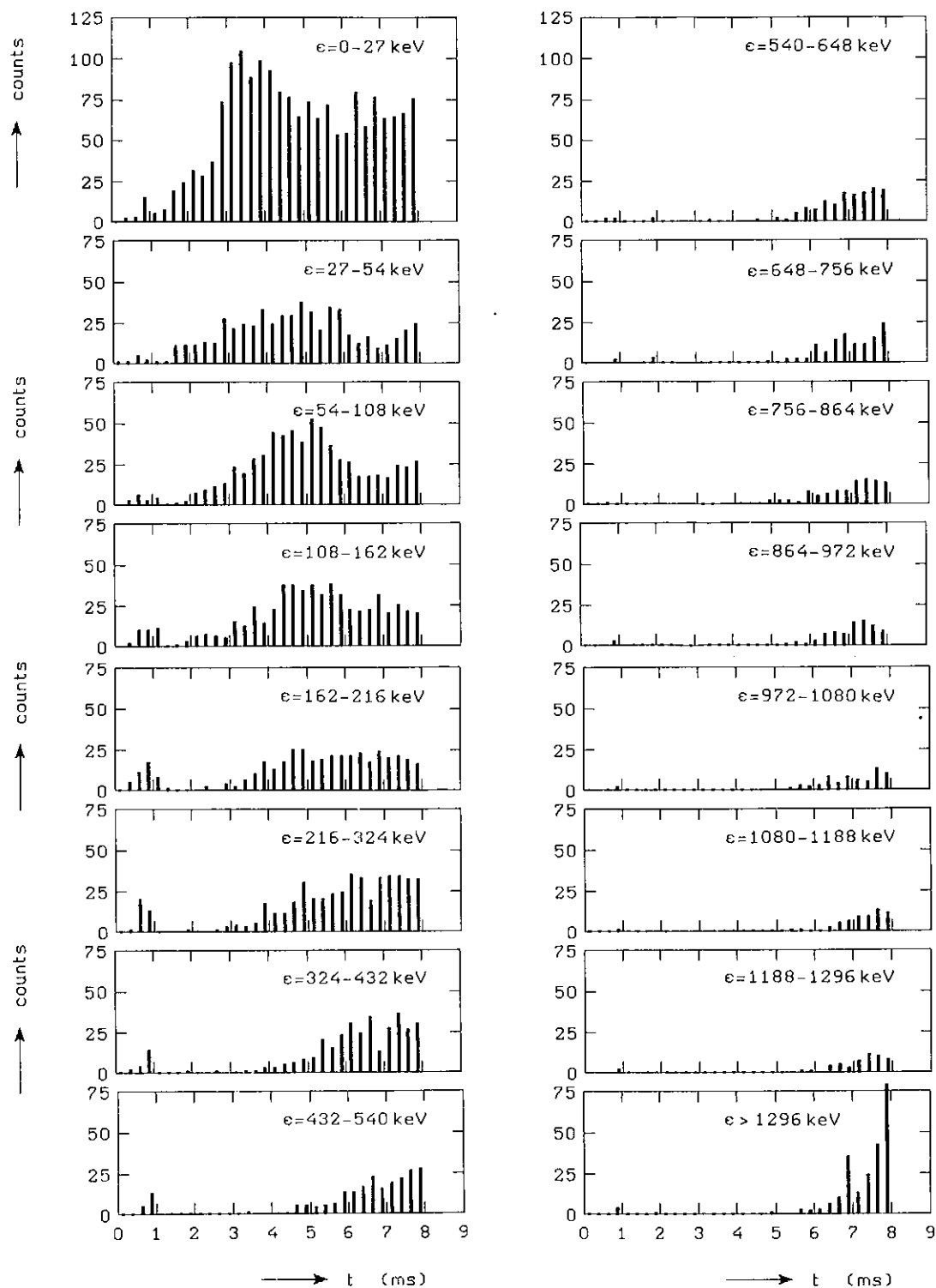


Fig. 4.A.11a. The evolution of the intensity in a series of spectral intervals (NaI(Tl) detector).

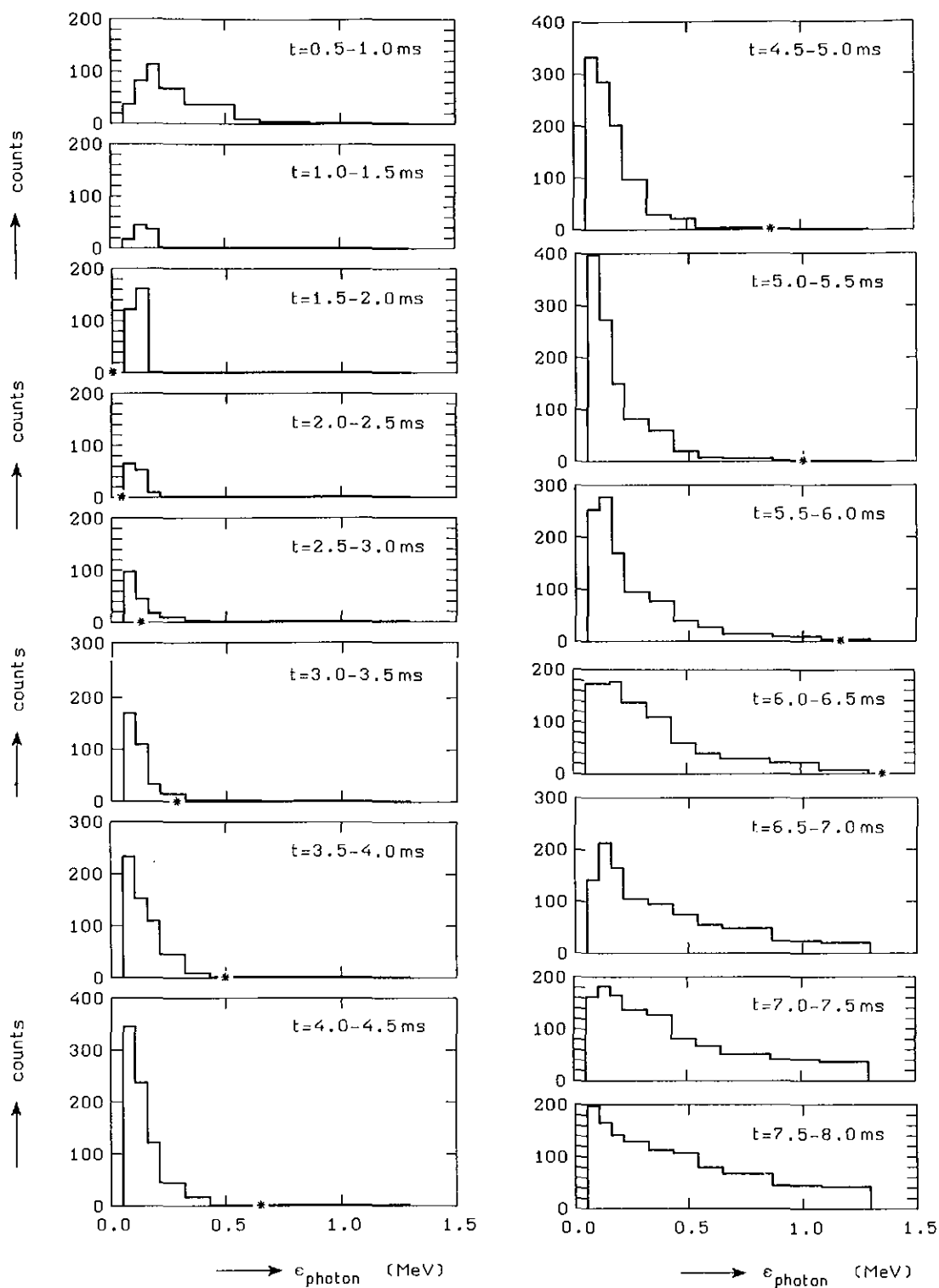


Fig. 4.A.11b. The evolution of the hard X-ray spectrum (NaI(Tl) detector).  
\*: the energy of an electron that started a free fall at  $t = 1.5$  ms.  
The measuring range extends to 1.3 MeV.

More detailed information on the development of the tail is shown in Figs. 4.A.11a,b. In this experiment the signal from the NaI detector was stored in a 32 kbyte ADC, with a time resolution of 0.25  $\mu$ s. In this way, the individual pulses could be plotted for an interval of 8 ms per shot. The energy range was divided into sections of about 100 keV, and the pulses in each section were counted. Thus, from 9 shots, a crude spectrum was obtained with a time resolution of 0.5 ms. Here, spectral resolution has been sacrificed in the favour of time resolution. In Fig. 4.A.11b also the energy of a free falling electron is plotted as a function of time.

#### 4.B.1 Heating pulse, general results

Measurements of a number of plasma parameters are shown in Figs. 4.B.1a,b,c, on three different timescales. The first set, Fig. 4.B.1a, gives an impression of the heating pulse and its effects on a long timescale, so that a direct comparison with the basic discharge is possible.

More detailed information is conveyed by the set 4.B.1b. We see that the intensity  $S(k)$  of the low frequency (0 to 200 kHz) density fluctuations rises within 0.7 ms to a strongly enhanced value, whereafter it falls back to the initial value in 2 to 4 ms. We must remark that the rise might actually be faster than is shown in the figure; in the 0.5 ms following the pulse, measurements were hampered by a high noise level [9]. The central electron temperature, as measured by Thomson scattering and ECE rises steadily and reaches its maximum after 2 ms. The subsequent decay is characterized by a time constant  $\tau = 1.7$  ms, which is the energy confinement time, clearly. The central ion temperature shows roughly the same behaviour.

The electron temperature at  $r = 60$  mm shows a distinct dip, reflective of a sharpening of the peaked  $T_e$ -profile. This dip develops within 50  $\mu$ s after the heating pulse. On the same timescale, strong variations of  $n_e$  are observed (Thomson-scattering data), but the density recovers its normal value in about 0.5 ms.

On a  $\mu$ s timescale (Fig. 4.B.1c), a very fast heating effect is found in the plasma centre. It is accompanied by a density increase. Simultaneously cooling and rarefaction are observed at  $r = 60$  mm.

Sometimes Thomson-scattering spectra indicate a  $T_e \approx 3$  keV population at  $r = 60$  mm. Also ECE shows the existence of an  $\epsilon = 5$  to 10 keV population in the first 100  $\mu$ s after the pulse (100  $\mu$ s = ECE time resolution). These are all observations of fast transient effects: at  $t = 50$   $\mu$ s  $T_e$  and  $n_e$  have resumed their normal values.

The hard X-ray monitor records an intense burst 20 to 50  $\mu$ s after the pulse. Even faster an increase of the line radiation intensity of the low ionization states of impurities develops.

The functional dependence of  $S(k)$ ,  $T_e$  and  $T_i$  on the height of the current pulse is shown in Fig. 4.B.2. We observe that these quantities all scale linearly with  $(\Delta I_p)^2$ . It has been established experimentally that  $\Delta I$  scales linearly with the applied voltage  $\Delta V$  and that  $(\Delta I)^2 \sim \int_{\text{pulse}} IV dt$ . Hence,  $(\Delta I_p)^2$  is a measure of the energy input during the pulse. Furthermore, we notice that the electron heating breaks down for current pulses  $\Delta I_p > 35$  kA. This break-down is measured both with Thomson scattering and ECE. ECE records a violent oscillation of the  $T_e$ -profile ( $f \approx 10$  kHz,  $\Delta r \approx 5$  cm), and at times the  $T_e$ -profile is completely flat [5]. Strikingly, the ion heating remains effective for pulses up to 50 kA.

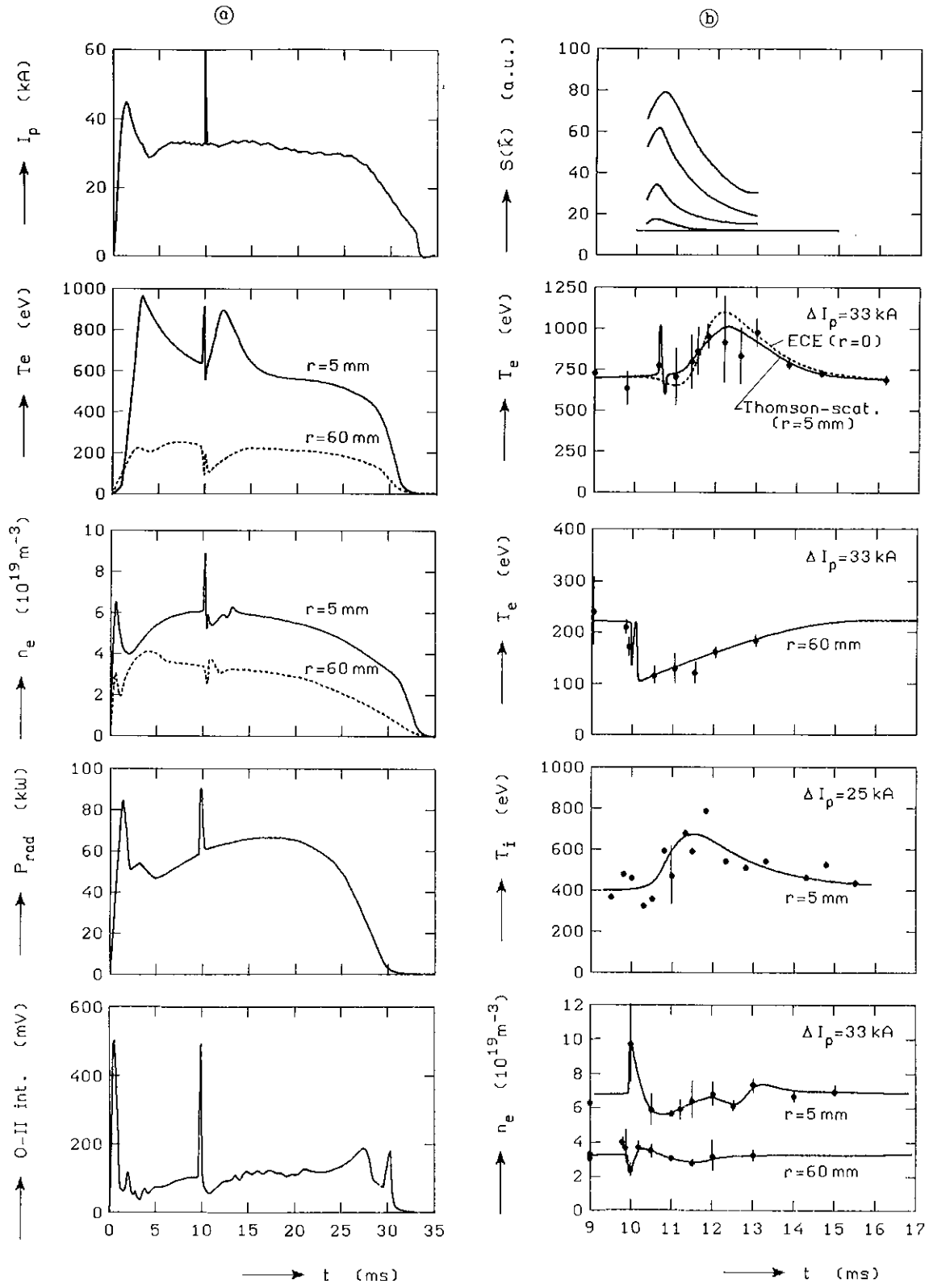


Fig. 4.B.1. a,b,c. Effects of the high-voltage pulse on various plasma parameters, shown on three different timescales.

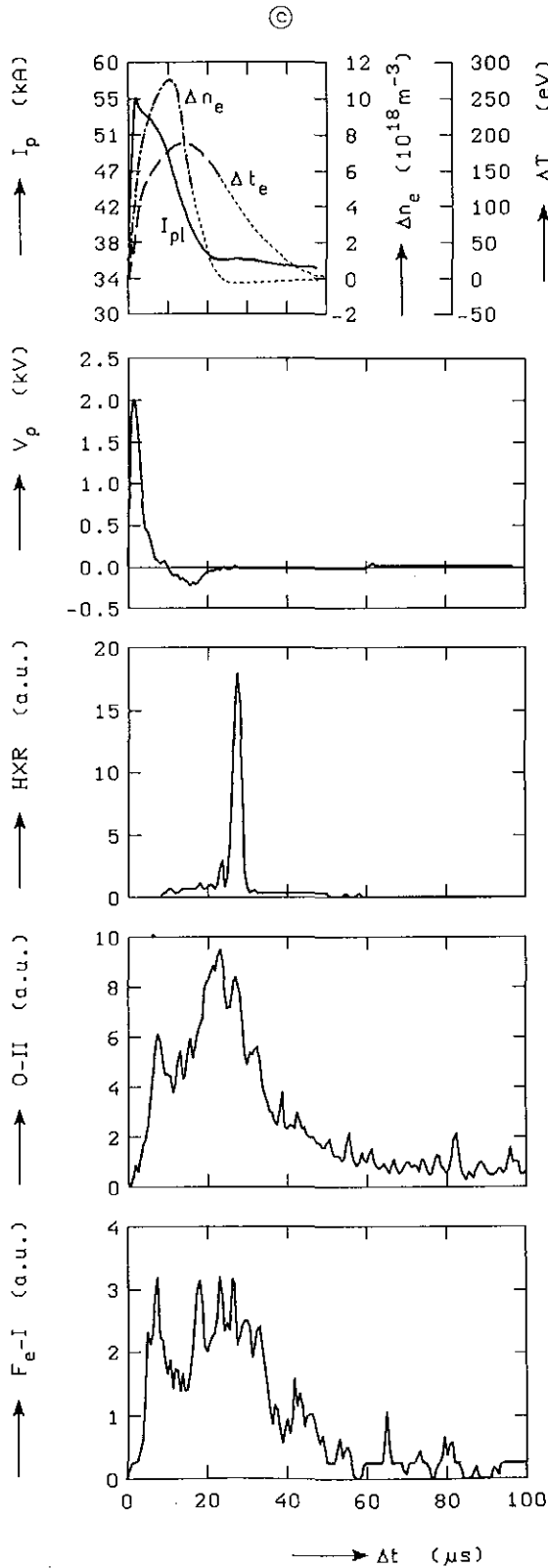


Fig. 4.B.1.c.

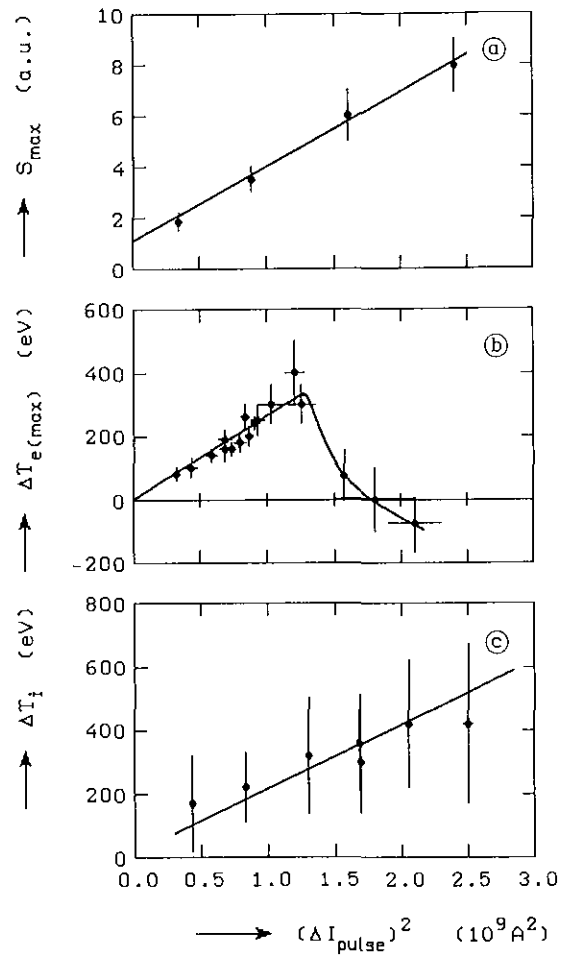


Fig. 4.B.2.

$\Delta T_e$ ,  $\Delta T_i$  and  $S(k)$  as a function of  $(\Delta I_p)^2$ .

#### 4.B.2 Heating pulse, X-ray measurements

As is shown in Fig. 4.B.1c, the hard X-ray monitor records an intense hard X-ray burst 20 to 50  $\mu$ s after the application of the heating pulse. In the period thereafter, however, the hard X-ray intensity is very low. In Fig. 4.B.3, spectra taken with the NaI scintillator are shown, recorded in the period before the pulse 4-7 ms, and directly after the pulse 7-9. In this experiment the heating pulse was triggered at 7.0 ms. It is observed that after the pulse the tail is truncated effectively. The explanation is that, due to the pulse, the population of fast electrons escapes to the wall, thereby generating the hard X-ray burst recorded with the monitor. The subject will be treated in more detail in Chapter 5.

The soft X-ray flux all but vanishes after the pulse. This phenomenon was recorded with several types of detectors: the channeltrons (Fig. 4.B.4a), the surface-barrier diodes (Fig. 4.B.4b), and the Si(Li) detector. Only the  $\epsilon \leq 2$  keV flux, dominant before the pulse, that shows this dip. The thermal continuum from the hot core remains intact, as will be shown next.

A series of measurements was dedicated to the study of the evolution of the soft X-ray spectrum in the milliseconds after the pulse. This series differed from the preceding ones in that gaspuffing was applied. Gas was puffed by the end of the discharge to suppress excessive hard X-ray radiation at the termination of the discharge. An additional gaspuff was applied during the discharge, 1 ms before the heating pulse. The gaspuffs turned out to have some influence on the discharge: the basic central electron temperature was lowered to 550 eV, the loop voltage was lowered to 3.5 V and the heating of the electrons by the heating pulse was much more effective:  $\Delta T_e = 290$  eV when  $\Delta I_p = 26$  kA with gaspuff, whereas  $\Delta T_e = 150$  eV for the same current pulse without gaspuff. A characterization of the gaspuffed discharge is given in Fig. 4.B.5.

For the X-ray spectra the lower loop voltage, resulting in a less populated runaway tail, means that the thermal continuum can be measured more purely, up to 5 keV. In order to measure the effect of the heating pulse on the spectrum in the region 3-20 keV, the softer photons were filtered out with 18 micron Al and 65 micron Be. Spectra taken in the four milliseconds after the pulse are shown in Fig. 4.B.6 on a semilog scale.

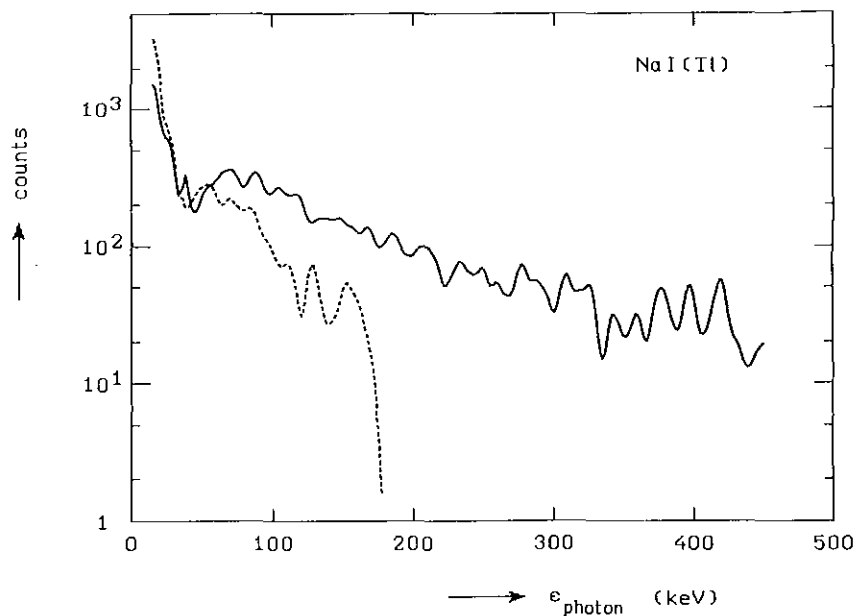


Fig. 4.B.3. Hard X-ray spectra before and directly after turbulent heating pulse: —  $t = 4 - 7$  ms,  $\cdots$   $t = 7 - 9$  ms,  $t_{\text{pulse}} = 7$  ms.

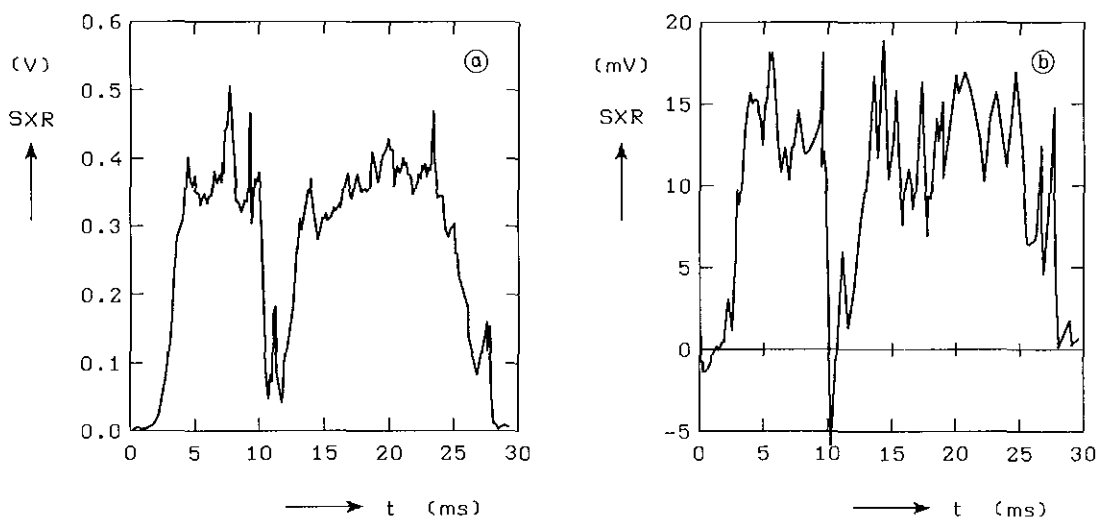


Fig. 4.B.4. The lull in the soft X-ray emission. a. channeltron signal; b. surface-barrier diode signal.

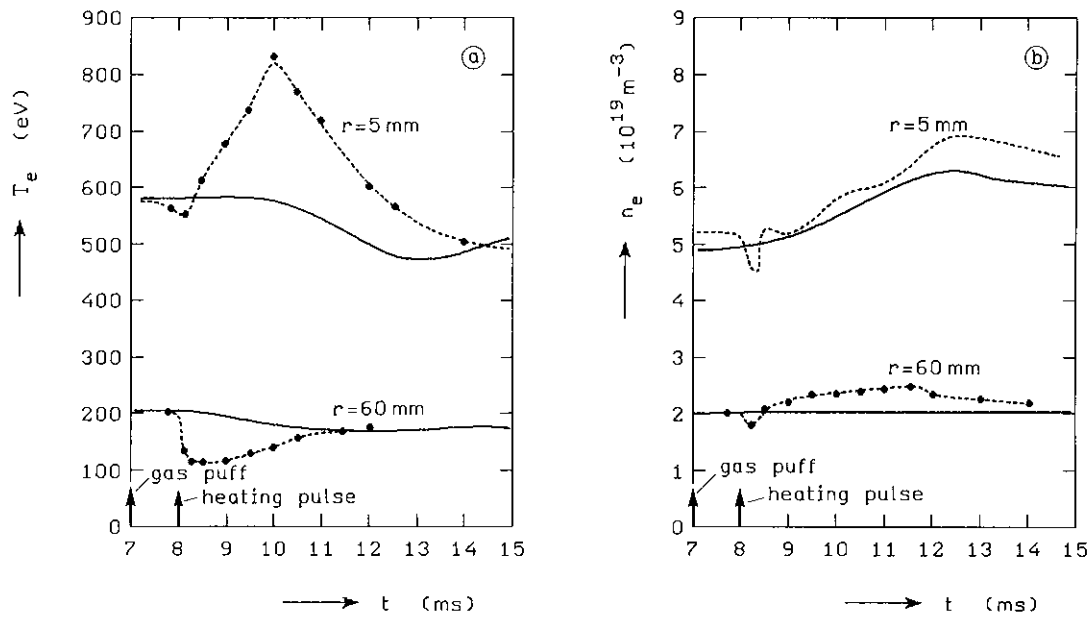


Fig. 4.B.5. Temperature and density evolution in a gaspuffed discharge.  
Solid line: basic discharge;  
Dotted line: discharge plus heating pulse.

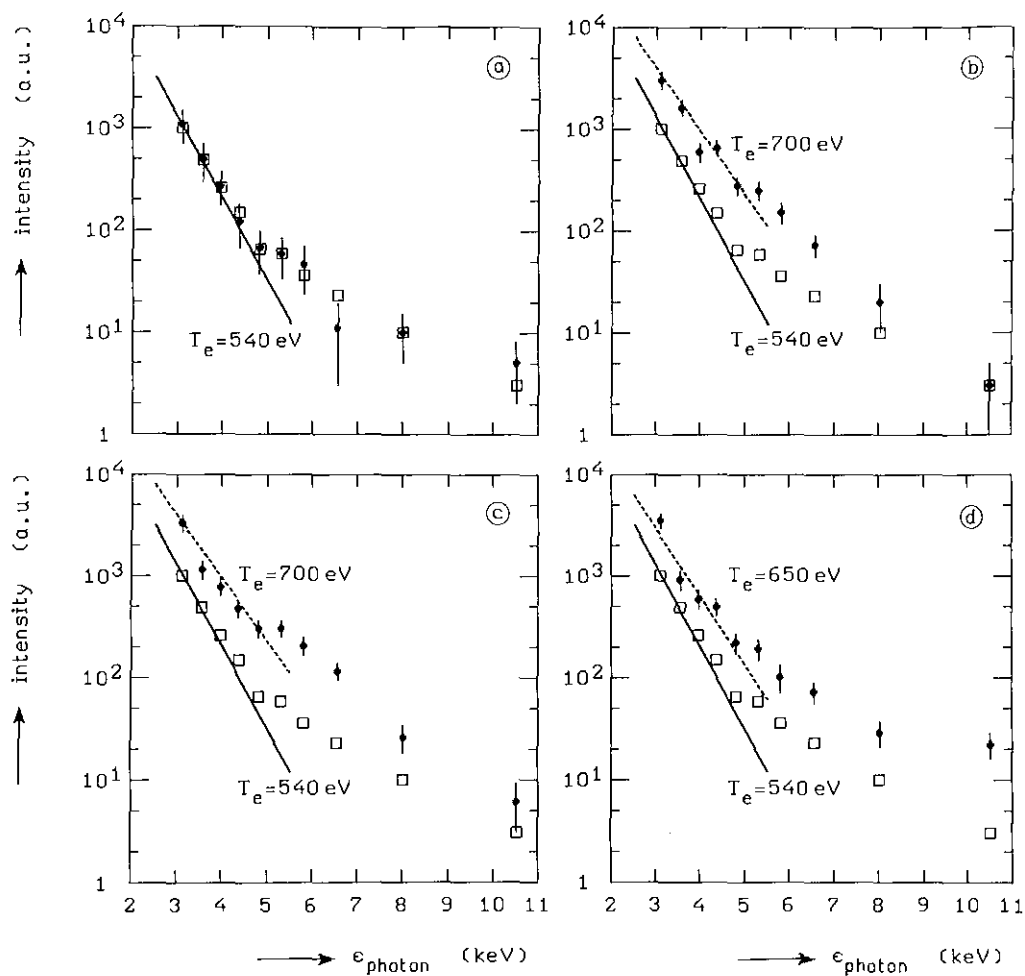


Fig. 4.B.6. The development of the soft X-ray spectra in the milliseconds after the pulse:  
 a.  $t = 8-9$  ms; b.  $t = 9-10$  ms; c.  $t = 10-11$  ms; d.  $t = 11-12$  ms.  
 Solid lines: spectrum of basic plasma. Broken lines: slope and intensity corresponding to the electron temperatures indicated.

References

- [1] H. de Kluiver et al., Phys. Lett. 94A (1983) 156.
- [2] TORTUR TEAM, Proc. 11th Eur. Conf. on Contr. Fusion and Plasma Phys., Aachen (1983) Part I, p. 409.
- [3] H. de Kluiver et al., Proc. 10th Int. Conf. on Plasma Phys. and Contr. Nucl. Fusion Res., London (1984) Vol. 1, p. 375.
- [4] P.C. Efthimion et al., Proc. 10th Int. Conf. on Plasma Phys. and Contr. Nucl. Fusion Res., London (1984) Vol. 1, p. 29.
- [5] R.M. Niestadt, "ECE measurements on the TORTUR III tokamak", Rijnhuizen Report 83-148 (1983).
- [6] L.L. House, Astrophys. J., Supplement Series, 18 (1968) 21.
- [7] CRC Handbook of Chemistry and Physics, 60th ed. (1979), CRC Press, Florida.
- [8] R.L. Kelly and L.J. Palumbo, "Atomic and ionic emission lines below 2000 Angstroms", NRL Report 7599 (1973).

## C H A P T E R 5

### INTERPRETATION OF THE X-RAY MEASUREMENTS

#### 5.1 Introduction

In this chapter the X-ray measurements are subjected to a more careful analysis. The different contributions to the flux are pulled apart and examined. Four spectral intervals are discussed in separate sections. Results of other diagnostics are mentioned if necessary for the interpretation. Though in some instances we prelude on the discussion of the effects of the heating pulse, the thorough discussion on this topic is deferred to Chapter 6. The scope of the present chapter is to investigate the information obtained from the X-ray measurements.

#### 5.2 The spectral region 1 to 2 keV

(Data presented in Sections 4.A.2 and 4.B.2.)

In the spectral region 1 to 2 keV a soft X-ray flux of high intensity is measured. In this section this flux is referred to as 'the flux'. The spectrum corresponds to radiation from a plasma with an apparent electron temperature of 150 eV, which is well below the central  $T_e$ . Both with PLATO and with the Si(Li) detector this flux has been measured, at three different diagnostic ports, and with various field angles. The flux starts to rise at  $t = 2$  ms, and decays at  $t = 15$  to 20 ms, well before the end of the discharge. If the heating pulse is applied, the flux drops sharply, to recuperate within 3 ms.

The question is where and how this flux is generated. By means of inspection pinholes in the Be-foils have been eliminated as a possible explanation of the observed spectrum [1]. Consequently, the source of the flux is sought in the plasma and then two distinct possibilities come to mind:

- A. Line radiation of heavy impurities such as iron is held responsible. The flux is generated in the plasma core in this case.
- B. The thermal radiation of the outer plasma zone is strongly enhanced either by recombination of impurity ions or by wall contact.

Possibility A is eliminated. First the relevant lines of iron lay in the energy range 950 to 1150 eV, whereas the enhanced flux stretches to 1.8 keV. One might argue that the measured spectrum is the far wing of strong lines at  $\sim 1$  keV. However, the system has too good a resolution. In Fig. 5.1 the Fe<sup>55</sup> calibration lines (these being the calibration lines of lowest energy available) are depicted on a semilog scale. If we were to interpret the high energy wing as thermal radiation from a plasma, we would find  $T_e$  (apparent) = 60 eV. At lower energy the resolution of the system is probably better. Furthermore, according to the VUV measurements, oxygen and carbon are the dominant impurities, and only little iron is present in the plasma. We also remark that not much is seen of iron K-lines (6.6 keV) in the X-ray spectra. Moreover, the soft flux declines well before the plasma has decayed, and it shows a dip after the heating pulse. These two effects cannot be explained if impurities in the plasma core were to account for the enhanced flux. Hence, we can reject possibility A and conclude that, anyhow, the flux is generated somewhere near the plasma boundary.

Two mechanisms to enhance the radiation of the edge plasma are considered: recombination of light impurities, e.g. oxygen and wall contact, e.g. bremsstrahlung production by fast plasma particles hitting the liner.

The possibility that the outer plasma is polluted with oxygen and as a consequence, exhibits a strongly enhanced soft X-ray flux has been the subject of a separate study [1], of which some results are mentioned here. The idea is that after the plasma formation, oxygen is released from the wall in the form of water or metallic oxides. The oxygen is ionized stepwise while it penetrates the plasma. The state O<sup>6+</sup> is reached within 2 ms, but further ionization is slow. For the diffusion rate we can only give an estimate on the basis of a scaling law for anomalous diffusion:  $D \sim I_p^2/n_e$  [2,3,4]. We found that it takes an oxygen blanket  $\sim 50$  ms to spread over the entire column. Thus it is marginally possible that an oxygen blanket is maintained during 15 ms, when the X-ray flux is maximal.

An oxygen density profile that amounts to Per = 50% (Per =  $\frac{\sum_j n_{Oj+}}{\sum_j n_{Oj+} + n_{H^+}}$ ) at the limiter and spreading 2 cm into the plasma was found to provide an explanation for the PLATO measurements (high absolute intensity and low foil method deduced temperatures), provided that the impurity content of the plasma core is low: 0.2% of

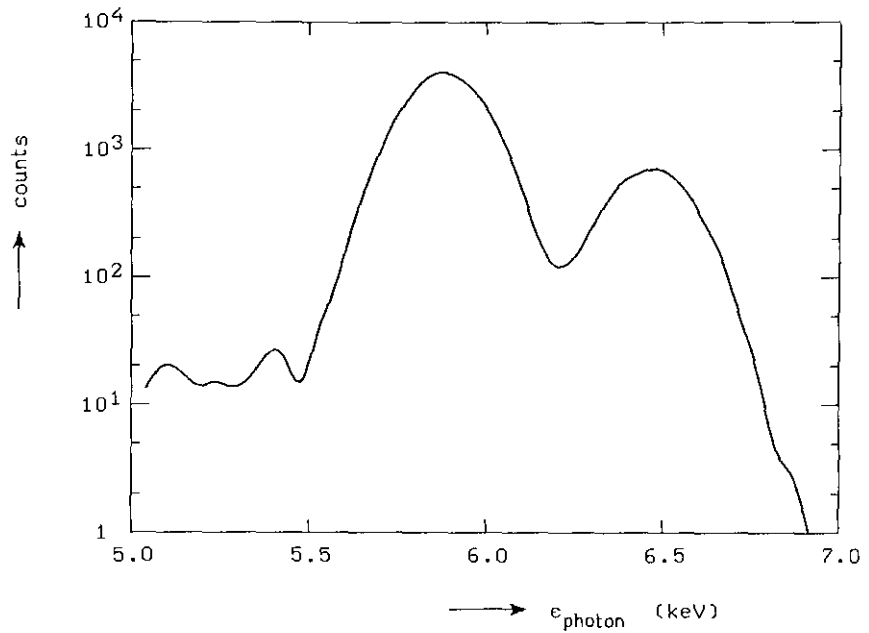


Fig. 5.1. Detail of the 5.9 and 6.5 keV calibration lines, measured with the Si(Li) detector.

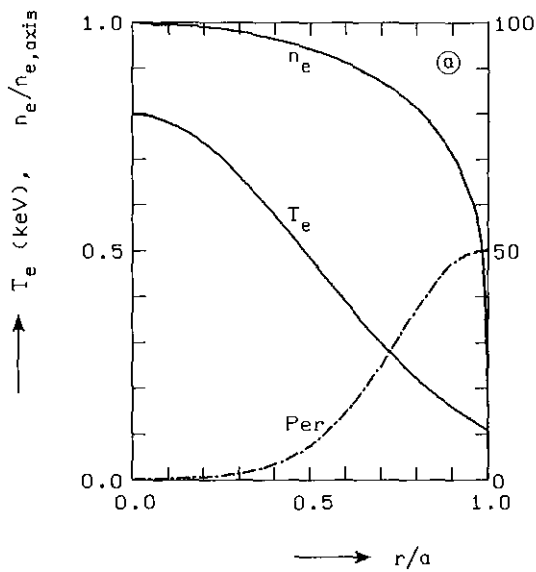


Fig. 5.2a.

The profiles of  $T_e$ ,  $n_e$  and the percentage of oxygen Per, which cause a soft X-ray emissivity profile that is peaked near  $r/a = 0.6$ . Such profiles could account for the temperature and absolute flux as measured with PLATO.

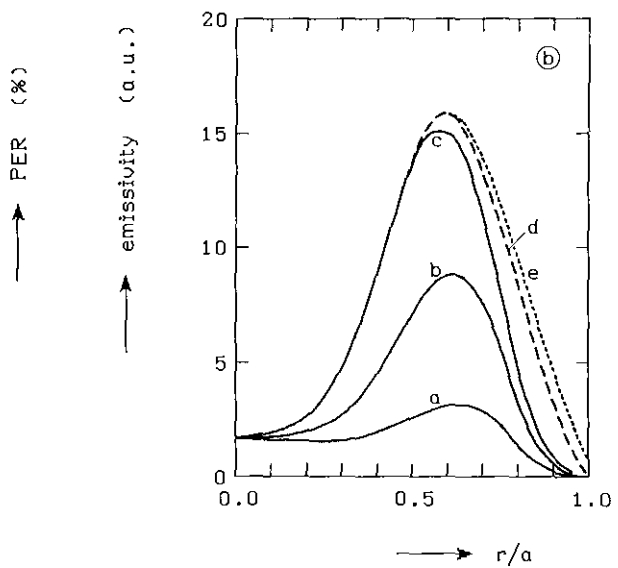


Fig. 5.2b.

The emissivity profiles resulting from the  $T_e$  and  $n_e$  profiles shown in Fig. 5.2a, with  $\text{Per} = 0.2 + A \exp(-8(1-x)^2)\%$ .  
 a:  $A = 5$ ; b:  $A = 20$ ; c:  $A = 50$ : local corona equilibrium.  
 d:  $A = 50$ , corona equilibrium evaluated for  $T_e^+ = T_e + 100$  eV.  
 e:  $A = 50$ , all oxygen fully ionized.

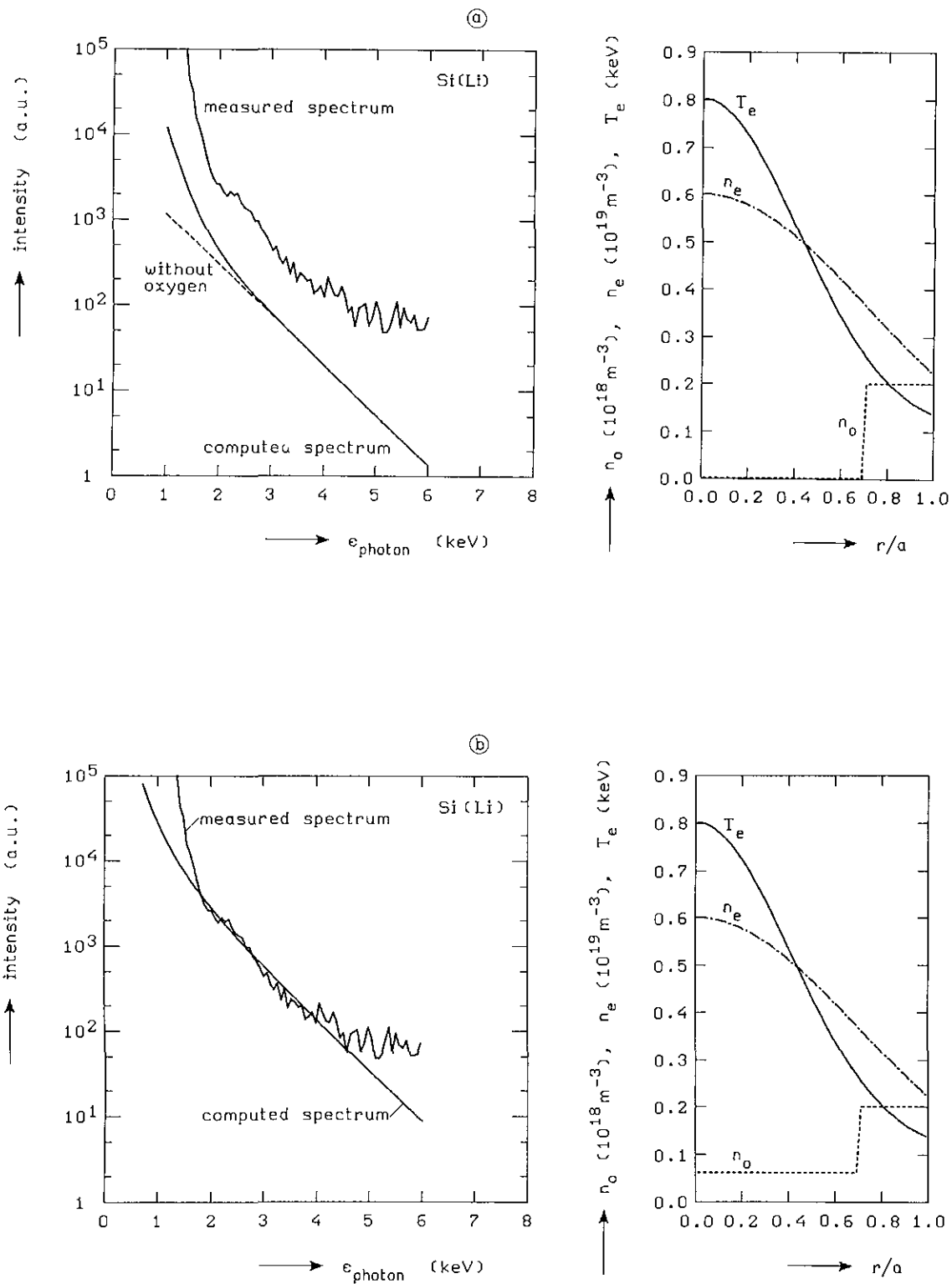


Fig. 5.3.a,b. Comparison of the measured spectrum with spectra calculated for the profiles shown in the right graphs.

oxygen. Figure 5.2a shows the radial profiles of  $n_e$ ,  $T_e$  and the oxygen content. The emissivity profiles that result from various oxygen density profiles are shown in Fig. 5.2b. Here, the emissivity is defined as the soft X-ray intensity of a test volume, as detected by a channeltron screened by  $46 \mu$  Be and  $8 \mu$  Makrofol. It is seen that the desired shape of the emissivity profile, e.g. peaked in the outer region, can be achieved readily.

Whereas the PLATO results can be explained with the oxygen blanket hypothesis, the latter is not fully compatible with the Si(Li) spectral measurements. In Fig. 5.3a, the calculated spectrum is shown together with the measured spectrum. Here the oxygen blanket is driven to its extreme: a rectangular profile with near to 100% oxygen at the limiter, in order to produce a knee in the spectrum as sharp as possible. The radial profiles of  $T_e$  and  $n_e$  are typical for the plasma of which the spectrum was taken. The absolute intensity of the calculated spectrum is computed for the collimation system used. In order to get agreement between the measured spectrum and the computed one in the thermal range 2-5 keV, we should account for an overall oxygen contamination that amounts to 1% in the centre. If we do so, the knee almost vanishes in the computed spectrum (see Fig. 5.3b). In the energy range 1 to 2 keV agreement is not achieved.

In the light of these observations we must now conclude that not only an oxygen blanket can be held responsible for the measured flux.

Next, we turn our attention to the possible generation of soft X-rays due to plasma-wall contact. Much care was taken to collimate the X-ray detection systems properly. The field of view of the Si(Li) detector has a cross-section of only a few millimetres. Therefore, it is most unlikely that radiation from the rim of the diagnostic port is detected. Also radiation from the limiters cannot reach the detector.

Then the part of the liner facing the diagnostic port is the most likely origin of the detected flux. This is in agreement with the observation that the measured spectrum does not depend critically on the field of view, nor on the diagnostic port used.

In Fig. 5.4, examples of PLATO signals are shown for different evolutions of the plasma current and the horizontal displacement. From these measurements we conclude that there is no clear correlation between the inward or outward displacement of the column and the soft X-ray intensity. A more allusive correlation is found between the soft X-ray intensity and  $dI/dt$ : if the current subsides, the flux collapses. The following interpretation is evoked by this observation.

The decreasing current is indicative of a narrowing current density profile: if  $dI/dt < 0$  while  $V_{loop}$  remains at the same level, we must have  $dL_i/dt > 0$ , where  $L_i$  is the internal self-inductance of the plasma current. But also a resistive effect may cause the narrowing: if the plasma cools, it does so first in the outer layer. Hence, that is where the resistivity rises and the current density drops. Anyway, the narrowing of the current density profile goes together with cooling in the outer plasma region, which reduces the generation of X-rays at the limiter.

The fact that the spectrum shows an apparent temperature of 150 eV signifies that the temperature and density profiles stretch to the limiter with high values, to show a sharp drop at the very edge of the plasma. Such a conclusion is in accord with the ECE-results which show a temperature of about 100 eV at the limiter radius. Further corroboration is obtained from the visible light spectrum, where the lowest ionization states dominate. Not much is seen of the states that correspond to the temperature range 10 to 50 eV. The VUV spectrum, on the other hand, mainly shows lines of  $O^{6+}$  and  $O^{7+}$ , emitted from the hot part of the plasma. The observations indicate that the  $T_e$ -profile has a sharp gradient in the range 10-50 eV, evidently because this is the radiation barrier of the light impurities. The low ionization states of oxygen are found in the scrape-off layer, where  $T_e$  is typically a few electron volts.

As a conclusion of this discussion we make the following statements:

- the X-ray flux in the spectral region 1.3 to 2 keV is generated near the plasma boundary and not in the core of the plasma,
- most likely, the flux is a result of loss (through diffusion) of 'hot' electrons made possible by the broad current density profiles.

The fall of the flux directly after the heating pulse is now explained as strong cooling of the edge plasma. Further discussion on this topic is found in Chapter 6.

### 5.3 The spectral region 2 to 5 keV

(Data presented in Sections 4.A.2 and 4.B.2.)

Measurements in the spectral region 2 to 5 keV were done exclusively with the Si(Li) detector. The intensity in this region is too low to use the time resolving detection system PLATO.

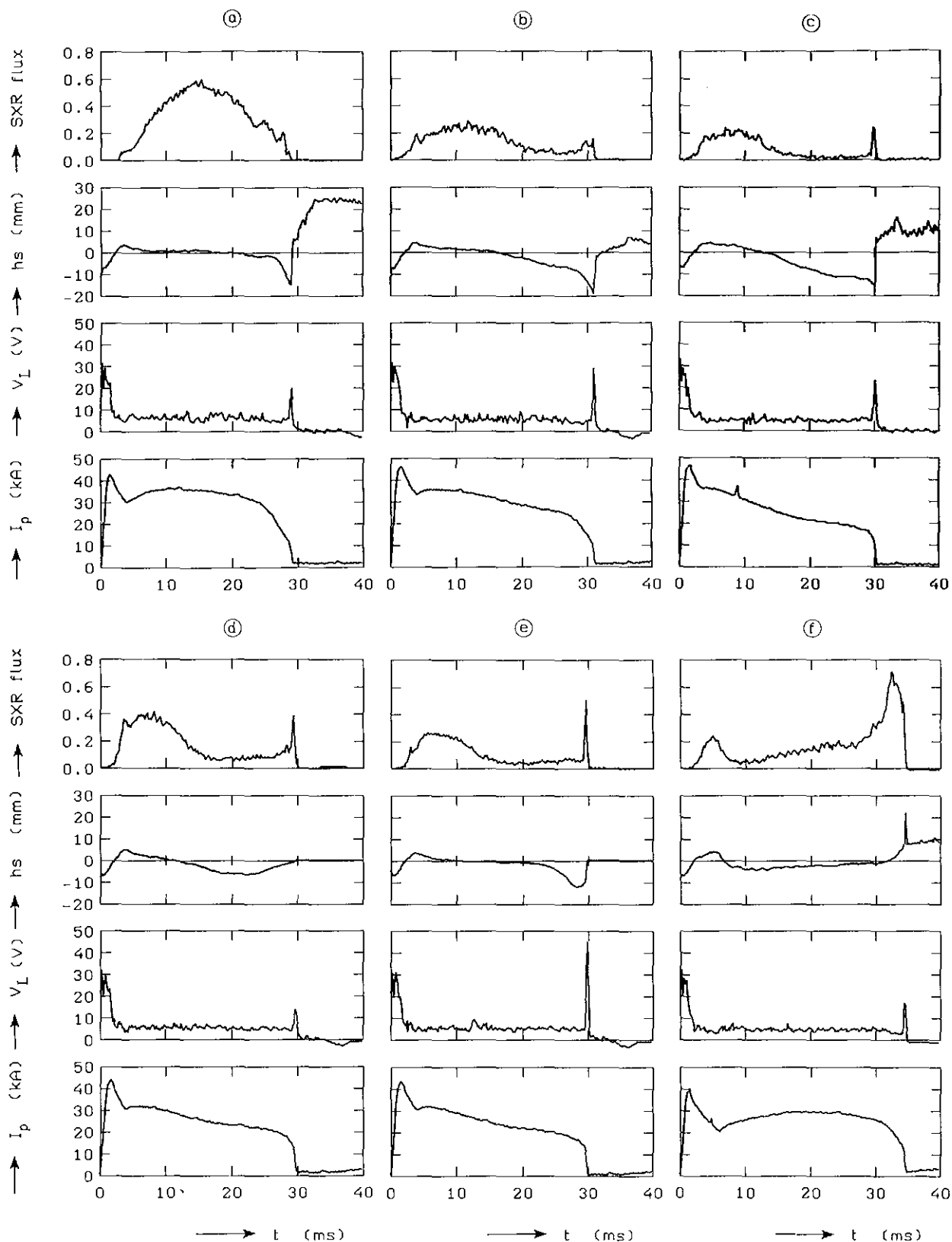


Fig. 5.4. PLATO signal for various discharge conditions. The soft X-ray (SXR) the flux, the horizontal shift (HS) of the column, the loop voltage and the plasma current are shown here.

The spectrum exhibits no peculiarities, it is a plain spectrum from a thermal plasma. The line radiation (Section 4.A.2) at  $\epsilon = 2$  to 3 keV does not hamper the determination of the electron temperature. The temperatures measured are in good agreement with the Thomson-scattering data.

Calculation of the field angle of the collimation system enables the direct comparison of shape and absolute intensities of the measured spectrum and the calculated spectrum. Figure 5.3b shows both spectra. In order to fit the slopes of the spectra, we must take  $T_e(0) = 800$  eV for the calculations, whereas the slopes correspond to  $T_e = 700$  eV. Of course, the value of  $T_e$  deduced from the slope of the spectrum somewhat underestimates the top-value of the  $T_e$ -profile, because also the near central plasma has a significant contribution to the flux. For the thermal continuum part an enhancement by a factor of 5 over thermal radiation of a pure hydrogen plasma is found. If oxygen is taken as the dominant impurity, we find a relative density (assuming corona equilibrium):

$$n_o/n_{ion} = 1 \pm 0.5\% .$$

The error is the estimated uncertainty in the calculation of the field angle of the collimation system.

The corresponding value of the effective ion charge is:

$$Z_{eff} = 1.5 \pm 0.3 .$$

In the TORTUR discharge corona equilibrium might not be reached, as the ionization of  $O^{6+}$  and  $O^{7+}$  takes on the order of 10 ms, largely depending on the local electron temperature and density [5]. If  $O^{6+}$  is taken as the dominant state, we find:

$$Z_{eff} = 2 \pm 0.5 .$$

For comparison: the density  $n_e$  was found to scale with  $I_p$  according to Murakami's limit, adopting  $Z_{eff} \approx 2$ .

#### 5.4 The spectral region 5 to 30 keV

(Data presented in Sections 4.A.3 and 4.B.2.)

First we remark that in this region the measurements with the Si(Li) detector are subject to two experimental difficulties: the low count rate and the danger of a pile-up contribution from the lower energy part of the spectrum. Therefore, we have poor spectral resolution in this region and the experimental error prohibits rigorous conclusions as to the identification of lines or subtle deformations of the electron energy distribution function. Moreover, we cannot distinguish between the contribution from the plasma column and that generated at the wall. The two melt together and in this region it is not clear which one is dominant. For these reasons, we must abstain from any quantitative interpretation in the region 10 to 30 keV. We can merely say that a tail is observed and we make the general observation that the intensity of the tail is lower in the discharges with gaspuff than in those without. This fact flows naturally from the higher electron temperature and higher loop voltage which enhance the ratio  $E/E_C$  and hence the runaway production in the discharges without gaspuff.

Information on the spectral region 15 to 30 keV is also obtained from measurements with the NaI(Tl) detector. Two observations are made. First: the intensity of the tail increases during the first 7 ms of the discharge (see Fig. 4.A.10) (at  $t = 7$  ms the measurement stopped, not the development of the tail). Second: in the 2 ms following the heating pulse, the tail intensity is increased at energies lower than 30 keV. The first effect reflects the rather slow development of the runaway tail, which is also shown clearly in Fig. 4.A.11a,b. The second observation is explained by the enhanced runaway production after the pulse, which results from the increase of  $T_e$  and, as we shall see, from the somewhat higher electric field.

We now return to a lower energy part of the spectrum. As is seen in Figs. 4.A.9 and 4.B.6 the spectra exhibit a little plateau around 5.5 keV. The probable explanation is line radiation, e.g. K-lines of Cr, Ni, and Fe; the main compounds of stainless steel. The intensity of the lines is low and in discharges without gaspuff they are drowned in the tail.

We could also seek the explanation of the plateau in a non-thermal feature of the electron energy distribution function  $g(\epsilon)$ . In order to investigate the effect of a hump in the distribution, we calculate the spectrum of a distribution of the form:

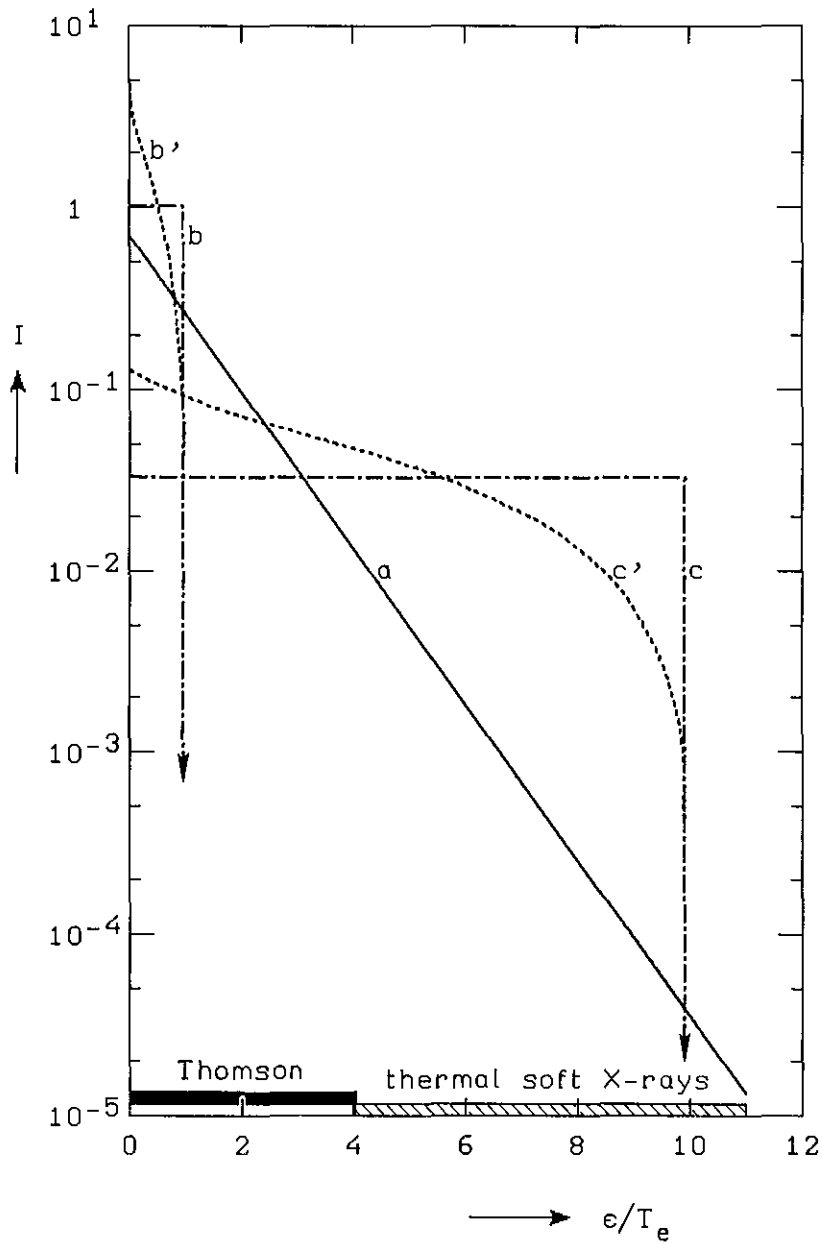


Fig. 5.5. Calculated soft X-ray spectra for electron populations of equal kinetic energy density, with different energy distribution functions:  
 a: thermal distribution,  
 b, c: 'hump' distribution at  $\epsilon_h = T_e$  and  $\epsilon_h = 10 T_e$ , respectively,  
 b', c': tail distribution stretching to  $\epsilon_t = T_e$  and  $\epsilon_t = 10 T_e$ , respectively. The measuring range of the Thomson scattering diagnostic and the thermal part of the soft X-ray spectrum are also indicated in the figure.

$$q(\varepsilon) = g_m(\varepsilon) + g_h(\varepsilon) ,$$

with a maxwellian part  $g_m(\varepsilon) = \frac{\sqrt{4}}{\pi} n_{e,m} \frac{\sqrt{\varepsilon}}{T_e^{3/2}} e^{-\varepsilon/T_e}$

and a sharp hump  $g_h(\varepsilon) = n_{e,h} \delta(\varepsilon - \varepsilon_h)$  .

The kinetic energy density in the maxwellian part is  $W_m = \int \varepsilon g_m(\varepsilon) d\varepsilon = 3/2 n_{e,m} T_e$ , in the hump  $W_h = n_{e,h} \varepsilon_h$ .

As particles of both parts of the distribution scatter on the same ion cloud, we may reduce the functional expression for the spectrum to

$$I(\varepsilon) = \text{const} \int_{\varepsilon}^{\infty} \frac{g(\varepsilon')}{\sqrt{\varepsilon'}} d\varepsilon' .$$

$$I_m(\varepsilon) = \text{const} n_{e,m} \frac{\sqrt{4}}{\pi} \frac{e^{-\varepsilon/T_e}}{\sqrt{T_e}} ,$$

$$I_h(\varepsilon) = \text{const} n_{e,h} \sqrt{\frac{1}{\varepsilon_h}} \quad \varepsilon < \varepsilon_h$$

$$= 0 \quad \varepsilon > \varepsilon_h .$$

Two parameters determine the spectral deformation due to the hump:  $\varepsilon_h$  and  $W_h/W_m$ . In Fig. 5.5, calculated spectra are shown for different values of  $\varepsilon_h$  and  $W_h/W_m$ . In order to get more general results, all energies are expressed in units of  $T_e$ .

A plateau as observed in the measured spectra could be the result of a hump in  $g(\varepsilon)$  at about 7 keV, with a total energy content of less than 1% of the energy in the thermal bulk.

For completeness, also the spectrum of a tail distribution is calculated:

$$g_t(\varepsilon) = n_{e,t} \frac{1}{\varepsilon_t} , \quad \varepsilon < \varepsilon_t$$

$$= 0 \quad \varepsilon > \varepsilon_t .$$

$$W_t = \frac{1}{2} n_{e,t} \varepsilon_t ,$$

$$I_t(\varepsilon) = \text{const.} n_{e,t} \frac{2}{\varepsilon_t} (\sqrt{\varepsilon_t} - \sqrt{\varepsilon}) \quad \varepsilon < \varepsilon_t$$

$$= 0 \quad \varepsilon > \varepsilon_t .$$

The analysis is completely analogous to the case of the hump. The results are shown in Fig. 5.5. It is observed that for the spectrum a hump and a tail are not that different: the deformation due to the tail is more smooth and is more pronounced on the low energy side.

Since we see that the little plateau in the spectrum is always found at  $\epsilon = 5.5$  keV (see Fig. 4.B.6) and that it does not alter much in the milliseconds after the pulse, when a new tail is growing, we conclude that it is indeed line radiation and not an effect of a hump in the tail distribution. The latter would be of a less stable nature.

Figure 5.5 also makes clear that if a hump or tail distribution is present that carries an energy comparable to the energy in the thermal population, such a distribution produces a giant deformation of the thermal spectrum. Nothing of the sort is observed (see Figs. 4.A.4, 4.A.10, 4.B.6), not before and not after the pulse. Hence, we conclude that such a superthermal population can only be present in the plasma during a time much shorter than the time resolution of the Si(Li) measurements: 1 ms after the pulse.

#### 5.5 The spectral region 30 keV to 2 MeV

(Data presented in Sections 4.A.3 and 4.B.2)

Measurements in this region involve the spectral measurements with the NaI(Tl) detector, the monitoring of the spectral evolution of the tail and the high time resolution measurement of the hard X-ray flux. The high energy tail under consideration here is partly generated at the wall. This part reflects the energy distribution of the escaping electrons rather than that of the trapped electrons. Furthermore, the spectrum is deformed by two effects: fluorescence of lead, leading to a peak at 80 keV, and, for photons of energy exceeding 0.5 MeV, the angle of view is drastically enlarged because the lead castle becomes transparent. Then, the emission of photons by relativistic electrons is peaked in the direction of the electron velocity.

Hampered by these distortions of the spectrum we are not able to make bold statements on the density of the runaway electrons or the energy distribution function of the tail. Still the measurements do convey much valuable information on the runaway electrons in the TORTUR III plasma.

The first, most general conclusion is that the tail stretches to energies exceeding 1.3 MeV, which ensures that we have got authentic runaways in the basic discharge. Evidently, if a tail truncating

mechanism is active, it is not fully effective.

The second observation is that the fastest electrons have experienced a free fall. In Fig. 4.A.12 we see that a flux of photons with energies exceeding 1.3 MeV begins to rise at  $t = 6$  ms. The electrons of longest confinement have been accelerated from  $t = 1.5$  ms on, when the runaways generated in the predischARGE are dumped. From Fig. 3.4 we see that 4.5 ms free fall in a field of 1.5 V/m brings an electron to an energy of about 1.3 MeV. Hence, the free-fall model applies for the runaways in the basic plasma.

Next, we observe that in the entire spectral region  $\epsilon > 500$  keV the flux starts to rise only at  $t = 6$  ms. If electrons of  $\epsilon_e > 1.2$  MeV are present in the plasma at  $t = 6$  ms, then obviously electrons of less energy are present already in an earlier stage of the discharge. They only do not come out. The third conclusion therefore is that the confinement time of the runaways in the energy range 0.5 to 1.2 MeV is at least 4.5 ms. Here, also a confirmation is found of the statement that part of the observed flux originates from electrons hitting the limiters.

In the interval 20 to 50  $\mu$ s after the heating pulse, a burst of hard X-rays is recorded by the monitor. Neither the monitor, nor the NaI(Tl) detector, nor the Si(Li) detector (used with low amplification) show any hard X-ray activity directly after the burst. As, especially in the  $\epsilon < 100$  keV region, the flux generated in the plasma by the runaway population should be detected, this observation indicates a total loss of the runaway population.

The spectrum taken in the period 0 to 2 ms after the pulse shows a short tail, stretching to about 150 keV (see Fig. 4.B.3). This tail has developed during the measuring interval.

In the ECE-spectra, non-thermal emission is found at wavelengths corresponding to positions in the outer half of the column. This is attributed to the relativistically shifted radiation from a tail population ( $\epsilon_e \approx 70$  keV) in the central plasma. After the pulse this emission vanishes, to come back within 4 ms. This observation, too, implies that the tail population in the central plasma gets lost after the pulse. Taking X-ray measurements and ECE-results together, we conclude that after the pulse all runaways are dumped. This indicates the breaking of the magnetic field lines. We stress that the runaways get lost on a typical MHD timescale. Normal transport operates on a timescale of milliseconds. In reverse, we deduce from the long confinement of runaways in the basic discharge that here the magnetic flux surfaces are undisturbed, which means that there is little MHD activity.

## 5.6 Conclusions

We recapitulate the conclusions we have deduced from the analysis of the X-ray measurements:

- \* The  $\epsilon < 2$  keV flux is generated in the edge plasma (presumably at the wall) and is mainly determined by the width of the current density profile.
- \* In the central plasma  $Z_{\text{eff}} \approx 1.5 - 2$ .
- \* Weak impurity lines are found at 2 to 3 keV (probably Cl and Nb) and at 5.5 to 7 keV (Cr, Fe, Ni).
- \* In the basic discharge, the confinement time of runaway electrons is at least 4.5 ms, indicative of a good MHD stability.
- \* At least part of the runaway electrons experience a free fall.
- \* Neither in the basic discharge, nor after the pulse, a superthermal population with an energy content comparable to  $nkT$  exists in the range 1 to 100 keV longer than 0.5 ms.
- \* Directly after the pulse, all runaways are dumped, presumably due to the braiding of the magnetic field lines by MHD activity.

## References

- [1] N.J. Lopes Cardozo, "Soft X-ray electron temperature measurements on TORTUR", Rijnhuizen Report 84-151 (1984).
- [2] J.E. Rice et al., "Continuum X-ray emission from the Alcator-A Tokamak", MIT Report PFC/JO-81-5 (1981).
- [3] F. de Marco et al., "Behaviour of oxygen impurities in the Frascati tokamak", Frascati Report 81.14 (1981).
- [4] R.J. Fonck et al., "Spatially resolved measurements of fully ionized low-Z impurities in the PDX-tokamak", PPPL 1908 (1982).
- [5] W. Lotz, "Electron impact ionization cross-section and ionization rate coefficients for atoms and ions from hydrogen to calcium", IPP 1/62 (1967).

## C H A P T E R 6

### GENERAL INTERPRETATION AND DISCUSSION

#### 6.1 Introduction

In the preceding chapters a synopsis was presented of the experimental data concerning the TORTUR III basic plasma and the effects of the application of a short high-voltage pulse. An effort has been made to come to an understanding of the measurements. As a result we now have an accumulation of experimentally established facts. The piecing together of a coherent physical picture will be the theme of the present chapter.

First, our attention is directed to the basic discharge, which is special for its anomalously high loop voltage and its broad profiles. Two papers concerning this topic have been published recently [1,2]. An account of our present view is presented in Section 6.2.

Second, we will focus on the heating pulse experiments. The first twenty microseconds after the triggering of the high-voltage capacitor bank are the subject of Section 6.3. They bring the penetration and extraction of the current pulse, the expulsion of the runaway electrons and the fast rise and decline of the temperature.

The third item to be tackled is the phenomenon of the delayed heating. This heating is proportional to the energy delivered by the pulse, which suggests that it is this energy which transforms into heat. However, the heating is observed 2 ms after the pulse, whereas the energy confinement time  $\tau_E$  is but 1.7 ms. Hence, we ask: 'where in the plasma is this energy stored and how does it survive so long?' Various schemes that have been proposed to explain the phenomenon of the delayed heating are discussed in Section 6.4. Also a new model is presented. In Section 6.5 this model is analysed quantitatively and checked against the experimental results. Section 6.6 is a summing up of the conclusions derived from the heating pulse experiments.

## 6.2 The basic discharge

The basic discharge is started up with a high loop voltage and a steeply rising (30 kA/ms) plasma current. During the current rise a current skin is maintained. Since the ions are cold in this phase, ion-acoustic turbulence is excited, which rapidly heats the electrons. When the current eventually has reached its plateau value, the plasma is hot:  $T_e \approx 3T_i \approx 1000$  eV at  $t = 3$  ms [1,2,3]. The temperatures take on their plateau values  $T_e \approx 2T_i \approx 700$  eV a few milliseconds later. We shall begin our discussion at this point.

First, we will attack the question: is the plateau plasma turbulent or not? In order to find the answer we calculate  $Z_{\text{eff}}$  with the assumption that the resistivity is classical (Spitzer resistivity). The following profile functions approximate the observed profiles

$$x = r/a, \quad (a: \text{limiter radius})$$

$$T_e(x) = 700 e^{-2x^2} \text{ eV},$$

$$n_e(x) = n_e(0) e^{-x^2} \quad \text{with } n_e(0) = 6 \times 10^{19} \text{ m}^{-3}.$$

The Spitzer resistivity is given by:

$$\eta_{\parallel} = \frac{m_e}{n_e \tau_{c,ei} e^2}, \quad \text{with } \tau_{c,ei} = 6.90 \times 10^{11} \frac{1}{Z^2} \frac{T_e^{3/2}}{n_i \ln \Lambda},$$

which is approximated by (take  $\ln \Lambda = 15$ ):

$$\eta_{\parallel} = 7.5 \times 10^{-4} Z_{\text{eff}} T_e^{-3/2} \quad (T_e \text{ in eV}).$$

Furthermore, the following relations are used:

$$j(x) = E/\eta(x) \quad \text{and} \quad I(x) = 2\pi a^2 \int_0^x j(x') x' dx'.$$

For the total current we find (with  $a = 0.08$  m and  $E \approx 1.5$  V/m):

$$I_{p,Spitzer} = \frac{1}{Z_{eff}} 240 \text{ kA} ,$$

whereas the measured plasma current is 30 to 35 kA. Matching the two values yields:

$$Z_{eff,Spitzer} = 7 \text{ to } 8 , \text{ compared to}$$

$$Z_{eff,exp} = 1.5 \text{ to } 2 , \text{ measured with soft X-rays.}$$

Evidently, the Spitzer resistivity expression is not valid and some resistivity-enhancing mechanism is active. We exclude  $Z_{eff}$  as a possible source of the enhanced resistivity. Hence, we conclude that the plasma is turbulent.

This turbulence is of a steady nature: plasma current and loop voltage are essentially constant over more than 20 ms. Moreover, the plasma finds back its basic discharge state even after the perturbation due to the turbulent heating pulse. For these reasons we think of a weak current-driven instability as the source of the enhanced resistivity. Such an instability depends only on the macroscopic discharge parameters and is insensitive to the variation of the runaway tail population. As was pointed out in Section 3.5, of the current-driven instabilities, the electrostatic ion-cyclotron type will be triggered easiest in our plasma conditions. We recall the onset condition:

$$v_D \geq u_{cr} = 20 (T_i/T_e)^{3/2} v_S \approx 7 v_S \quad (\text{for } T_e = 2T_i) .$$

If Spitzer resistivity alone were to limit  $v_D$ , this threshold would be reached: in the centre, with  $Z_{eff} = 2$ ,  $v_D/v_S \approx 7$ . Hence, we may expect the instability to be triggered and we shall assume that the effective resistivity is given by the marginal stability condition:

$$v_D = \gamma v_S , \text{ with } \gamma > 1 \text{ and } \gamma \sim n_e^{-1/2} .$$

This relation refers to  $v_D$  averaged over many growth times of the instability. The next step will be to calculate the current-density profile according to this concept:

$$v_D = \gamma_0 \sqrt{\frac{n_e(0)}{n_e}} v_S = 2.6 \times 10^5 \gamma_0 e^{-\frac{1}{2}x^2} .$$

In Fig. 6.1a, the thus calculated profiles of  $j$  and  $q$  are compared to those following from classical resistivity. For the total plasma current we now find:

$$I_p = \gamma_0 26 \text{ kA} .$$

Matching this value to the experimental  $I_{p,exp} = 30$  to  $35$  kA yields:

$$\gamma_0 = 1.3 ,$$

which satisfies the condition  $\gamma > 1$ . The mean drift velocity is  $0.2$  to  $0.4 u_{cr}$ , but is high enough in fluctuations to mildly excite the electrostatic ion-cyclotron waves in the way sketched in Section 3.2.

A general expression for the effective collision frequency induced by collective oscillations is of the form:

$$v_{eff} = \text{const.} \frac{W}{nkT} \omega_{pe} , \quad (6.1)$$

where  $W$  is the wave energy density [4,10]. The constant is of the order of  $0.1$  to  $1$ . We see that only  $W \approx 10^{-3} nkT$  need to be present in waves to account for the resistance anomaly of a factor of four. (See Table 1.3.)

Experimental evidence of the occurrence of ion-cyclotron oscillations is found in the density fluctuation spectrum. It follows from theory that the excited waves have maximum growth for

$$(k_{\perp} r_{ci})^2 \approx 1 \quad \text{at } \omega \approx 1.2 \omega_{ci} \quad [5,6] .$$

Substituting TORTUR III values, we find:

$$k_{\perp} \approx 1000 \text{ m}^{-1} \quad (\lambda_{\perp} \approx 6 \text{ mm}) \quad \omega \approx 350 \text{ MHz} .$$

These waves are observed in the 4-mm scattering spectrum. Also contributions at  $100$ - $200$  kHz (drift waves) and around  $1$  MHz are observed.

In conclusion, we think that the electrostatic ion-cyclotron current-driven instability is the source of the enhanced resistivity. It may couple to magnetic sound [5] and drift waves. However, the precise mechanism is not fully understood. If we want to know how the anomalous resistivity depends on the current and other plasma parameters, we can best use experimental data. For variation of the plasma current  $I_p$  we found [1]:

$$T_e \sim I_p, \quad (6.2a)$$

$$n_e \sim I_p, \quad (6.2b)$$

$$\eta_{an}/\eta_{cl} \sim I_p. \quad (6.2c)$$

The drift velocity is constant for variation of  $I_p$  in our case, as  $v_D \sim I_p/n_e$ .

For the scaling of  $\eta_{an}$  with  $j$ ,  $n_e$  and  $T_e$ , we write

$$\eta_{an} \sim j^{\alpha_1} n_e^{\alpha_2} T_e^{\alpha_3}. \quad (6.3)$$

From the above experimentally established relations, we derive

$$\alpha_1 + \alpha_2 + \alpha_3 = -\frac{1}{2}. \quad (6.4)$$

We cannot derive the specific dependencies because the variations of  $I_e$ ,  $n_e$  and  $T_e$  are coupled in our case. As a second input we use the relation:

$$\gamma \sim n_e^{-1/2} \rightarrow j n_e^{-1} T_e^{-1/2} \sim n_e^{-1/2}.$$

In the stationary phase of a discharge, the electric field  $E$  is constant over the cross-section, hence:

$$\eta_{an} \sim j^{-1} \sim n_e^{-1/2} T_e^{-1/2}. \quad (6.5)$$

Combining Eqs. (6.3), (6.4), (6.5) yields

$$\eta_{an} \sim j^{1/2} n_e^{-1/2} T_e^{-1/2}. \quad (6.6)$$

The  $\eta_{an} \sim n_e^{-1/2}$  dependence is consistent with the general expression (6.1) for the effective collision frequency due to collective oscillations:

$$v_{\text{eff}} \sim \omega_{pe} \sim \sqrt{n_e} \rightarrow \eta_{\text{an}} \sim v_{\text{eff}}/n_e \sim n_e^{-1/2} .$$

The experimental results (6.2a,b,c) are consistent with the TFR scaling law for  $\tau_e$ . The latter reads:

$$\tau_e \sim n_e \sqrt{q} \sim n_e I_p^{-1/2} .$$

Hence,

$$\begin{aligned} I^2 R \tau_e &\sim I_p^{5/2} n_e T_e^{-3/2} && (\text{use } \eta_{\text{cl}} \sim T_e^{-3/2}) , \\ &\sim I_p^2 && (\text{use (6.2a) and (6.2b)}) , \end{aligned}$$

whereas by definition

$$\begin{aligned} I^2 R \tau_e &\sim n_e T_e \\ &\sim I_p^2 && \text{for TORTUR III ((6.2a) and (6.2b)) .} \end{aligned}$$

The general impact of Eq. (6.6) is that  $\eta_{\text{an}}$  declines with increasing  $T_e$  much slower than  $n_{\text{cl}}$ . This means that in a mildly turbulent plasma ohmic heating is effective to higher temperatures than is the case in a classical plasma. Furthermore,  $\eta_{\text{an}}$  does not rise sharply with increasing current density. These results are found quite generally in mildly turbulent plasmas [7,8].

The reason that the current-driven instability does not impose a hard limit upon  $j$  (or rather:  $v_D$ ) is that the mean drift velocity is still well below the critical value  $u_{\text{cr}}$ . The anomalous resistivity arises from the repeated rise and quenching of the instability, which process takes many growth times of the particular mode. Only if the mean drift velocity is driven up to  $u_{\text{cr}}$ , the anomalous resistivity rises sharply, typically a factor  $10^4$  or more [9,10].

Finally, we want to remark that it is most unlikely that the shape and population of the runaway tail are important parameters in our discharge. As is seen from X-ray measurements the runaway tail grows steadily, then is cut off by the heating pulse, whereafter its growth starts again. Moreover, in some experiments gas puffing was applied, in which case runaway production was suppressed effectively as follows from X-ray spectra and from the production of hard X-rays during the termination of the discharge. With these different tail populations always essentially the same macroscopical behaviour was found.

### 6.3 During the current pulse and shortly after

In this section we will discuss the immediate effect of the fast heating pulse. First, we investigate the effect on the current density profile. A pictorial description is presented in Fig. 6.1. In the first 5 microseconds the current enters the plasma and flows in a skin of width 2-3 cm. The skin formation has been investigated by Kalfsbeek [9], who showed that due to turbulent processes the skin width of 2-3 cm is attained rapidly. In this phase the electric field is strong in the skin:  $E/E_C \approx 10$ . Thomson scattering and ECE show that a tail population is formed which immediately is cut off at  $\epsilon \approx 5$  keV and becomes isotropic. This truncation is ascribed to the Parail and Pogutse instability [11]. The tail population is observed with Thomson scattering as a hot population,  $T_e \approx 5$  keV, which exists in the plasma boundary during 0-10  $\mu$ s after the triggering of the pulse. The conditions under which this population is observed indicate that it exists only in the outer 2-3 cm of the column. In the skin, current-driven instabilities of the ion-acoustic as well as the ion-cyclotron type are excited. The group velocity of the excited waves is perpendicular to B and can transport particles and energy towards the plasma centre [12]. A few microseconds after the start of the pulse, tearing modes develop and begin to break up the magnetic field structure, which greatly facilitates the radial transport. The current spreads over the entire column, establishing a monotonic q-profile. In the plasma centre, compression and heating are observed almost simultaneously with the rise of the current, followed by rarefaction and cooling. Sometimes, a fluctuation of  $T_e$  and  $n_e$  with a typical frequency of 0.5 MHz is observed. This fluctuation is measured by Thomson scattering as well as ECE. The first density rise can amount to 30%. We note that such a pinch effect could never occur if the toroidal field were to be compressed together with the plasma. Hence, we have three indications of the snapping of the field lines: the rapid spread of the current skin (as measured by Kalfsbeek), the strong fluctuations of  $T_e$  and  $n_e$  in the centre and the loss of the runaway population. The process is fast enough to explain the heating effect as being due to adiabatic compression. During the compression in the centre, rarefaction and cooling are observed in the outer plasma.

After 5 microseconds the decline of  $I_p$  sets in, entering the plasma like a negative current skin. In contrast to the case of the positive current penetrating, the q-profile now remains of a stable

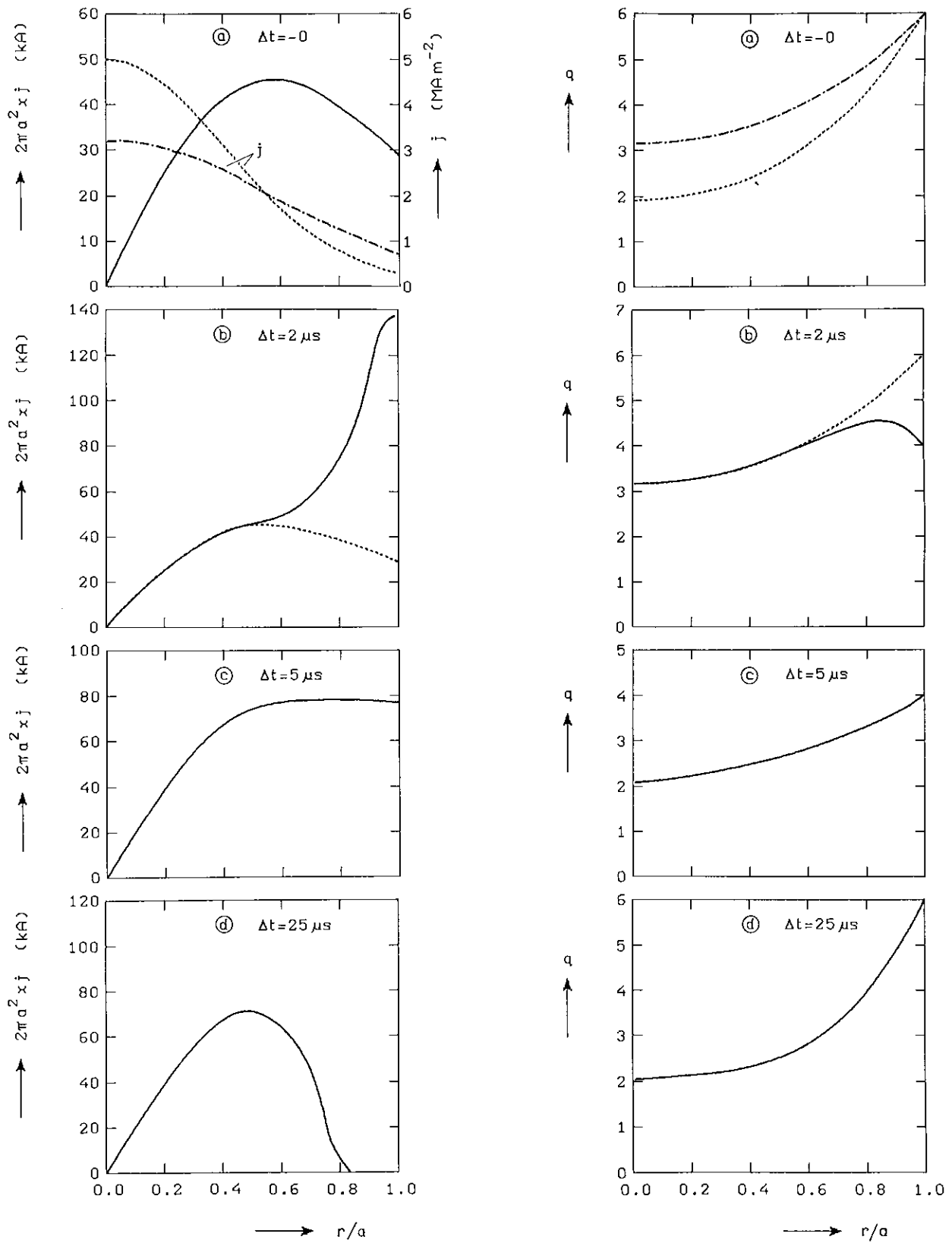


Fig. 6.1. Sketches of the probable development of the  $j$ -profile and the  $q$ -profile during the current pulse. a. before pulse (also depicted (...):  $j(x)$  and  $q(x)$  as would result from Spitzer resistivity); b. penetration of current skin; c. after implosion of current skin; d. after extraction of additional current.

shape and consequently the negative current skin penetrates into the plasma only as deep as is necessary to get the total current back to its original value, which depth is estimated  $\sim 3$  cm. In the outer zone, even a layer of negative current may be formed and may persist for some time, as was actually measured by Kalfsbeek.

After these processes a current-density profile is established that again carries the basic plasma current  $I_p = 30-35$  kA, but is substantially narrower than in the relaxed state before the application of the heating pulse. The subsequent relaxation will take place within a few milliseconds, as will be shown in Section 6.5.

In the outer zone of the plasma cold ions may enter the plasma, together with some lowly ionized impurity ions. They give rise to the temporal enhancement of emission in lines in the visible light observed at  $t = 20-50$   $\mu$ s after the pulse and cool the outer part of the plasma.

Let us consider the energy balance at  $t = 50$   $\mu$ s after the start of the pulse: the integral of  $IV$  over this period, i.e. the Poynting flux through the toroidal surface with minor radius  $a$ , yields a net extra power input of 180 J at  $\Delta I_p = 30$  kA. Where is this energy when the current pulse has passed? It is either lost, or transformed into particle movement (in the form of heat or drift) or stacked in magnetic field energy.

The bolometer records an extra loss of  $\sim 30$  J. The total loss is estimated about the double: 60 J. Remains some 120 J. Neither ECE, nor Thomson scattering, nor  $T_i$ -measurements, nor soft X-rays or hard X-rays detect any non-thermal population that carries 120 J kinetic energy. Also the temperatures  $T_e$  and  $T_i$  are not increased, they are back on their prepulse value. Hence, we must conclude that the energy is not present in a kinetic term.

Next, we will investigate the possibility that the energy is stored in an increase of the poloidal magnetic field energy. We have already argued that the current-density profile has been reshaped by the pulse into a more peaked form. We will now estimate the amount of energy associated with this narrowing. For the total amount of field energy due to the poloidal field we have:

$$W_L = \int_0^{r_0} \frac{B^2}{2\mu_0} 2\pi r dr + \int_{r_0}^a \frac{B^2}{2\mu_0} 2\pi r dr ,$$

where  $r_0$  is the radius of the current channel and  $a$  is the limiter

radius. The first term can be shown to be fairly independent of  $r_0$ , provided the shape (not the width) of the  $j$ -profile does not change drastically (see Appendix B). Then the change  $\Delta W_L$  is determined mainly by the coaxial term:

$$\Delta W_L \approx \frac{1}{2} I_p^2 \Delta L_{\text{coax}} = \frac{1}{2} I_p^2 \mu_0 R \left( \ln \frac{a}{r_{0,\text{after}}} - \ln \frac{a}{r_{0,\text{before}}} \right).$$

Substituting  $I_p = 33$  kA and  $R = 0.46$  m, we find that for  $\Delta W_L = 120$  J the  $j$ -profile should shrink from  $r_0 = 8$  cm to  $r_0 = 5$  cm, which agrees well with our estimate based on the evolution of the current profile. The subject will be discussed in more detail in Section 6.5.

Taking into account all observations and following the heuristic reasoning given above, we think that the main effects of the current pulse, evaluated at  $t = 50$   $\mu$ s after the pulse, are: (for  $\Delta I_p = 30$  kA):

- narrowing of the current-density profile,
- storage of the net power input  $\sim 120$  J in poloidal magnetic field energy,
- no substantial net effect on the distribution functions of the
- electrons and the ions,
- introduction of a modest amount of cold gas and impurities in the outer plasma,
- loss of the entire runaway population.

#### 6.4 The delayed heating

In this section the phenomena connected with the second, delayed, rise of  $T_e$  and  $T_i$  are examined. We review the experimental observations: rise and decline of the density fluctuation level within 2 ms; increase of the central  $T_e$  and  $T_i$  during 2 ms, followed by a decline with a time constant of  $\sim 1.7$  ms; fast drop and subsequent slow recovery of  $T_e$  ( $r = 60$  mm); drop and recovery of the soft X-ray flux from the plasma edge and of the hard X-ray intensity; linear dependence of  $\Delta T_e$ ,  $\Delta T_i$  and  $\Delta S(k)$  on  $(\Delta I_p)^2$ , with  $(\Delta I_p)^2 \sim \int_{\text{pulse}} IV dt$ .

We shall briefly discuss some explanations of the delayed heating that have been proposed in the recent past. It is our purpose to check them against the experimental data in order to see which are valuable elements and what can be rejected. Then, we will present a new explanation, which has been precluded to in Section 6.3. This model will be subjected to a quantitative analysis in Section 6.5.

The explanations for the delayed heating that have been proposed previously, differ in the essentials of their physical bases. We give a classification:

I impurity penetration: if after the pulse impurities are introduced in the plasma, this might enhance the ohmic power input;

II velocity space effects: in this type of explanation the idea is that energy delivered by the pulse is stored in a deformation of the velocity distribution function, e.g. in a superthermal population.

III improvement of the energy confinement.

All the types have their own motivation. Type I has been raised as the unsophisticated explanation that should be checked before embarking on more involved and physically more interesting arguments. It will be shown to lack all experimental support. Type II has a better motivation: it is inspired by the linear dependence of  $\Delta T_{e,i}$  on  $(\Delta I_p)^2$ , which suggests that the energy which eventually is seen as heating, is injected in the plasma by the pulse. It assumes that a population of fast electrons is generated that thermalizes in 2 ms. Explanation III, in contrast, examines the possibility that the heating does not result from extra energy input but from reduced loss.

#### I Impurity influx

We state that no influx of impurities of any importance takes place after the heating pulse. The experimental evidence is as follows:

- Neither the VUV-spectrometer, nor the bolometer, nor the X-ray diagnostics, nor the visible light diagnostics give any indication of an enhancement of the impurity content after the pulse.
- In experiments with two to four subsequent pulses with intervals of 1 to 2 ms (not reported on here, see Ref. 14), the delayed heating was found to repeat. This is not compatible with the impurity influx hypothesis, as the particle confinement time is much longer than  $\tau_e$ . Hence, impurities supposedly introduced by one pulse would still be present in the plasma when the next pulse is applied.
- Since in the basic discharge the resistivity is only for one third classical (determined by  $Z_{eff}$ ) and for two thirds current-driven, an enormous amount of impurities is required to induce a significant enhancement of the ohmic power input. The ohmic power input due to classical resistivity with  $Z_{eff} = 2$  is about 50 kW. To achieve the heating observed, this power should at least be doubled, which implies  $Z_{eff} > 4$  or  $> 25\% O^{6+}$ .
- The electron density is not raised after the pulse.

## II Velocity space effects

The possibility has been put forward that during the pulse a population of fast electrons is generated carrying the energy which is greeted as an increase of  $T_e$  and  $T_i$  two milliseconds later. The formation of a ' $T_e$ ' = 5 keV population in the outer shell of the plasma was actually measured (Thomson scattering and ECE), but it was observed to disappear within 10-20  $\mu$ s. This disappearance is conform the expectation, as the electron-electron energy equipartition time is 5-20  $\mu$ s. Could it be that somehow a superthermal population survives and escapes detection?

If the population were a hot thermal distribution, it should be seen by Thomson scattering, ECE, and X-ray diagnostics. If it were beam-like, with  $\epsilon_b \approx 5$  keV, it might escape observation by Thomson scattering and ECE, but in the soft X-ray spectra it should be found very clearly. Furthermore, the beam should not carry too big a part of the plasma current or the ohmic power input would collapse. If for instance,  $I_b \approx 1/10 I_p \approx 3$  kA, the kinetic energy content of the beam,  $W_{k,b}$  calculated from:

$$I_b = \frac{eN_b}{2\pi R} \sqrt{\frac{2\epsilon_b}{m_e}}, \quad W_{k,b} = N_b \epsilon_b, \quad \epsilon_b = 5 \text{ keV}$$

amounts to  $W_{k,b} \approx 1$  J, far less than is necessary for the observed heating. For non-relativistic  $\epsilon_b$ ,  $W_{k,b}$  is proportional to  $\sqrt{\epsilon_b}$ . To store  $W_{k,b} \sim 100$  J with  $I_b = 3$  kA, a runaway population is needed, with  $\epsilon_b \approx 3$  MeV. Runaways, however, do not thermalize. Moreover, we already have seen that all runaways are dumped after the pulse.

Finally, if anywhere in the plasma a beam is generated, it is in the outer shell, since there the electric field (during the pulse) is maximal. The heating, however, is observed in the centre.

We conclude that the delayed heating is not produced by a slowly thermalizing superthermal electron population.

## III Improvement of energy confinement

In Section 6.3 it was shown that after the heating pulse the current-density profile has narrowed. It has been proposed that the more slender column suffers less losses. Especially the convective loss term could be diminished. The bolometer does not record a decrease of the power flux to the wall. However, the bolometer records but 75 kW

of the total power loss of 175 kW. The remaining 100 kW is not measured. This loss term could decrease unnoticedly after the pulse. The decrease of the power loss would appear as an additional power input, which lasts until a new equilibrium is reached. If we assume that during 2 ms the mean additional power input is 50 kW, the apparent energy input is 100 J, sufficient to explain the observed heating. This is an upper limit estimate. It is difficult to give a more precise estimate.

The evidence is, however, that the delayed heating is not the result of diminished loss. First: what has happened with the  $\sim 100$  J injected during the current pulse? Second: the predominant heating would occur in the plasma boundary and not in the centre.

In conclusion, we have little reason to believe that the energy confinement is improved after the pulse.

A new concept: conversion of magnetic energy into heat.

In the preceding paragraphs we have discussed various schemes that have been proposed as possible explanations of the delayed heating. It was shown that none is compatible with the experimental data. Certainly, a quantitative theory has not yet been proposed.

At this point we take up the heuristic theory developed in Section 6.3. We ended up with the picture that the pulse induces a narrowing of the current channel, while the energy delivered by the pulse is stored mainly in the increase of the poloidal field energy. The subsequent expansion of the current channel takes  $\sim 2$  ms. As long as the relaxation process is not completed, the ohmic dissipation density ( $j^2 \eta$ ) is enhanced in the centre and lowered in the outer region. As a net effect the total dissipation is enhanced. During the relaxation process a conversion takes place of the energy  $\Delta W_L$  stored in the poloidal magnetic field into thermal energy. The increased current density in the centre induces an enhanced level of the current-driven ion-cyclotron waves. This may explain the observed increase of the low-frequency modes which are coupled to the ion-cyclotron mode. The additional dissipation is localized in the plasma centre, which complies with the fact that there the strong heating is observed, whereas the outer plasma remains cool.

We see that the peaking of the  $j$ -profile can account in a natural way for the experimental findings. In the next section we will expand on this concept and subject it to a quantitative analysis.

### 6.5 The relaxation of the pinched current-density profile

In Fig. 6.2 the current-density profile and the electric field  $E(r)$  are sketched in the relaxed state and in the perturbed state directly after the pulse. The relaxation process evolves with a time constant which is estimated

$$\tau_R = (a/2)^2 \mu_0 / \bar{\eta} ,$$

the resistive skin time of a plasma layer of thickness  $a/2$ . For  $\bar{\eta}$  we take the mean value  $\bar{\eta}$  given by

$$\bar{\eta} = R_D \frac{a^2}{2R} = 10^{-6} \Omega m ,$$

which yields

$$\tau_R \approx 2 \text{ ms} .$$

This figure should be regarded as a rough estimate, its purpose being merely to show that the relaxation of the  $j$ -profile may take place on the same long timescale as the delayed heating. This is consistent with the experimental finding that  $T_e$  ( $r = 60 \text{ mm}$ ) and the very soft X-ray flux recover on a milliseconds timescale.

In order to parametrize the relaxation, we will approximate the current-density profile by

$$j(r) = (a/r_0)^2 j_0(r \frac{a}{r_0}) \quad 0 \leq r \leq r_0 ,$$

$j_0(r)$ : unperturbed profile

i.e., the  $j$ -profile is pinched by a factor  $a/r_0$ , but not altered of shape. We can now describe the relaxation process by the single parameter  $r_0$ :

$$r_0(t) = a - (a - r_0(0)) e^{-t/\tau} ,$$

where  $\tau$  is the relaxation time, estimated  $\sim 2 \text{ ms}$ , both from experiment and from theory (see above). We have taken  $t = 0$  directly after the pulse has vanished.

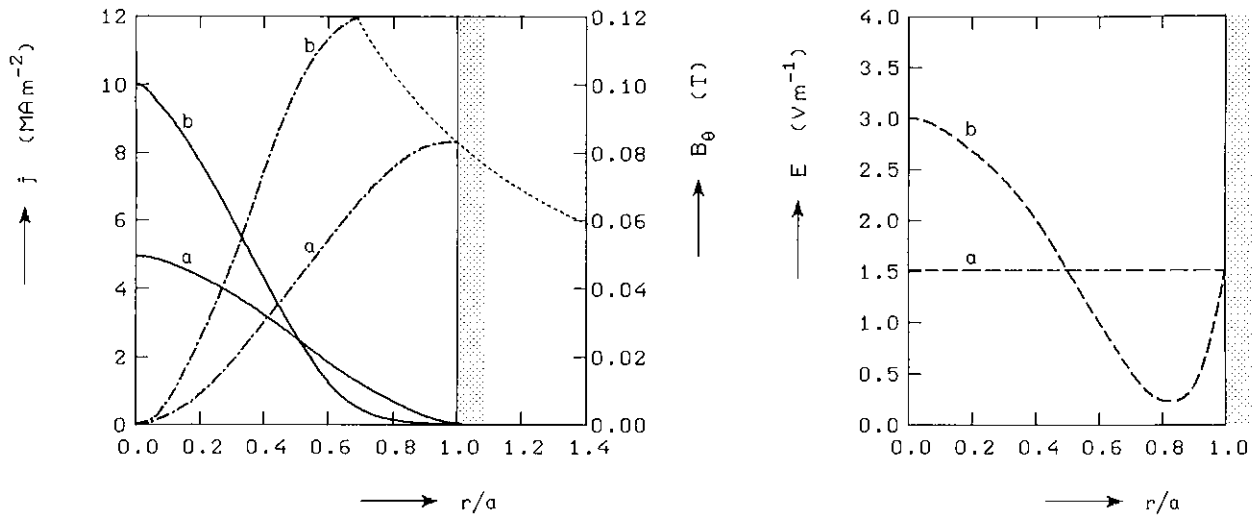


Fig. 6.2. Sketches of the current-density profile (—), the poloidal magnetic field (-.-) and the electric field (---) in the basic discharge (a) and in the perturbed state after the pulse.

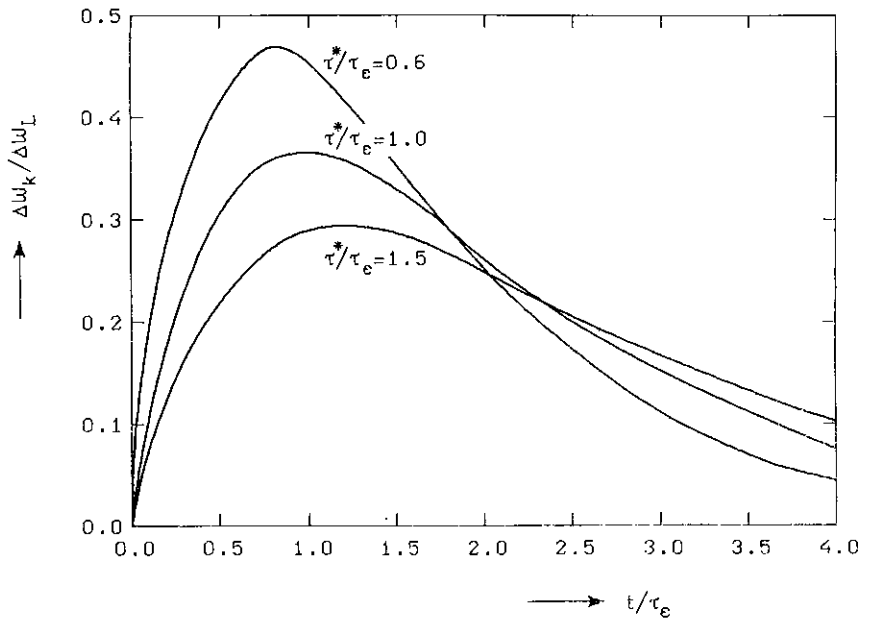


Fig. 6.3. The increase of the kinetic energy content ( $\Delta W_k$ ) due to the gradual dissipation of  $\Delta W_L$ . (See text p. 100.)

The amount of magnetic energy stored in the increase of  $L$ ,  $\Delta W_L$ , is given by (see Appendix B):

$$\Delta W_L = 300 \ln(a/r_0(0)) \text{ J} \quad (\text{for } I_p = 33 \text{ kA}) .$$

We shall now derive a relation between  $a/r_0(0)$  and the height of the pulse  $\Delta I_p$ . Experimentally, the following relation was established

$$\Delta W_{\text{pulse}} = 180 \times 10^{-9} (\Delta I_p)^2 \text{ J A}^{-2} ,$$

where

$$\Delta W_{\text{pulse}} = \int_{\text{pulse}} IV dt .$$

Allowing for 30 J extra loss measured by the bolometer and about as much extra loss to the limiter at  $\Delta I_p = 30 \text{ kA}$ , we estimate:

$$\Delta W_{\text{pulse}} - \Delta W_{\text{loss}} = 120 \times 10^{-9} (\Delta I_p)^2 \text{ J A}^{-2} .$$

Setting  $\Delta W_L$  equal to  $\Delta W_{\text{pulse}} - \Delta W_{\text{loss}}$  yields

$$300 \text{ J} \ln \frac{a}{r_0(0)} = 120 \times 10^{-9} (\Delta I_p)^2 \text{ J A}^{-2} ,$$

$$\text{hence, } \frac{a}{r_0(0)} = \exp(0.4 \times 10^{-9} (\Delta I_p)^2) \quad (\Delta I_p \text{ in A}) . \quad (6.7)$$

We introduce the notation  $y = 0.4 \times 10^{-9} (\Delta I_p)^2$ . Since  $\Delta I_p$  is varied up to  $\Delta I_p \approx 40 \text{ kA}$ , it follows that  $y \leq 0.6$ . We make the Taylor expansion:

$$\frac{a}{r_0(0)} = \exp(y) = 1 + y + O(y^2) .$$

$$\text{Hence, } \frac{a}{r_0(t)} = 1 + ye^{-t/\tau} .$$

During the relaxation of the  $j$ -profile the ohmic dissipation ( $\dot{W}_\Omega$ ) is on an enhanced level. The increased dissipation tends to lower  $I_p$ , which effect is counteracted by the release of energy stored in

self-inductance of the plasma: the decreasing self-inductance acts as a current supply.  $\dot{W}_\Omega$  is given by

$$\dot{W}_\Omega = \int_0^a j^2(r) n(r) 2\pi r dr .$$

Accounting for a slight  $j$ -dependence of  $n$  (see Appendix C) this can be approximated by

$$\dot{W}_\Omega = \dot{W}_{\Omega,0} (1 + \alpha y e^{-t/\tau}) \quad \text{with } \alpha = 0.8 \text{ to } 1.4 .$$

$\dot{W}_{\Omega,0}$  denotes the dissipation level in the unperturbed state.

The ohmic energy input at a time  $t$  after the pulse is computed:

$$W_\Omega(t) = \int_0^t \dot{W}_\Omega dt ,$$

hence,

$$\Delta W_\Omega = \lim_{t \rightarrow \infty} \int_0^t (\dot{W}_\Omega - \dot{W}_{\Omega,0}) dt = 60 \times 10^{-9} \alpha \tau (\text{ms}) (\Delta I_p)^2 \quad \text{J A}^{-2} .$$

From this calculation we see that if the relaxation takes place with a time constant  $\sim 2$  ms, the energy injected by the heating pulse is entirely dissipated. This agrees with the observation that, averaged over 2 ms,  $I_p V_L$  is on its basic level after the pulse. If the relaxation were slower, the increased plasma resistivity would lead to a decreasing plasma current or, at constant  $I_p$ , to a rise of  $V_L$ . If, on the other hand, the relaxation were faster, energy would be transferred to the external circuit.

The fact that  $I_p$  does not collapse indicates that the resistivity does not rise sharply with increasing current density. This confirms the findings of Section 6.2. If, in contrast, the plasma resistance were proportional to the intensity of the low-frequency density fluctuations,  $S(k)$ ,  $R_p$  would increase by a factor of 3 at  $\Delta I_p = 30$  kA.

We now have established the coherent picture that the energy reservoir  $\Delta W_L$  releases its contents with a time constant  $\tau = 2$  ms. We consider the energy balance equation:

$$\dot{W}_k = -\frac{1}{\tau_\epsilon} W_k + I_p V_L + \frac{1}{\tau} \Delta W_L e^{-t/\tau} .$$

$W_k$  is the total kinetic energy content of the plasma,  $\tau_\epsilon$  is the energy confinement time ( $\approx 1.5$  to  $2$  ms),  $I_p V_L$  is the basic ohmic power input which is taken constant, and the last term describes the gradual dissipation of  $\Delta W_L$ . The change of  $W_k$  with respect to the basic level  $W_k(0) = W_k(\infty)$  is given by:

$$\Delta W_k(t) = \frac{1}{\tau} \Delta W_L (1 - e^{-t/\tau^*}) \tau^* e^{-t/\tau_\epsilon}$$

with

$$\tau^* = \left( \frac{1}{\tau} - \frac{1}{\tau_\epsilon} \right)^{-1} .$$

In Fig. 6.3,  $\Delta W_k(t)$  is shown for  $\tau/\tau_\epsilon = 0.6$ ,  $1.0$ , and  $1.5$ . It is seen that for  $\tau/\tau_\epsilon = 1$ , which is a good estimate for our case, the maximum value of  $\Delta W_k$  is reached at  $t = \tau_\epsilon$  and is about  $0.37 \Delta W_L$ :

$$\text{(Model)} \quad \Delta W_k(\text{max}) = 45 \times 10^{-9} (\Delta I_p)^2 \quad \text{J A}^{-2} . \quad (6.8)$$

This relation should be checked against the experimentally established relation

$$\Delta T_e(5 \text{ mm}) \approx \Delta T_i = 250 \times 10^{-9} (\Delta I_p)^2 \quad \text{eV A}^{-2} .$$

Taking into account the changed profiles of  $T_e$  and  $T_i$  this relation translates to

$$\Delta W_k(\text{max}) = 40 \times 10^{-9} (\Delta I_p)^2 \quad \text{J A}^{-2} . \quad (6.9)$$

The agreement between the results of the simple model (6.8) and the experiment (6.9) is satisfactory.

The next quantity we calculate is the value of  $\Delta I_p$  for which  $q = 1$  is reached in the centre, according to the model. We have

$$q(0) = 3 \text{ for } r_0 = a .$$

Since  $q$  is proportional to  $j^{-1}$ , with  $j = j_0(a/r_0)^2$ , we find

$$q(0) = 1 \quad \text{for } a/r_0 = 1.7 ,$$

and using (6.7)

$$\Delta I_{p,crit.} \approx 36 \text{ kA} .$$

For  $\Delta p > \Delta I_{p,crit.}$  we expect the occurrence of a sawtooth relaxation. This effect limits further peaking of the  $j$ -profile and flattens the top of the  $T_e$ -profile. Furthermore,  $\Delta I_p \approx 34 \text{ kA}$  marks the occurrence of  $q(a) = 3$ . The development of  $m = 3$  MHD modes in the plasma boundary may seriously enhance the power loss to the liner and may thus cool the plasma. This is observed in many tokamaks. These effects are proposed as an explanation for the breakdown of the electron heating in the centre, which occurs for  $\Delta I_p \approx 35 \text{ kA}$ .

#### 6.6 Conclusions concerning the heating pulse experiment

- The extra current induced on top of the running plasma current spreads within  $5 \mu\text{s}$  over the entire plasma, due to turbulent processes.
- Simultaneously, magnetic field lines are broken, permitting radial particle transport.
- After the current pulse is extracted, a sharpened  $j$ -profile has been established.
- The net energy input due to the pulse,  $\Delta W_L$ , is stored as  $\frac{1}{2}\Delta L I_p^2$ , where  $\Delta L$  is the increase of the self-inductance of the plasma corresponding to the narrowing of the  $j$ -profile.
- The outer plasma zone cools due to an influx of cold plasma and the subsequent ionization of hydrogen and impurities.
- The runaway population is lost, due to the breakage of magnetic field lines.
- The relaxation of the  $j$ -profile takes place with a typical time  $\tau \approx (\frac{1}{2}a)^2 \mu_0 / \eta \approx 2 \text{ ms}$ .
- During the relaxation the ohmic dissipation is enhanced in the centre and lowered in the outer plasma.
- The net extra dissipation is about equal to  $\Delta W_L$ .
- The fluctuation level is increased according to the enhanced drift velocity, but the anomalous resistivity remains more or less constant.

References

- [1] H. de Kluiver et al., Phys. Lett. 94A (1983) 156.
- [2] TORTUR TEAM, Proc. 11th Eur. Conf. on Contr. Fusion and Plasma Phys., Aachen (1983) Part I, p. 409.
- [3] A.W. Kofschoten, "Experimental studies of anomalous plasma heating in TORTUR II", part of Thesis University of Utrecht, 1982, Rijnhuizen Report 82-141 (1982).
- [4] H. de Kluiver, private communications.
- [5] B.B. Kadomtsev, "Plasma turbulence", Academic Press, New York (1965).
- [6] J.M. Kindel and C.F. Kennel, J. Geophys. Res. 76 (1971) 3055.
- [7] R.J. Bickerton and B.E. Keen, in "Plasma Physics" (ed. B.E. Keen) Conf. series 20, The Institute of Physics, London and Bristol (1974).
- [8] H. de Kluiver, "Current-driven turbulence in plasmas", Rijnhuizen Report 77-106 (1977).
- [9] H.W. Kalfsbeek, "Magnetic field profiles during turbulent heating in a toroidal hydrogen plasma", Part of Thesis University of Utrecht, 1979, Rijnhuizen Report 78-114 (1978).
- [10] K. Papadopoulos, Rev. Geophys. and Space Phys. 15 (1977) 113.
- [11] V.V. Parail and O.P. Pogutse, Nucl. Fusion 18 (1978) 303.
- [12] R.L. Stenzel, Phys. Rev. Lett. 38 (1977) 394.
- [13] H. de Kluiver et al., Proc. 10th Int. Conf. on Plasma Phys. and Contr. Nucl. Fusion Res., London (1984) Vol. 1, p. 375.

A C K N O W L E D G E M E N T S

The author wishes to express his gratitude to the TORTUR group, and particularly to Prof. H. de Kluiver. He thanks Dr. C. Bobeldijk for his continued support and Prof. C.M. Braams and Prof. F. Engelmann for their comments on the manuscript.

This work was performed as part of the research programme of the association agreement of Euratom and the "Stichting voor Fundamenteel Onderzoek der Materie" (FOM) with financial support from the "Nederlandse Organisatie voor Zuiver-Wetenschappelijk Onderzoek" (ZWO) and Euratom.

A P P E N D I X A

The channeltron is represented by the circuit shown in Fig. A1. The idea behind the scheme is that the multiplication process can be thought of as being built up of  $n$  discrete steps with multiplication  $(\text{Gain})^{1/n}$ . Evidently the most exhaustive charge drain occurs in the end of the channel. We state that only the last multiplication step suffers from saturation, while the others behave linearly. The first steps are represented by a resistance  $R_1$ . The last, saturated step is represented by a RC-circuit. Every single cascade is assumed to discharge  $C$  completely, so that the total gain is equal to the charge on  $C$ , and consequently proportional to  $V_2$ . After a discharge, recovery takes place with time constant

$$\tau = \frac{R_1 \times R_2}{R_1 + R_2} \cdot C = \frac{n-1}{n} \cdot (R_1 + R_2) C .$$

It is seen that the actual value of  $n$  hardly affects  $\tau$ , as long as  $n \gg 1$ .

The pulse-height distribution of a channeltron is adequately approximated by a triangle (see Fig. A2). The position of its top is proportional to  $V_2$ . A decrease of  $V_2$  causes the triangle to shrink with respect to the horizontal direction. Hence, the fraction of the pulses that falls beneath the discrimination level ( $D$ ) increases with the decrease of  $V_2$ . The values of  $\tau$  and  $D$  were determined experimentally.

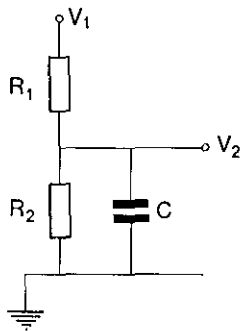


Fig. A1.  
RC-circuit representing a channeltron.

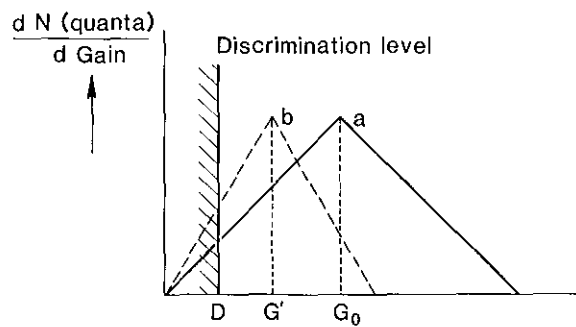


Fig. A2. → Gain  
Pulse-height distributions of a channeltron used in the model: a) unsaturated, b) saturated.

A P P E N D I X B

The self-inductance of the plasma column

The self-inductance  $L$  is defined by

$$\frac{1}{2}LI^2 = \int_{\text{vol}} B^2/2\mu_0 dV .$$

The integral should be taken over the volume encompassed by the surface  $r = a$  at which the loop voltage is measured. The field outside a does contribute to the self-inductance, but this term is part of the external circuit.

Consider a current running in a channel of width  $r_0 < a$ , with

$$j(x) = j_0 p(x) \quad x = r/r_0$$

$p(x)$  = profile function

$$I(x) = 2\pi r_0^2 j_0 \int_0^x x' p(x') dx' = 2\pi r_0^2 j_0 P(x)$$

with 
$$P(x) = \int_0^x x' p(x') dx' .$$

The total current  $I_0$  is given by

$$I_0 = I(1) = 2\pi r_0^2 j_0 P(1) .$$

Furthermore: 
$$B(x) = \frac{I(x)}{2\pi x r_0} .$$

For the total amount of field energy within the current channel, we get:

$$W_i = \frac{\mu_0}{4\pi} \frac{1}{2} I_0^2 \frac{1}{P^2(1)} \int_0^1 \frac{P^2(x)}{x} dx ,$$

where  $\ell = 2\pi R$ , the circumference of the torus and  $P^2(x)$  denotes  $(P(x))^2$ . Finally, for the internal self-inductance we find:

$$L_i = \frac{\mu_0}{2\pi} \ell \text{ PF} \quad \text{with PF} = \frac{1}{P^2(1)} \int_0^1 P^2(x) x^{-1} dx .$$

PF is a profile factor, which does not depend on  $r_0$ . In Table A.1 it is listed for some profile functions. The total self-inductance  $L$  is given by  $L_i$  plus the coaxial term:

$$L = \frac{\mu_0}{2\pi} \ell \left( \text{PF} + \ln \frac{a}{r_0} \right) .$$

TABLE B.1

$p(x)$	PF
1	0.25
$1 - x$	0.52
$1 - x^2$	0.46
$(1 - x^2)^2$	0.61

A P P E N D I X C

We consider a triangular j-profile:

$$j(x) = \beta^2(1 - \beta x)j_0, \quad 0 \leq \beta x \leq 1, \quad x = \frac{r}{a}, \quad \beta = \frac{a}{r_0};$$

$\beta = 1$  in the basic discharge.

The resistivity in the basic discharge is given by:

$$\eta(x) = \frac{\eta_0}{1 - x}.$$

If we assume that  $\eta$  is unaltered by the pinching of the j-profile, the ohmic dissipation is given by:

$$\dot{W}_\Omega = \dot{W}_{\Omega,0} \int_0^{1/\beta} 6\beta^4 \frac{(1 - \beta x)^2}{(1 - x)} x dx.$$

If we take  $\eta \sim j^{1/2}$  (see Section 6.2), the relation takes the form:

$$\dot{W}_\Omega = \dot{W}_{\Omega,0} \int_0^{1/\beta} 6\beta^5 \frac{(1 - \beta x)^{5/2}}{(1 - x)^{3/2}} x dx.$$

In Fig. C.1 these integrals are plotted against  $\beta$ . In the range of interest,  $1 < \beta \leq 1.5$ , the following approximated relation is found:

$$\begin{aligned} \frac{\dot{W}_\Omega}{\dot{W}_{\Omega,0}} &\approx \exp[\alpha(\beta - 1)] \\ &= 1 + \alpha(\beta - 1) + O(\alpha^2(\beta - 1)^2), \end{aligned}$$

with  $\alpha = 0.8$  for  $\eta \sim j^0$   
and  $\alpha = 1.4$  for  $\eta \sim j^{1/2}$ .

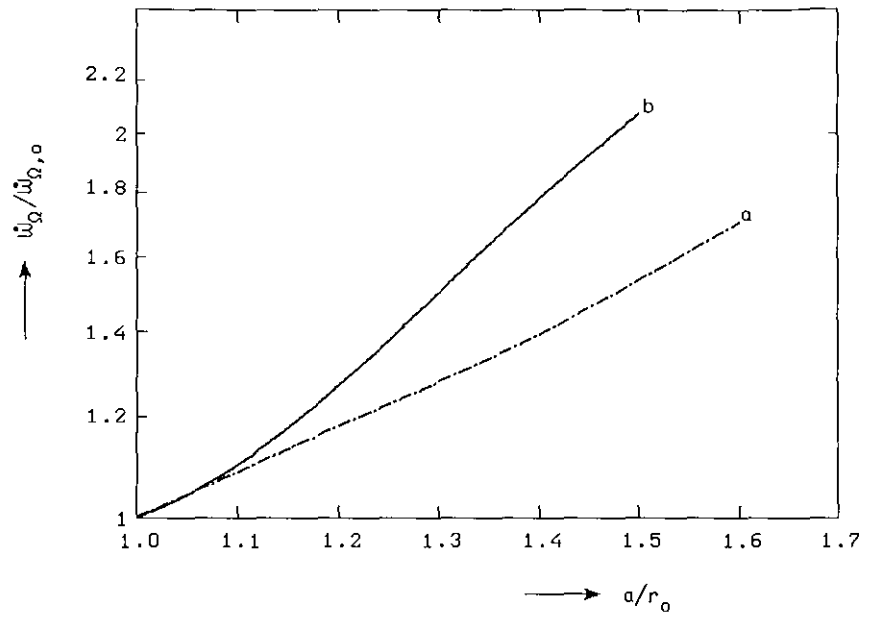


Fig. C.1. The normalized ohmic dissipation as a function of the width ( $r_0$ ) of the current-density profile, calculated for a triangular  $j$ -profile with the assumption  $\eta \sim j^0$  (a) and  $\eta \sim j^{1/2}$  (b).

A P P E N D I X D

In this Appendix a synopsis is presented of the diagnostics development I have been involved with.

In the four-channel analyser PLATO two of the original four channeltrons were replaced by surface-barrier diodes. This modification allowed the test and application of the hybrid foil method (a method to deduce  $T_e$  from soft X-ray measurements). The hybrid foil method is described in Ref. 1. Results obtained with PLATO are published in Ref. 2 and in this thesis.

Two new multichannel soft X-ray diagnostic systems were designed and built, one for the TORTUR III tokamak and one for the SPICA II screw-pinch experiment. Both are so-called pinhole cameras.

The camera for TORTUR III has a spatial resolution of 0.5 cm and a time resolution of 50  $\mu$ s in eight detection channels. An iterative Abel-inversion code has been developed to reconstruct the radial X-ray emissivity profile. First results were obtained early in 1985.

The camera for SPICA II has sixteen detection channels, arranged in a  $2 \times 8$  matrix. It offers radial resolution in eight double detection channels, with resolution  $\Delta r = 1$  cm and a time resolution of 2  $\mu$ s. The double channels enable application of the absorber-foil method to determine the electron temperature ( $T_e$ ). To that end two foil exchangers are mounted in the instrument.

In both cameras microchannelplates are applied as X-ray sensitive detectors. A research programme was carried out to investigate i) the pulse-height distribution of a 'chevron' (two cascaded microchannelplates) as a function of the bias voltages and ii) the performance of a chevron subjected to pulsed and continuous high intensity.

For these experiments an electron beam facility of controlled intensity was built.

From the results of the first experiment and from a theoretical statistical analysis it was concluded that the typical quasi-gaussian pulse-height distribution of the chevron is not due to saturation of the second plate. Instead, the pulse-height distribution of the

chevron is a nearly linear magnification of that of the first plate [3].

The high counting rate experiments showed that the recovery of a channel that is 'fired' proceeds with an initial fast phase (typical time constant  $\tau_1 = 0.5$  ms) to continue slower ( $\tau_2 \approx 5$  ms). Generally, only the slow phase is found in literature. We have investigated whether lateral currents could be responsible for the fast, partial, recovery second plate (as is widely assumed). To that end we measured the bulk resistivity ( $\eta_b$ ) of the channelplates. We found  $\eta_b = 10^{10}$   $\Omega\text{m}$ , compared to  $\eta > 10^{16}$   $\Omega\text{m}$  specified for Corning 8161 glass (the bulk material of standard Galileo microchannelplates). This result implies that lateral conduction is not negligible in a channelplate. It cannot, however, account for the observed fast initial recovery [4].

#### References

- [1] N.J. Lopes Cardozo, Rev. Sci. Instrum. 55 (1984) 1077.
- [2] N.J. Lopes Cardozo, "Soft X-ray electron temperature measurements on TORTUR", Rijnhuizen Report 84-151 (1984).
- [3] N.J. Lopes Cardozo, "An experimental and theoretical investigation into the pulse-height distribution of microchannelplates", submitted for publication to IEEE Trans. Nucl. Sci.
- [4] N.J. Lopes Cardozo and J. Renes, "On saturation and recovery of microchannelplates", to be published.